DETECTION OF LUNG CANCER USING

OPTICAL SPECTROSCOPY

Martin Bard

DETECTION OF LUNG CANCER USING

OPTICAL SPECTROSCOPY

Detectie van longkanker gebruikmakend van optische spectroscopie

Proefschrift

ter verkrijging van de graad van doctor aan de

Erasmus Universiteit Rotterdam

op gezag van de

rector magnificus

Prof.dr. S.W.J. Lamberts

en volgens besluit van het College voor Promoties.

De openbare verdediging zal plaatsvinden op

woensdag 28 september 2005 om 13.45 uur

door

Martin Philippe Louis Bard

geboren te Antony, Frankrijk

Promotie commissie

Promotor:	Prof.dr. H.C. Hoogsteden
Overige leden:	Prof.dr. P.C. Levendag
	Prof.dr. J.W. Oosterhuis
	Prof.dr. J.P. van Meerbeeck
Copromotoren:	Dr. H.J.C.M. Sterenborg
	Dr. J.G.J.V. Aerts

Voor mijn ouders

Annelies, Thomas en Emma

pardon pour le temps volé

Contents

This thesis has been prepared at:

Erasmus Medical Center Rotterdam, The Netherlands
 Department of Respiratory Diseases
 Center for Optical Diagnostics and Therapy, Department of Radiation Oncology
 Department of Pathology
 Department of Statistics

Sint Franciscus Hospital Rotterdam, The Netherlands
 Department of Respiratory Diseases
 Department of Pathology

Delft University of Technology
 Faculty of Electrical Engineering, Mathematics and Computer Science

CHAPTER 1

Introduction and aim of the thesis

1. Lung cancer

   1.1. Epidemiology

   Lung cancer is the most frequent cancer worldwide and its incidence has risen sharply since the last 50 years. Lung cancer represents 12.3 % of all new cancers and there are an estimated 1.2 million new cases in 2000 (1, 2). The disease is more common in men and the areas of highest incidence are Eastern Europe, North America, Australia/New Zeeland and South America. Tobacco smoking is well established as the main cause of lung cancer and about 90% of cases are thought to be tobacco related. There is a clear dose-response relation between lung-cancer risk and the number of cigarettes smoked per day, degree of inhalation, and age the smoker starts his habit (3-6). In general, someone who has smoked all his life has a 20–40 times greater risk of developing lung cancer than a non-smoker. Among the more than 60 carcinogens identified in tobacco smoke, the two major classes are polycyclic aromatic hydrocarbons and nitrosamines. These carcinogens induce sequential mutations of various genes especially those involved in the regulation of the cell-cycle (7-9). The accumulation of genetic and molecular abnormalities leads to an uncontrolled growth of clonal cells and to an increased capacity of these cells to migrate. Other factors known to increase risk of lung cancer are occupational exposure to asbestos, some metals (e.g. nickel, arsenic, cadmium), radon, and ionising radiation. The effect of some of these agents, particularly asbestos, on lung-cancer risk may be synergistic with smoking (10). Prognosis of lung cancer is severe and most patients die within 1 year of diagnosis, making lung cancer the leading cause of cancer death. One of the explanations for the very poor survival of patients is that most patient initially present with disease at an advanced stage. At the time of diagnosis, only 20% of all lung cancer patients will have local disease, while 25% will have disease spread to regional lymph nodes, and 55% will have distant metastasis. Even in those patients with supposedly localized disease, overall 5-year survival is only 30-40% (11, 12).

1.2. Pathology

1.2.1. Classification

The diagnosis of lung cancer is made by examining histologic or cytologic specimens from the lung itself or from metastases. The common types of lung carcinomas are: adenocarcinoma, squamous cell carcinoma, large cell carcinoma and small cell carcinoma (13). Adenocarcinoma is a glandular epithelial malignancy usually peripherally located. Bronchial adenocarcinoma forms glands and produces mucin. The cells of adenocarcinoma are usually large, with large nuclei, a high nucleus-to-cytoplasmic ratio, and prominent eosinophilic nucleoli. Squamous cell carcinoma is defined as a malignant epithelial tumor with features of squamous differentiation such as keratin formation and intercellular bridges. In contrast to adenocarcinoma, the majority of these tumors arise centrally from major bronchi. The microscopic appearance of the tumor depends of the degree of differentiation. The tumor usually grows as large solid nests of cells that have dense eosinophilic cytoplasm with large hyperchromatic nuclei. The nuclei are irregular in shape and may not show prominent nucleoli. The nuclear-to-cytoplasmic ratio is low. Undifferentiated large cell carcinoma is a non-small cell carcinoma that displays no evidence of squamous or glandular maturation with light microscopy. These tumors may be central or peripheral. The most commonly identified form is a uniform type with sheets of closely packed cells with high nuclear-to-cytoplasm ratio and areas of necrosis. Small cell carcinoma is a malignant epithelial tumor with the cytologic features of scant cytoplasm, finely granular chromatin, absent nucleoli, and frequent mitoses. Usually arising centrally around the hilum, this tumor is frequently associated with lymph node involvement. Small cell carcinoma usually appears as monotonous sheets of hyperchromatic cells with foci of necrosis. These round-to-oval cells have a high nucleus-to-cytoplasm ratio. Mitotic count is very high.

1.2.2. Pre-neoplastic lesions

Bronchogenic carcinoma is not a result of a sudden radical change in the bronchial cells, but a multistep process in which a sequence of morphological and genetic changes is occurring. Preneoplastic lesions are morphological phenotypes of the different steps in the progression from normal to malignant tissue (14). Pre-neoplastic lesions are frequently found in association with malignancy or in patients with high risk of developing lung cancer (15, 16). Moreover, frequent genetic changes are common between tumors and their associated preneoplastic lesions (17-20). For squamous cell carcinoma, precursor lesions are widely recognized in the sequence hyperplasia-metaplasia-dysplasia-carcinoma in situ (CIS). These lesions are characterized by morphological changes, illustrated in figure 1, with a progressive increase of pleomorphic and atypic cells inducing a thickening of the epithelial layer of the bronchial mucosa.
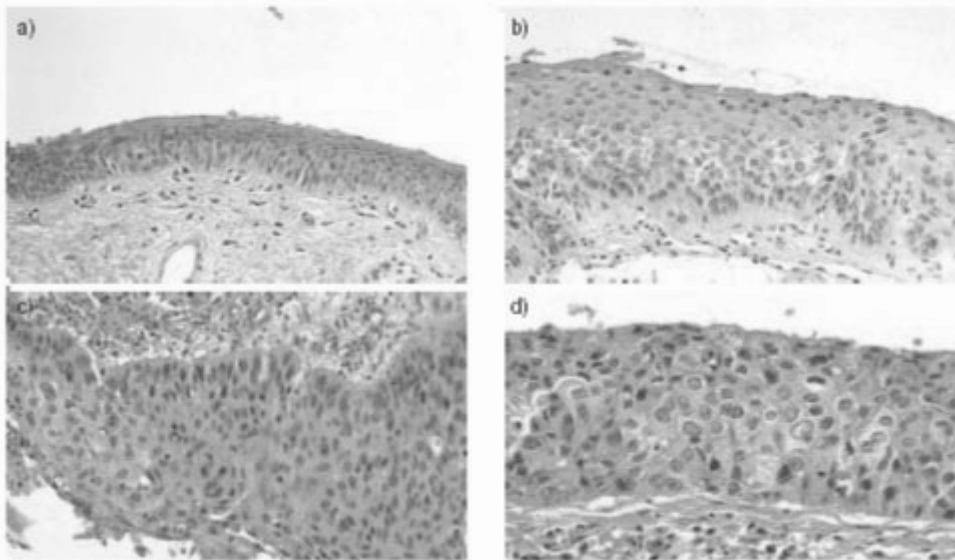
Figure 1. Histological patterns of bronchial squamous cell carcinoma precursors (Brambilla, Eur Respir J 2001). a) Mild dysplasia: mildly increased thickness, mild pleiomorphism, nuclei are vertically oriented, mitoses absent. b) Moderate dysplasia: moderately increased thickness, moderate anysocytosis and pleomorphism; nuclei are vertically oriented, mitotic figures in lower third. c) Severe dysplasia: markedly increased thickness, marked anisocytosis and pleomorphism, irregular nuclei vertically oriented in lower third, mitosis in lower two-thirds. d) Carcinoma in situ: markedly increased cell size and pleomorphism, cellular crowding throughout epithelium, no consistent orientation of nuclei, irregular nuclei, mitotic figures through full thickness.

Each lesion of the sequence can be divided into three broad categories. Reactive changes, such as hyperplasia and metaplasia, which are very frequent in smokers but which have no increased risk. Intermediate changes, such as mild and moderate dysplasia, which have moderately increased risk. High risk lesions, such as severe dysplasia and carcinoma in situ, which have considerably increased risk and for which a therapy is discussed. For adenocarcinoma, progenitor lesions may be the adenomatous hyperplasia, and atypical adenomatous hyperplasia. No preneoplastic lesion has been clearly identified for small cell carcinoma (13, 14). The detection of preneoplastic lesions may allow an early cure of still localised lesions, allowing a more positive prognosis of lung cancer (21).

1.3. Early diagnosis of lung cancer

It is commonly accepted that the earlier a cancer is discovered, the greater the chances of survival. Patient with stage I (small size localized tumor) non small cell lung cancer have a 5 years survival ranging from 40% to 80% (11, 12). However, no consensus exists about the value of early detection of lung cancer. This lack of consensus has been based on a general acceptance that screening for lung cancer in randomised trials has not yet demonstrated a reduction in mortality. Various techniques have already been studied for lung cancer screening.

1.3.1. Imaging technique

Thorax X ray has been the first imaging technique used for lung cancer screening. In the years 70s-80s, three studies sponsored by the National Cancer Institute have studied the interest of periodic chest radiographs for lung cancer screening. More than 30.000 patients were enrolled but, although a significant shift toward earlier diagnosis and an increased rate of operable cancer were reported, no disease-specific mortality benefit was observed (22).

13

Chest radiographs have also been shown to be insensitive for detecting early parenchymal abnormalities and central airway tumours (23). Several recent studies have documented the effectiveness of low dose spiral computer tomography (CT) scan to detect lesions that cannot been seen on a chest radiograph. The results of these studies are promising, allowing diagnosis at earlier and thus more curable stages (24-26). However, the impact on lung cancer mortality has not yet been demonstrated. A major problem of CT scan screening is the high rate of false positive findings and a challenge is to avoid unnecessary procedures for benign or indolent nodules. Dynamic imaging techniques such as positron emission tomography (PET) scan seem to be interesting but need to be studied more extensively (27).

1.3.2. Sputum cytology

The cytological analysis of sputum samples has been combined to imaging techniques (chest radiography and/or CT scan) in various studies aiming the early detection of lung cancer. No advantage for the patient, particularly no mortality benefit, can be concluded from the already published literature (28). Although sputum cytology is a highly specific technique (>98%), its sensitivity is very low (20-30%). As well as its lack of sensitivity, sputum cytology is also a time consuming technique (29). Moreover, opinions vary on the reliability of the sputum examination. The variation in intra- and inter-observer agreement seems to depend on experience among cytopathologists and the type of lesion studied (the higher degree of agreement is obtained for higher grades of dysplasia and CIS).

Various tools can be used to improve the sensitivity of sputum-examination. Immunostaining techniques, PCR techniques, computer-assisted image analysis are some examples of recently developed techniques that can help the cytological examination of sputa (30, 31). Moreover, the recent improvement in molecular biology, the advances in gene chip

technology might become feasible to probe for expression of multiple genes in sputum of asymptomatic individuals (32-35).

1.3.3. Bronchoscopy

Bronchoscopy is, with thoracic imaging (CT-scan and PET-scan), the cornerstone technique for both diagnosis and staging of lung cancer. Proximal exophytic endobronchial tumors are generally easy to localize with white light bronchoscopy, but more subtle changes of the bronchial mucosa as those associated with dysplasia or CIS have been reported to be only visible to experienced bronchoscopists (36). Recent improvement in video system quality, development in video chip technology have permitted the development of video-endoscope allowing high quality imaging of the tracheobronchial tree. Other recent progress has been made in the development of combined endoscopes allowing a simultaneous visualization of the bronchi under white and ultraviolet-blue light.

Autofluorescence bronchoscopy (AFB) implements the modifications of autofluorescence property that occur in unhealthy mucosa and which are extensively discussed in the paragraph dedicated to the fluorescence spectroscopy. Ultraviolet laser or violet-blue light lamps are used to excite the endogeneous fluorophores contained in the bronchial mucosa; the fluorescence emission is collected and processed in order to produce an image allowing a distinction between normal and unhealthy mucosa (37, 38).

Various AFB imaging systems are commercially available. The LIFE system, developed fifteen years ago by the Canadian company Xillis, uses a helium-cadium (442 nm) laser for the fluorescence excitation and acquires digitized autofluorescence images by the ratios of red to green fluorescence light emission. More recently developed systems are the D-light (Storz, Germany), the SAFE (Pentax, Japan) and the DAFE (Richard Wolf, Germany) systems that

use no laser but a violet-blue lamp for fluorescence excitation and fluorescence filters for the acquisition of autofluorescence images.

These various AFB systems, but more especially the LIFE system, have been compared to WLB (39-50). In a great majority of these studies, AFB has been reported to be better than WLB for the detection of proximal endobronchial tumors. Sensitivity values ranging from 70% to 96% have been commonly reported for AFB, superior to the 30%-60% sensitivity observed with conventional WLB. The variation of AFB sensitivity reported by these various authors is explained by the differences existing in the population studied (amount of patients with a positive sputum cytology for example) and by differences existing in the criteria chosen by the bronchoscopists for the definition of the bronchial lesions. Concerning the detection of pre-malignant lesions such as severe dysplasia and CIS, higher sensitivity values have also been reported for AFB in comparison with WLB. Sutedja and coll recently reviewed the sensitivity of several AFB systems for the detection of endobronchial premalignant lesions (37). These authors reported that most AFB systems yield comparable results with sensitivity values around 80% (Table I).

System (amount biopsies)	WLB	AFB
Life Xillis (n = 4173)	40%	86%
D-light Storz (n = 771)	25%	83%
Safe Pentax (n = 157)	21%	79%

Table I. Sensitivity rates for moderate, severe dysplasia and carcinoma in situ of different autofluorescence bronchoscopy systems (adapted from Sutedja et al, Lung Cancer 2001). WLB; white light bronchoscopy, AFB; autofluorescence bronchoscopy

Recently, a prospective comparison of the LIFE and the D-Light systems was reported, demonstrating hardly any discrepancy for the detection of endobronchial lesions between these laser and non-laser AFB systems (51). The D-Light systems was however reported to be cheaper, easier to use, with a shorter examination time (51).

Controversy still exists about the value of fluorescence endoscopy for the detection of lung cancer (36-38, 43, 52, 53) and pre-malignant lesions of the bronchial tree (54-60). The lack of comparison of AFB with the most recent white light video-bronchoscope hampers any conclusion over the real superiority of AFB to WLB for the detection of early cancer and pre-malignant lesions. Moreover, AFB is characterized by a low specificity for the detection of pre-malignant lesions with a high rate of false positive findings. Specificity values ranging from 55% to 70% have been typically reported for AFB, largely inferior to the 80-90% specificity commonly observed with WLB. Such low specificity of AFB induces unnecessary biopsies at greater cost and longer examination duration and is a major problem hampering the general use of AFB for lung cancer screening. If AFB is at present the technique with the best sensitivity for the detection of endobronchial (pre-)malignant lesions, additional techniques are needed to improve its specificity.

2. Light induced spectroscopy

Pre-neoplastic and malignant disease are accompanied by local metabolic and architectural changes at cellular and subcellular level that are likely to affect the optical properties, i.e. the scattering, absorption and fluorescence properties of the tissue. Therefore, optical spectroscopy may be able to provide functional information to identify focal (pre-) cancerous lesions (61-64).

2.1. Autofluorescence spectroscopy (AFS)

2.1.1. Principle

Energy in the form of a photon can excite certain molecules within a tissue to a higher energy level. The subsequent radiative relaxation of the molecule is accompanied by the release of a reemission photon in a process termed "fluorescence". Molecules that can fluoresce are called "fluorophores". Most endogenous fluorophores are associated with the structural matrix of tissue or are involved in cellular metabolic processes. The most important of the former are collagen and elastin. Fluorophores involved in cellular metabolism include reduced nicotinamide adenine dinucleotide (NADH) and flavins. Other fluorophores include the aromatic amino acids (e.g. tryptophan, tyrosin, phenylalanine), various porphyrins and lipopigments. In addition, red porphyrin fluorescence due to bacteria may be significant in certain body sites (oral cavity) and/or lesions (62). Each fluorophore has a distinct excitation and emission spectrum. Moreover, any given tissue contains a mixture of many fluorophores of different concentrations and the fluorophores are not uniformly distributed in tissue. Changes in tissue fluorescence properties depend on modifications of the fluorophore concentrations or spatial distributions, the fluorophore metabolic status (e.g. NADH is fluorescent only in its reduced form), the tissue architecture such as mucosal thickening or loss of layered structure, and the wavelength dependent light attenuation due to the

18

concentration and distribution of (non-fluorescent) chromophores, particularly haemoglobin. Some of these changes occur early in oncogenesis and may be observed in pre-malignant lesions.

Reports in animal models suggest that the fluorescence spectroscopic changes occurring in epithelial tissue throughout the dysplasia-carcinoma sequence may precede the morphologic tissue changes (65). In humans, decreased NADH and flavin fluorescence have been observed in cancerous bronchial cells in comparison with normal bronchial epithelial cells (66). Decreased density of elastin tissue has been associated with a decrease of autofluorescence intensity without change of the spectral shape in human bronchi (67). In the colon, changes in basement membrane type IV collagen have been reported to be responsible for the fluorescence modification observed in malignant tissue (68). An increased haemoglobin absorption would also contribute to the decreased fluorescence of adenomatous colonic polyps in comparison with normal mucosa (69). Moreoever, the dysplastic changes occurring in colon epithelium have been reported to be associated with an increase of cytoplasmic fluorescence due to a rise in mitochondrial reduced NADH concentration (70). Finally, in uterine cervix and oesophagus mucosa, low collagen en high NADH fluorescence were associated with the autofluorescence changes observed in high grade dysplastic lesions (71)

2.1.2. Application in human cancer

Most autofluorescence spectroscopic systems currently used for the detection of human cancer consist of a source of monochromatic light (laser or lamp with appropriate filters to obtain specific wavelength), an optical fiber probe, and a spectrometer to record fluorescence intensities in a specific wavelength region. A typical fluorescence spectrum measured using

405 nm excitation in bronchial mucosa is shown in figure 2. The greatest intensity occurs in the green region around 500nm.
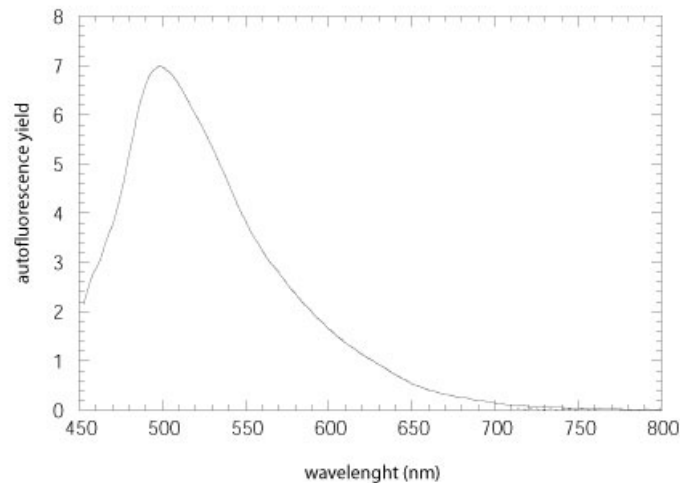
Figure 2. Typical autofluorescence spectra measured in bronchial mucosa. The greatest intensity occur in the green region around 500nm wavelength.

In their pioneering work, the group of Lam and Palcic reported that autofluorescence spectra measured in cancerous bronchial lesions were characterized by a decrease in intensity without changes in the spectral shape (72). Most interesting was the report that the autofluorescence spectra of dysplastic and CIS lesions were also characterized by a decreased intensity. More recently, the group of Wagnieres examined autofluorescence spectra of human bronchial tissue (normal, dysplastic and cancerous) using a larger excitation wavelength range (from 350 to 480 nm). These authors reported that the excitation wavelengths yielding the highest contrast were between 400 and 480nm with a peak at 405nm (73, 74). They also observed a decrease in AF intensity in dysplastic and cancerous lesions. Coupling spectrofluorometry to laser-induced fluorescence imaging, a Japanese group reported the same results in the human bronchial tree with a decreased autofluorescence intensity in cases of cancerous lesions, carcinoma in situ and dysplastic lesions in comparison with normal bronchial mucosa (44). Such a decreased intensity of fluorescence is not restricted to

bronchial mucosa but has already been reported in cancer occurring in various organs such as the oral cavity (75-78), the digestive tract (79-81), the bladder (82, 83), the uterine cervix (84, 85), the breast (86), and the skin (87).

Thus, alterations of autofluorescence in epithelial tissue seems to be a common consequence of biological and morphological changes occurring during oncogenesis. Therefore, use of autofluorescence spectroscopy, mostly coupled with imaging (endoscopy) techniques, may improve the detection of (pre-)malignant lesions.

2.2. White light reflectance spectroscopy

2.2.1. Principle

Reflectance spectroscopy is the study of light that has been reflected or scattered from a solid, liquid, or gas as a function of wavelength. As the photons enter an object, some of the light is absorbed, some is reflected (scattered), and some passes through the object unperturbed (transmitted). Significant light absorbers of biological tissue are haemoglobin, melanin, proteins and DNA. Various cellular and extracellular components of living tissue contribute to light scattering. In the cell, the membrane-bound subcellular organelles such as the nuclei, nucleoli, mitochondria, secretory vacuoles and other similarly sized intracytoplasmic granules can influence light scattering because of refractive differences at the membrane interface (88-92). In the extracellular matrix, collagen and elastin are the predominant scatterers. Typical reflectance spectra measured in bronchial mucosa is shown in figure 3. The signal dips observed below 600nm correspond to the absorption of light by haemoglobin.
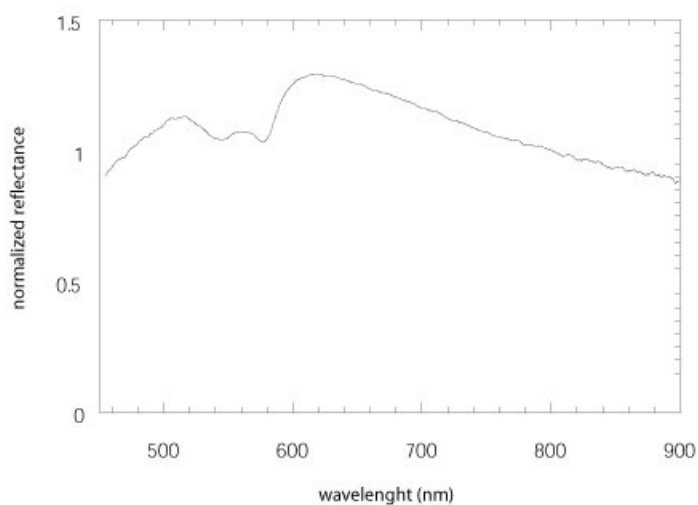
Figure 3. Typical reflectance spectra measured in the bronchial mucosa. The signal dips observed below 600nm correspond to the absorption of light by haemoglobin.

Reflectance spectroscopy is particularly useful for the analysis of cancerous tissue because major scattering and absorption changes occur during the development of cancer. Cellular changes include modifications in the size, shape, and orientation of the nuclei, an increase in nucleus chromatin content, variations in the nucleus-cytoplasma ratio, and changes in the intra-cytosolic content (13). Additionally, major architectural changes occur, inducing an increase in the total amount of cells, with commonly a thickening of the epithelial layer. Cancerous tissue is also frequently associated with an increased metabolism and an abnormal microvasculature network (neoangiogenesis) (93) inducing dramatic changes in both the concentration of blood and the oxygenation of hemoglobin (94, 95).

Therefore, white light reflectance spectroscopy may be useful in lung oncology for various purposes:

1)   To study *in vivo* and non-invasively several light absorbers (such as haemoglobin) and light scatterers (such as nuclei and cytosolic organelles) contained in tumor tissue .

2)   To correlate the optical and the histological changes occurring in tumor tissue in the aim to (early) detect (pre-)malignant lesions.

2.2.2. Application in human cancer

2.2.2.1. Analysis of light absorption

The volume and the oxygenation of blood have been studied in adenomatous polyps of the colon using diffuse reflectance spectroscopy (96). Reflectance spectra were measured using a fiberoptic probe during colonoscopy. Both the total blood concentration and the oxygen saturation of hemoglobin were extracted from the reflectance spectra using mathematical modelling. In comparison with normal colon mucosa, adenomatous polyps were characterized by an increased concentration of blood, while there was no observable difference in hemoglobin oxygenation. Using a similar technique, an increased blood concentration was reported in bladder carcinoma in comparison with normal mucosa (97). Near-infrared reflectance spectroscopy has been used on uterus and breast tissue (98, 99). A decrease in hemoglobin oxygenation has been reported in high-grade squamous intra-epithelial lesions of the cervix in comparison with normal cervical tissue (98) and in ductal carcinomas of the breast in comparison with benign fibroadenomas (99).

Reflectance spectroscopy can thus be used to evaluate the concentration and oxygenation of blood in tumor tissue and could be useful for the monitoring of several therapies targeted on the tumor hypoxia and the neoangiogenesis.

2.2.2.2. Analysis of light scattering

The reflectance signal is composed of photons reflected (scattered) from the various light scatterers contained in the tissue. Moreover, the reflectance signal is the sum of photons which have been only one-time scattered (single scattering signal) and photons which have

undergone multiple scatter events in the tissue (diffuse scattering signal). As a consequence, the contribution of a particular scatterer to the scattered signal is particularly hard to distinguish. An additional difficulty is related to our poor knowledge of the exact dependence of the scattered signal on the composition of cells and tissue.

The G.R. Harrison Spectroscopy laboratory from M.I.T. aimed to use reflectance spectroscopy to analyse the nuclear composition in pre-malignant and cancerous epithelia. They hypothesized that nuclei are the main scatterers in epithelial tissue, and they mathematically modeled diffuse reflectance spectra measured in tissue in order to distinguish the single scattered signal from the diffusely scattered signal (100). They observed a periodic component in the modeled single scattering signal that they used to calculate both the concentration and the size of the epithelial nuclei. Using this so called light scattering spectroscopy (LSS) technique, they studied patients suffering from dysplastic and cancerous epithelial lesion of the uterine cervix (101), the oesophagus (102-104) and the oral cavity (93, 105). In each of these organs, they measured enlarged nuclei in cancerous but also in dysplastic epithelium in comparison with normal mucosa. In the attempt to validate their signal modeling method, these authors used polarized light spectroscopy to directly measure the single scattering part of the light reflectance signal. Principle of polarized light spectroscopy is that linearly polarized light loses its polarization as it traverses a turbid medium such as biological tissue and is multiply scattered. By removing the unpolarized component of the reflected light signal emerging from the tissue, the contribution due to the single scattered signal can be distinguished. Polarized light spectroscopy was used ex vivo for the analysis of oesophageal, colon, bladder, and oral epithelia. Higher nuclear size and density were observed in both dysplastic and cancerous lesions in comparison with normal mucosa (106, 107).

The pioneering work of the M.I.T. group demonstrated the feasibility and the potential interest of light reflectance spectroscopy for the study of epithelial cancerous lesion. However, the LSS results are controversial because they are theory dependant. Indeed, the assumption that the nucleus is the principal scatterer in the epithelium is probably inaccurate. Recent *ex vivo* reports in human tissue and tissue phantoms suggest that intra-cytosolic particles with a 2-μm size (possibly the mitochondria) may contribute mostly to the scattering of cells and tissue (88-91, 108). Furthermore, it is highly debatable to resume the single scattered component of light-induced reflected signal to a difference between a measured and a modeled diffuse reflectance signal. More accurate techniques are then needed for the analysis of the optical properties of epithelial tissue.

2.2.2.3. detection of (pre-)malignant lesions

The feasibility of reflectance spectroscopy to classify and detect pre-malignant and cancerous lesions has been evaluated in various organs.

In uterine cervix, AFS and DRS have been used to distinguish normal from dysplastic and cancerous epithelium (109, 110). Sensitivities higher than 70% were reported associated with specificity values ranging from 65 to 80% depending on the types of lesion studied (normal *versus* dysplasia or *versus* cancer lesion). High sensitivity and specificity were also reported for the distinction of breast (86) and ovary (111) carcinomas by combination of AFS and DRS.

The M.I.T. team evaluated the classification property of three light spectroscopic techniques, i.e. AFS, DRS and LSS, in several organs such as the uterus (101), the oesophagus (104) and the oral cavity (105). LSS was able to distinguish normal epithelium from cancerous lesions but also from pre-malignant dysplatic lesions with the best sensitivity and specificity. The combination of the three spectroscopic techniques yielded very accurate

results with, for example, sensitivity and specificity of 92% and 71% respectively for the distinction between cervical squamous intraepithelial lesions and normal cervical tissue (101).

At present, no data are available for the lung due to the difficulty to measure light reflectance spectra in the bronchial tree. Recently, Lam and colleagues reported the development of an integrated endoscopy system allowing the simultaneous acquisition of images and light-induced spectra from bronchial mucosa illuminated with both white and blue light (112). This group aims to increase the diagnostic accuracy of the bronchoscopic imaging technique (white light and autofluorescence bronchoscopy) by the simultaneous use of AFS and DRS. These authors did not report any data concerning the use of this instrument on patients. However, the reflectance spectra analysed by this instrument are collected from a large tissue area and penetrate deep in the tissue impairing the specific analysis of localized lesions and of lesions limited to the most superficial layer of the bronchial mucosa, i.e. the epithelium. New optical instruments are therefore needed for the detection of intra-epithelial pre-malignant and cancerous lesions.

Aim of the Thesis

The aim of the study was to use optical spectroscopy during bronchoscopy for the detection and the analysis of pre-malignant and cancerous lesions of the tracheobronchial tree. For this study we developed a fiberoptic instrument allowing the simultaneous measurement of three kinds of light induced spectroscopy, i.e. autofluorescence spectroscopy, reflectance spectroscopy and differential path-length spectroscopy. Differential path-length spectroscopy is an original spectroscopic technique which allows the analysis of the most superficial layer of the tissue, i.e the epithelium.

In **chapter 2**, we describe the original optic instrument developed by our group for the analysis of epithelial optical properties. This fiberoptic-based tool improves the detection of the scattering events occurring close to the probe tip, thanks to the use of a single fiber for both the delivery and the collection of light. The sensitivity of this instrument for the scattering signal detection is tested in various tissue phantoms. We demonstrate that our instrument is sensitive to the scattering events occurring in the most superficial (first 150-200 μm) of the tissue surface.

In **chapter 3**, we describe a new spectroscopic method, differential path-length spectroscopy (DPS), that allows the analysis of the optical properties of the most superficial layer of tissue. Because blood is the main absorber in tissue, informations concerning the blood content, the blood oxygenation and the diameter of microvasculature can also be extracted from DPS spectra. DPS method is described in detail and preliminary data in bronchial mucosa are reported.

In **chapter 4**, we report the results of DPS measurements in the bronchial tree in a large group of patients with known or suspected malignancies of the lung. DPS was measured during bronchoscopy in various kinds of bronchial lesions. We observed that bronchial tumors were characterized by a lower blood oxygen saturation and a higher blood content

than normal mucosa. No differences were observed between normal and metaplastic/mild dysplastic mucosa.

In **chapter 5**, we study the relation between the hypoxia-related parameters measured using DPS and one of the most important prognosis factors of lung cancer, i.e. the cancer cell type. Small-cell carcinomas and poorly differentiated large-cell carcinomas were associated with the lowest blood oxygenation and the lowest blood content in comparison with other lung cancer cell types. No difference in microvessel size was observed. Significant differences in scattering property were also observed in cases of small-cell carcinomas.

In **chapter 6**, we report the results of a pilot study aiming to establish the importance of autofluorescence and diffuse reflectance spectroscopy for the improvement of autofluorescence imaging. D-light Storz autofluorescence bronchoscopy system was used for the detection of endobronchial lesions. Autofluorescence and diffuse reflectance spectra were measured in all detected lesions and histology of all lesions were obtained. We observed that the combination of AFS and DRS increases the specificity of autofluorescence imaging.

In **chapter 7**, we compare the accuracy of AFS, DRS and DPS to distinguish endobronchial cancerous lesions from healthy bronchial mucosa. Spectroscopic measurements were done during bronchoscopy in a large cohort of patients with known or suspected malignancies of the lung. The three spectroscopic techniques, especially DRS and DPS, allowed to classify malignant tissue with a high accuracy. The specificity of autofluorescence bronchoscopic imaging for the detection of endobronchial tumors was markedly improved by the addition of the three spectroscopic techniques.

In **chapter 8**, we review the results obtained in the previous chapters. We describe the relevance of our findings and the potential application of light induced spectroscopy for the analysis and the detection of cancer of the bronchial tree.

REFERENCES

1. Parkin DM, Bray FI, Devesa SS. Cancer burden in the year 2000. The global picture. Eur J Cancer 2001;37:S4-S66.
2. Tyczynski JE, Bray F, Parkin DM. Lung cancer in Europe in 2000: epidemiology, prevention, and early detection. Lancet Oncol 2003;4:45-55.
3. Jerzy ET, Bray F, Parkin DM. Lung cancer in Europe in 2000: epidemiology, prevention, and early detection. Lancet Oncol 2003;4:45-55.
4. Doll R, Peto R, Boreham J, Sutherland I. Mortality in relation to smoking: 50 years' observations on male British doctors. BMJ 2004;328:1519.
5. Alberg AJ, Samet JM. Epidemiology of lung cancer. Chest 2003;123:21S-49S.
6. Proctor RN. Tobacco and the global lung cancer epidemic. Nature Reviews 2001;1:82-86.
7. Mina JD, Roth JA, Gazdar AF. Focus on lung cancer. Cancer Cell 2002;1:49-52.
8. Roland M, Rudd RM. Genetics and pulmonary medicine. 7. Somatic mutations in the development of lung cancer. Thorax 1998;53:979-983.
9. Rom WN, Hay JG, Lee TC, Jiang Y, Tchou-Wong K-M. Molecular and genetic aspects of lung cancer. Am J Respir Crit Care Med 2000;161:1355-1367.
10. Lee PN. Relation between exposure to asbestos and smoking jointly and the risk of lung cancer. Occup Environ Med 2001;58:145-153.
11. Mountain CF. The international system for staging lung cancer. Sem Surg Oncol 2000;18:106-115.
12. Naruke T, Tsuchiya R, Kondo H, Asamura H. Prognosis and survival after resection for bronchogenic carcinoma based on the 1997 TNM-staging classification: The Japanese experience. Ann Thorac Surg 2001;71:1759-1764.
13. Brambilla E, Travis WD, Colby TV, Corrinz B, Shimosato Y. The new World Health Association classification of lung cancer. Eur Respir J 2001;18:1059-1068.
14. Greenberg AK, Yee H, Rom WN. Preneoplastic lesions of the lung. Respir Res 2002;3:20.
15. Paris C, Benichou J, Bota S, Sagnier S, Metayer J, Eloy S, et al. Occupational and nonoccupational factors associated with high grade bronchial pre-invasive lesions. Eur Respir J 2003;21:332-341.
16. Peters EJ, Morice RC, Benner SE, Lippman S, Lippman S, Lukeman J, et al. Squamous metasplasia of the bronchial mucosa and its relationship to smoking. Chest 1993;103:1428-1432.
17. Wakamatsu K, Nakanishi Y, Takayama K, Miyazaki H, Hayashi K, Hara N. Frequent expression of p53 protein without mutation in the airway epithelium of human bronchus. Am J Respir Cell Mol Biol 1999;21:209-215.
18. Brambilla E, Gazzeri S, Lantuejoul S, Coll JL, Moro D, Negoescu A, et al. p53 mutant immunophenotype and deregulation of p53 transcription pathway (Bcl2, Bax, and Waf1) in precursor lesions of lung cancer. Clin Cancer Res 1998;4:1609-1618.
19. Brambilla E, Gazzeri S, Moro D, Lantuejoul S, Veyrenc S, Brambilla C. Alterations of Rb pathway (Rb-p16INK4-cyclin D1) in preinvasive bronchial lesions. Clin Cancer Res 1999;5:243-250.
20. Koty PP, Zhang H, Franklin WA, Yousem SA, Landreneau R, Levitt ML. In vivo expression of p53 and Bcl-2 and their role in programmed cell death in premalignant and malignant lung lesions. Lung Cancer 2002;35:155-163.
21. Chyczewski L, Niklinski J, Chyczewska E, Niklinska W, Naumnik W. Morphological aspect of carcinogenesis in the lung. Lung Cancer 2001;34:S17-S25.

22. Berlin NI, Buncher CR, Fontana RS, Frost JK, Melamed MR. The National Cancer Institute Cooperative Early Lung Cancer Detection Program: Results of the initial screen (prevalence). Early lung cancer detection: Introduction. Am Rev Respir Dis 1984;130:545-549.

23. Soda H, Tomita H, Kohno S, Oka M. Limitation of annual screening chest radiography for the diagnosis of lung cancer. A retrospective study. Cancer 1993;72:2341-2346.

24. Henschke CI, Naidich DP, Yankelevitz DF, McGuinness G, McCauley DI, Smith JP, et al. Early lung cancer action project. Cancer 2001 2001;92:153-159.

25. Kaneko M, Kusumoto M, Kobayashi T, Moriyama N, Naruke T, Ohmatsu H, et al. Computed tomographyscreening for lung carcinoma in Japan. Cancer 2000;89:2485-2488.

26. Sone S, Takashima S, Li F, Yang Z, Honda T, Maruyama Y, et al. Mass screening for lung cancer with mobile spiral computed tomography scanner. Lancet 1998;351:1242-1245.

27. Herder GJM, Breuer RHJ, Comans EFI, Risse EKJ, van Mourik JC, Postmus PE, et al. Positron emission tomography scans can detect radiographically occult lung cancer in the central airways. J Clin Onco 2001;19:4271-4272.

28. Humphrey LL, Teutsch S, Mark Johnson M. Lung cancer screening with sputum cytologic examination, chest radiography, and computed tomography: An update for the U.S. preventive services task force. Ann Intern Med 2004;140:740-753.

29. Petty TL. Sputum cytology for the detection of early lung cancer. Curr Opin Pulm Med 2004;9:309-312.

30. Thunissen FB. Sputum examination for early detection of lung cancer. J Clin Pathol 2003;56:805-810.

31. Palcic B, Garner DM, Beveridge J, Sun XR, Doudkine A, MacAulay C, et al. Increase of sensitivity of sputum cytology using high-resolution image cytometry: Field study results. Cytometry (Clin. Cytometry) 2002;50:168-176.

32. Brambilla C, Fievet F, Jeanmart M, de Fraipont F, Lantuejoul S, Frappat V, et al. Early detection of lung cancer: role of biomarkers. Eur Respir J 2003;21:36s-44s.

33. Hirsch FR, Franklin WA, Gazdar AF, Bunn PA. Early detection of lung cancer: clinical perspectives of recent advances in biology and radiology. Cancer Research 2001;7:5-22.

34. Hirsch FR, Merrick DT, Franklin WA. Role of biomarkers for early detection of lung cancer and chemoprevention. Eur Respir J 2002;19:1151-1158.

35. Mc Williams A, MacAulay C, Gazdar AF, Lam S. Innovative molecular and imaging approachesz for the detection of lung cancer and its precursor lesions. Oncogene 2002;21:6949-6959.

36. Kennedy TC, Lam S, Hirsch FR. Review of recent advances in fluorescence bronchoscopy in early localization of central airway lung cancer. Oncologist 2001;6:257-262.

37. Sutedja TG, Venmans BJ, Smit EF, Postmus PE. Fluorescence bronchoscopy for early detection of lung cancer. A clinical perspective. Lung Cancer 2001;34:157-168.

38. Banerjee AK, Rabbitts PH, George J. Lung cancer. 3: Fluorescence bronchoscopy: clinical dilemmas and research opportunities. Thorax 2003;58:266-271.

39. Hirsch FR, Prindiville SA, Miller YE, Franklin WA, Dempsey EC, Murphy JR, et al. Fluorescence versus white-light bronchoscopy for detection of preneoplastic lesions: a randomized study. J Natl Cancer Inst 2001;93:1385-1391.

40. Kennedy TC, Hirsch FR, Miller YE, Prindiville S, Murphy JR, Dempsey EC, et al. A randomized study of fluorescence bronchoscopy versus white-light bronchoscopy for early detection of lung cancer in high risk patients. Lung Cancer 2000;29(S1):244-245.

41. Kennedy TC, Miller YE, Prindiville S. Screening for lung cancer revisited and the role of sputum cytology and fluorescence bronchoscopy in a high-risk group. Chest 2000;117:72S-79S.

42. Lam S, Kennedy T, Unger M, Miller YE, Gelmont D, Rusch V, et al. Localization of bronchial intraepithelial neoplastic lesions by fluorescence bronchoscopy. Chest 1998;113:696-702.

43. Lam S, MacAulay C, LeRiche JC, Palcic B. Detection and localization of early lung cancer by fluorescence bronchoscopy. Cancer 2000;89:2468-2473.

44. Kusunoki Y, Imamura F, Uda H, Mano M, Horai T. Early detection of lung cancer with laser-induced fluorescence endoscopy and spectrofluorometry. Chest 2000;118:1776-1782.

45. Sato M, Saito Y, Usuda K, Takahashi S, Sagawa M, Fujimura S. Occult lung cancer beyond bronchoscopy visibility in sputum-cytology positive patients. Lung Cancer 1998;20:17-24.

46. Sato M, Sakurada A, Sagawa M, Minowa M, Takahashi H, Oyaizu T, et al. Diagnostic results before and after introduction of autofluorescence bronchoscopy in patients suspected of having lung cancer detected by sputum cytology in lung cancer mass screening. Lung Cancer 2001;32:247-253.

47. Kurie JM, Lee JS, Morice RC, Walsh GL, Khuri FR, Broxson A, et al. Autofluorescence bronchoscopy in the detection of squamous metaplasia and dysplasia in current and former smokers. J Natl Cancer Inst 1998;90:991-995.

48. Goujon D, Zellweger M, Radu A, Grosjean P, Weber BC, van den Bergh H, et al. In vivo autofluorescence imaging of early cancers in the human tracheobronchial tree with a sprectrally optimized system. J Biomed Opt 2003;8:17-25.

49. Homasson JP, Capron F, Angebault M, Nguyen Bich N. Lung autofluorescence. Preliminary study of two systems without laser illumination or photosensitization. Rev Pneumol Clin 2001;57:202-207.

50. Beamis JF, Ernst A, Simoff M, Yung R, Mathur PN. A multicenter study comparing autofluorescence bronchoscopy to white light bronchoscopy using a non light simulation system. Chest 2004;125:148S-149S.

51. Herth FJF, Ernst A, Becker HD. Autofluorescence bronchoscopy - A comparison of two systems (LIFE and D-Light). Respiration 2003;70:395-398.

52. Furukawa K, Ikeda N, Mieura T, Kakihana M, Saito M, Kato H. Is autofluorescence bronchoscopy needed to diagnose early bronchogenic carcinoma? Pro: autofluorescence bronchoscopy. J Bronchol 2003;10:64-69.

53. Mehta AC, Gildea TR. Is autofluorescence bronchoscopy needed to diagnose early bronchogenic carcinoma? Con: autofluorescence bronchoscopy. J Bronchol 2003;10:70-74.

54. Banerjee AK, Rabbitts PH, Jeremy P, George M. Are all high-grade preinvasive lesions premalignant, and should they all be treated? Am J Respir Crit Care Med 2002;165:1452-1453.

55. Bota S, Auliac J-B, Paris C, Metayer J, Sesboue R, Nouvet G, et al. Follow-up of bronchial precancerous lesions and carcinoma in situ using fluorescence endoscopy. Am J Respir Crit Care Med 2001;164:1688-1693.

56. Mathur PN, Edell E, Sutedja TG, Vergnon J-M. Treatment of early stage non-small cell lung cancer. Chest 2003;2003:176S-180S.

57. Venmans BJW, van Boxem TJM, Smit EF, Postmus PE, Sutedja TG. Outcome of bronchial carcinoma in situ. Chest 2000;117:1572-1576.

58. Pasic A, van Vliet E, Breuera RH, Risseb EJ, Snijdersb PJ, Postmus PE, et al. Smoking behavior does not influence the natural course of pre-invasive lesions in bronchial mucosa. Lung Cancer 2004;45(153-154).

59. Moro-Sibilot D, Fievet F, Jeanmart M, Lantuejoul S, Arbib F, Laverrie MH, et al. Clinical prognostic indicators of high-grade pre-invasive bronchial lesions. Eur Respir J 2004;24:24-29.

60. Stanzel F. Fluorescent bronchoscopy: contribution for lung cancer screening? Lung Cancer 2004;45:S29-S37.

61. Ramanujam N. Fluorescence spectroscopy of neoplastic and non-neoplastic tissues. Neoplasia 2000;2:89-117.

62. Wagnières GA, Star WM, Wilson BC. In vivo fluorescence spectroscopy and imaging for oncological applications. Photochem Photobiol 1998:603-632.

63. Sokolov K, Follen M, Richards-Kortum R. Optical spectroscopy for detection of neoplasia. Cur Opin Chemical Biol 2002;6:651-658.

64. Sokolov K, Nieman LT, Myakov A, Gillenwater A. Polarized reflectance spectroscopy for pre-cancer detection. Technol Cancer Res Treat 2004;3:1-14.

65. Coghlan L, Utzinger U, Richards-Kortum R, Brookner C, Zuluaga A, Gimenez-Conti I, et al. Fluorescence spectroscopy of epithelial tissue throughout the dysplasia-carcinoma sequence in an animal model: spectroscopic changes precede morphologic changes. Lasers Surg Med 2001;29:1-10.

66. Pitts JD, Sloboda RD, Dragnev KH, Dmitrovsky E, Mycek M-A. Autofluorescence characteristics of immortalized and carcinogen-transformed human bronchial epithelial cells. J Biomed Optics 2001;6:31-40.

67. Kobayashi T, Shibuya K, Hoshino H, Fujisawa T. Spectroscopic analysis of the autofluorescence from human bronchus using an ultraviolet laser diode. J Biomed Opt 2002;7:603-608.

68. Banerjee B, Miedema BE, Chandrasekhar HR. Role of basement membrane collagen and elastin in the autofluorescence spectra of the colon. J Investig Med 1999;47:326-332.

69. Zonios GI, Cothren RM, Arendt JT, Wu J, van Dam J, Crawford JM, et al. Morphological model of human colon tissue fluorescence. IEEE Trans Biomed Eng 1996;43:113-122.

70. Pavlova I, Sokolov K, Drezek R, Malpica A, Follen M, Richards-Kortum R. Microanatomical and biochemical origins of normal and precancerous cervical autofluorescence using laser-scanning fluorescence confocal microscopy. Photochem Photobiol 2003;77:550-555.

71. Georgakoudi I, Jacobson BC, Müller MG, Sheets EE, Badizadegan K, Carr-locke DL, et al. NAD(P)H and collagen as in vivo quantitative fluorescent biomarkers of epithelial precancerous changes. Cancer Research 2002;62:682-687.

72. Hung J, Lam S, LeRiche JC, Palcic B. Autofluorescence of normal and malignant bronchial tissue. Lasers Surg Med 1991;11:99-105.

73. Zellweger M, Goujon D, Conde R, Forrer M, van den Bergh H, Wagnieres G. Absolute autofluorescence spectra of human healthy, metaplastic, and early cancerous bronchial tissue in vivo. Appl Optics 2001;40:3784-3791.

74. Zellweger M, Grosjean P, Goujon D, Monnier P, van den Bergh H, Wagnieres G. In vivo autofluorescence spectroscopy of human bronchial tissue to optimize the detection and imaging of early cancers. J Biomed Opt 2001;6:41-51.

75. Gillenwater A, Jacob R, Richards-Kortum R. Fluorescence spectroscopy: a technique with potential to improve the early detection of aerodigestive tract neoplasia. Head & Neck 1998;20:556-562.

76. de Veld DC, Skurichina M, Witjes MJH, Duin RPW, Sterenborg HJ, Roodenburg JLN. Clinical study for classification of benign, dysplastic, and malignant oral lesions using autofluorescence spectroscopy. J Biomed Opt 2004;9:940-950.

77. Betz CS, Mehlman M, Rick K, Stepp H, Grevers G, Baumgartner R, et al. Autofluorescence imaging and spectroscopy of normal and malignant mucosa in patients with head and neck cancer. Lasers Surg Med 1999;25:323-334.

78. Wang C-Y, Chiang HK, Chen C-T, Chiang C-P, Kuo Y-S, Chow S-N. Diagnosis of oral cancer by light induced autofluorescence spectroscopy using double excitation wavelenghts. Oral Oncology 1999;35:144-150.

79. Mayinger B, Horner P, Jordan M, Gerlach C, Horbach T, Hohenberger W, et al. Endoscopic fluorescence spectroscopy in the upper GI tract for the detection of GI cancer: Initial experience. Am J Gastroenterol 2001;96:2616-2621.

80. Mayinger B, Jordan M, Horner P, Gerlach C, Muehldorfer S, Bittorf BR, et al. Endoscopic light-induced autofluorescence spectroscopy for the diagnosis of colorectal cancer and adenoma. J Photochem Photobiol B: Biol 2003;70:13-20.

81. Mycek M-A, Schomacker KT, Nishioka NS. Colonic polyp differentiation using time-resolved autofluorescence spectroscopy. Gastrointest Endos 1998;48:390-394.

82. Koenig F, McGovern FJ, Enquist H, Larne R, Deutsch TF, Schomacker KT. Autofluorescence guided biopsy for the early diagnosis of bladder carcinoma. J Urol 1998;159:1871-1875.

83. Zheng W, Lau W, Cheng C, Soo KC, Olivo M. Optimal excitation-emission wavelenghts for autofluorescence diagnosis of bladder tumors. Int J Cancer 2003;104:477-481.

84. Mitchell MF, Cantor SB, Ramanujam N, Tortolero-Luna G, Richards-Kortum R. Fluorescence spectroscopy for diagnosis of squamous intraepithelial lesions of the cervix. Obstet Gynecol 1999;93:462-470.

85. Ramanujan N, Mitchell MF, Mahadevan A, Thomsen S, Malpica A, Wright T, et al. Spectroscopic diagnosis of cervical intraepithelial neoplasia (CIN) in vivo using laser-induced fluorescence spectra at multiple excitation wavelengths. Lasers Surg Med 1996;19:63-74.

86. Breslin TM, Xu F, Palmer GM, Zhu C, Gilchrist KW, Ramanujan N. Autofluorescence and diffuse reflectance properties of malignant and benign breast tissues. Ann Surg Oncol 2004;11:65-70.

87. Brancaleon L, Durkin AJ, Tu JH, Menaker G, Fallon JD, Kollias N. In vivo fluorescence spectroscopy of nonmelanoma skin cancer. Photochem Photobiol 2001;73:178-183.

88. Bartlett M, Huang G, Larcom L, Jiang H. Measurement of particle size distribution in mammalian cells in vitro by use of polarized light spectroscopy. Appl Optics 2004;43:1296-1307.

89. Beauvoit B, Kitai T, Chance B. Contribution of the mitochondrial compartment to the optical properties of the rat liver: A theoretical and practical approach. Biophys J 1994;67:2501-2510.

90. Beauvoit B, Chance B. Time-resolved spectroscopy of mitochondria, cells and tissue under normal and pathological conditions. Mol Cell Bioch 1998;184:445-455.

91. Boustany NN, Drezek R, Thakor NV. Calcium-induced alterations in mitochondrial morphology quantified in situ with optical scatter imaging. Biophys J 2002;83:1691-1700.

92. Chance B, Liu H, Kitai T, Zhang Y. Effects of solutes on optical properties of biological materials:Models, cells, and tissues. Anal Biochem 1995;227:351-362.

93. Shijubo N, Kojima H, Nagata M, Ohchi T, Suzuki A, Abe S, et al. Tumor angiogenesis of non–small cell lung cancer. Microsc Res Tech 2003;60:186-198.

94. Höckel M, Vaupel P. Tumor hypoxia: definitions and current clinical biologic, and molecular aspects. J Natl Cancer Inst 2001;93:266-276.

95. Vaupel P, Kelleher DK, Höckel M. Oxygen status of malignant tumors: pathogenesis of hypoxia and significance for tumor therapy. Semin Oncol 2001;28:29-35.

96. Zonios G, Perelman LT, Backman V, Manoharan R, Fitzmaurice M, Van Dam J, et al. Diffuse reflectance spectroscopy of human adenomatous colon polyps in vivo. Appl Optics 1999;38:6628-6637.

97. Koenig F, Larne R, Enquist H, McGovern FJ, Schomacker KT, Kollias N, et al. Spectroscopic measurement of diffuse reflectance for enhanced detection of bladder carcinoma. Urology 1998;51:342-345.

98. Hornung R, Pham TH, Keefe KA, Berns MW, Tadir Y, Tromberg BJ. Quantitative near-infrared spectroscopy of cervical dysplasia in vivo. Hum Reprod 1999;14:2908-2916.

99. Tromberg BJ, Shah N, Lanning R, Cerussi A, Espinoza J, Pham TH, et al. Non-invasive in vivo characterization of breast tumors using photon migration spectroscopy. Neoplasia 2000;2:26-40.

100. Perelman LT, Backman V, Wallace M, Zonios G, Manoharan R, Nusrat A, et al. Observation of periodic fine structure in reflectance from biological tissue: A new technique for measuring nuclear size distribution. Phys Rev Lett 1998;80:627-630.

101. Georgakoudi I, Sheets EE, Müller MG, Backman V, Crum CP, Badizadegan K, et al. Trimodal spectroscopy for the detection and characterization of cervical precancers in vivo. Am J Obstet Gynecol 2002;186:374-382.

102. Georgakoudi I, Jacobson BC, van dam J, Backman V, Wallace MB, Muller MG, et al. Fluorescence, reflectance, and light-scattering spectroscopy for evaluating dysplasia in patient with Barrett's esophagus. Gastroenterology 2001;120:1620-1629.

103. Georgakoudi I, Van Dam J. Characterization of dysplastic tissue morphology and biochemistry in Barret's esophagus using diffuse reflectance and light scattering spectroscopy. Gastrointest Endosc Clin N Am 2003;13:297-308.

104. Wallace MB, Perelman LT, Backman V, Crawford JM, Fitzmaurice M, Seiler M, et al. Endoscopic detection of dysplasia in patients with Barrett's esophagus using light-scattering spectroscopy. Gastroenterology 2000;119:677-682.

105. Müller MG, Valdez TA, Georgakoudi I, Backman V, Fuentes C, Kabani S, et al. Spectroscopic detection and evaluation of morphologic and biochemical changes in early human oral carcinoma. Cancer 2003;97:1681-1692.

106. Gurjar R, Backman V, Perelman LT, Georgakoudi I, Badizadegan K, Itzkan I, et al. Imaging human epithelial properties with polarized light-scattering spectroscopy. Nature Medicine 2001;7:1245-1248.

107. Backman V, Wallace MB, Perelman LT, Arendt JT, Gurjar R, Müller MG, et al. Detection of preinvasive cancer cells. Nature 2000;406:35-36.

108. Johnson LJ, Hanley DF, Thakor NV. Optical light scatter imaging of cellular and subcellular morphology changes in stressed rat hyppocampal slices. J Neurosci Meth 2000;98:21-31.

109. Mirabal YN, Chang SK, Atkinson EN, Malpica A, Follen M, Richards-Kortum R. Reflectance spectroscopy for in vivo detection of cervical precancer. J Biomed Opt 2002;7:587-594.

110. Nordstrom RJ, Burke L, Nilodd JM, Myrtle JF. Identification of cervical intraepithelial neoplasia (CIN) using UV-excited fluorescence and diffuse-reflectance spectroscopy. Lasers Surg Med 2001;28:118-127.

111. Utzinger U, Brewer M, Silva E, Gershenson D, Blast RC, Follen M, et al. Reflectance spectroscopy for in vivo characterization of ovarian tissue. Lasers Surg Med 2001;28:56-66.
112. Zeng H, Petek M, Zorman MT, Mc Williams A, Palcic B, Lam S. Integrated endoscopy system for simultaneous imaging and spectroscopy for early lung cancer detection. Opt Letters 2004;29:587-589.

CHAPTER 2

Single-scattering spectroscopy for the endoscopic analysis of particle size in superficial layers of turbid media

Amelink A., M.P.L. Bard, S.A. Burgers, H.J.C.M. Sterenborg

Single-scattering spectroscopy for the endoscopic analysis of particle size in superficial layers of turbid media

Arjen Amelink, Martin P. L. Bard, Sjaak A. Burgers, and Henricus J. C. M. Sterenborg

We report on the development of an optical-fiber-based diagnostic tool that is sensitive to single-scattering events close to the fiber-optic probe tip. By using a single fiber to deliver and detect white light we optimized the detection probability of singly scattered photons from small depths. The sampling depth of this delivery-and-collection fiber was investigated by use of a tissue phantom. We found that for our phantom 90% of the single-scattering signal in the delivery-and-collection fiber originated from less than 200 μm from the fiber tip. The contribution of multiply scattered light from a greater depth to the signal was measured with an additional collection fiber. Several tissue phantoms demonstrated our fiber-optic probe's sensitivity to light scattering from superficial layers of tissue and thereby its potential to detect superficial precancerous epithelial lesions. © 2003 Optical Society of America

OCIS codes: 170.6510, 170.7050, 170.3660, 170.4580, 170.3890.

1. Introduction

In situ measurement of the optical properties of biological tissue is an important challenge in biomedical science. Changes in the optical properties of a tissue may reflect morphological and physiological changes such as those that occur in precancerous or cancerous conditions. Detection of malignancies in an early, mostly asymptomatic stage, such as carcinoma *in situ*, augments the cure rate considerably.[1] It is still unknown whether detection of earlier dysplastic changes has a similar effect on the clinical outcome, but this is at least partially because of the lack of adequate tools for detecting these changes.[2] Therefore the development of a technique that can reveal relevant differences in the optical properties of tissues is of great importance.

Precancerous lesions such as metaplasia, dysplasia, and carcinoma *in situ* are characterized by a thickening of the epithelial layer, an increase in the epithelial nucleus/cytoplasm ratio, and an enlargement of the epithelial nuclei.[3] Previous attempts have been made to use light-scattering spectroscopy to distinguish normal tissue from dysplastic tissue.[4–7] The development of such a noninvasive optical tool for the detection of dysplasia was based on the assumption that the epithelial nuclei are efficient scatterers of light because they have a larger refractive index than the surrounding cytoplasm. The size of the nuclei is associated with a scattering behavior described by Mie theory[8] and is characterized by a periodicity with the wave number. The period and amplitude of the oscillations vary with nuclear-size distribution. Therefore the assumption was made that single-scattering spectroscopy of epithelial nuclei could be a suitable technique to detect premalignant changes in the superficial epithelial layer. Although it is still uncertain whether nuclei or other subcellular structures are the dominant backscatterers in tissue, the development of a fiber-optic probe sensitive to light scattering from the epithelial layer could contribute significantly to the early diagnosis of epithelial malignancies.

Perelman *et al.*[4] used a fiber-optic probe with a central delivery fiber surrounded by six collection fibers to measure the light-scattering signal. A disadvantage of this probe is its large sampling depth, beyond the location of early superficial premalignant abnormalities. The thickness of a normal epithelial layer is usually less than 10 μm, and this might increase to several hundred micrometers for early precancerous or cancerous abnormalities. The optical-penetration depth of light in tissue greatly exceeds this thickness, unless very short wavelengths

are used. For the probe geometry used by Perelman *et al.* the measured reflected signal contains only a small fraction of singly scattered light from the epithelium and a large component of diffusely reflected light from the underlying tissue. In an attempt to detect changes in the backscatter signal from the epithelial nuclei, Perelman *et al.* modeled the signal from the underlying tissue and subtracted it from the total signal to obtain the single-scattering component. However, the same authors correctly state that "this approach must be specifically adapted to each different type of tissue studied, and its accuracy is theory dependent."[7] To optimize the use of light-scattering spectroscopy as a noninvasive diagnostic tool, it is necessary to develop a more robust method for reducing the contribution of multiply scattered light to the total signal.

It has been demonstrated that with the use of polarized light it is possible to isolate the single-scattering component of the reflected signal.[7] However, development of a fiber-based instrument that uses polarized light is technically challenging, and current approaches to polarized-light-scattering spectroscopy exclude environments accessible only with an endoscope. For the endoscopic detection of dysplasia a fiber-based instrument that can separate the singly scattered light from the multiply scattered light is required.

Another approach to significantly reducing the contribution of multiply scattered light is using a probe geometry that optimizes the detection of singly scattered photons. It has been shown that the use of a single optical fiber rather than two separate fibers to deliver and collect white light to and from the tissue has some important geometrical advantages.[9] Most important, the single-fiber approach is more sensitive to backscattering from small depths, which increases the probability of measuring singly scattered light from the epithelial layer. However, using a single fiber does not allow single backscattering from the epithelial layer to be distinguished from multiply scattered light from the underlying tissue. Since Canpolat and Mourant[9] did not demonstrate that the contribution of multiply scattered light in a single-fiber setup is negligible, we propose the use of an additional fiber to measure the contribution of the diffuse background to the signal.

In this paper we report on the development of a fiber-based instrument designed to measure singly backscattered light originating from the surface of a tissue phantom. We investigate the sampling depth of a single fiber used to deliver and collect light to and from the tissue. The contribution of multiply scattered light to the signal is measured with a second fiber.

2. Methods

A. Experimental Setup

The setup designed to measure the light-scattering signal of a superficial epithelial layer is schematically shown in Fig. 1. At the heart of the setup is a fiber
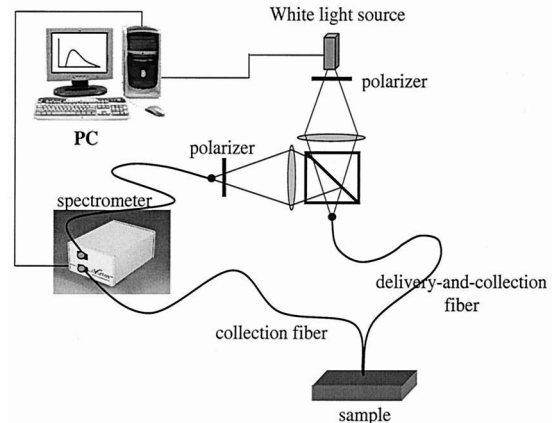

Fig. 1. Schematic diagram of the experimental setup.

probe that is small enough to fit through the working channel of a clinical endoscope. The probe is placed in contact with the tissue phantom under examination. It consists of two identical fibers, 440 μm in diameter with a core of 400 μm, fitted into a small metal tube. The two fibers are touching to minimize the distance between them. To optimize the probability of measuring singly scattered photons superficially, we use one fiber to deliver and collect white light simultaneously; the other fiber is used exclusively as a collection fiber. White light from a tungsten-halogen lamp (Avantes HL-2000-FHSA) is coupled into the delivery-and-collection fiber through a lens and a 50/50 beam splitter. Reflected light from the sample reentering the delivery-and-collection fiber is coupled through the beam splitter into the first (master) channel of a dual-channel spectrometer (Avantes SD2000). Two Glan–Thompson polarizers are used in closed configuration to remove specular reflections from the entrance facet of the delivery-and-collection fiber. Reflected light entering the probe's second collection fiber is coupled into the second (slave) channel of the spectrometer. We assume that when the two fibers are spaced close enough they collect the same amount of light from the deeper, underlying tissue. Essentially we hypothesize that the fiber that simultaneously delivers light to the tissue and collects light from the tissue collects singly backscattered photons from the epithelial layer as well as multiply scattered photons from the underlying tissue. Furthermore, the adjacent fiber collects mainly multiply scattered photons from the underlying tissue, and we assume that both fibers collect multiply scattered photons in equal amounts. The difference between the signals from the two fibers is then the signal from the superficial epithelial layer, which is the signal we are primarily interested in.

B. Theoretical Analysis of the Measured Signals

Throughout this paper all wavelength-dependent parameters are presented as boldfaced characters, e.g., $f(\lambda) = \boldsymbol{f}$. Parameters appearing as nonbold charac-

ters are implicitly assumed to be wavelength independent.

The total intensity $\boldsymbol{I}$ measured by the delivery-and-collection fiber connected to the master spectrometer channel can be written as

$$\boldsymbol{I} = (\boldsymbol{R}_n + \boldsymbol{R}_{\mathrm{ss}}^{\mathrm{shal}} + \boldsymbol{R}_{\mathrm{ss}}^{\mathrm{deep}} + \boldsymbol{R}_{\mathrm{ms}})\boldsymbol{T}_{\mathrm{master}}\boldsymbol{L}, \qquad (1)$$

where $\boldsymbol{R}_n$ is the reflection coefficient for specularly reflected light at the probe–sample interface (due to the difference in the refractive index of the fiber and the tissue phantom), $\boldsymbol{R}_{\mathrm{ss}}^{\mathrm{shal}}$ is the reflection coefficient for singly scattered light that has traveled a relatively small distance from the fiber tip picked up by the delivery-and-collection fiber, $\boldsymbol{R}_{\mathrm{ss}}^{\mathrm{deep}}$ is the reflection coefficient for singly scattered light that has traveled a relatively large distance from the fiber tip picked up by the delivery-and-collection fiber, and $\boldsymbol{R}_{\mathrm{ms}}$ is the reflection coefficient for multiply scattered light (diffuse scattering) picked up by the delivery-and-collection fiber. $\boldsymbol{T}_{\mathrm{master}}$ is the combined transmission function of the probe delivery-and-collection fiber, the optical components [50/50 beam splitter, polarizer, lens, and additional fiber (Fig. 1)], and the master spectrometer channel. Finally $\boldsymbol{L}$ is the light distribution at the probe–phantom interface.

Similarly the total intensity $\boldsymbol{J}$ measured by the collection fiber connected to the second spectrometer channel can be written as

$$\boldsymbol{J} = (\boldsymbol{R}_{\mathrm{ms}} + \boldsymbol{R}_{\mathrm{ss}}^{\mathrm{deep}})\boldsymbol{T}_{\mathrm{slave}}\boldsymbol{L}, \qquad (2)$$

where we have implicitly assumed that both fibers pick up the same amount of multiply scattered light and deeply singly scattered light, which is a reasonable assumption if the separation between the two fibers of the probe is small enough.

The reflection coefficient $\boldsymbol{R}_n$ for specularly reflected light at the probe–sample interface is determined approximately by placing the fiber probe in contact with a medium that has the same refractive index as the tissue phantom under investigation, in which case we have

$$\boldsymbol{I}_n = \boldsymbol{R}_n\boldsymbol{T}_{\mathrm{master}}\boldsymbol{L}. \qquad (3)$$

In this case we used water with a water-soluble absorbing dye (Avecia S109564, specific absorption coefficient $\mu_a \approx$ 1–2 ml mg^{-1} mm^{-1} for $350 < \lambda < 1000$ nm) to make sure that only specular reflections from the fiber–water interface were measured (thus $\boldsymbol{R}_{\mathrm{ss}} = \boldsymbol{R}_{\mathrm{ms}} = 0$).

The quantity $\boldsymbol{T}_{\mathrm{slave}}\boldsymbol{L}$ is measured by use of a water-submersed, white reflective tile (Avantes WS-2) with a reflection coefficient >99% over the measured wavelength range:

$$\boldsymbol{J}_{\mathrm{WS2}} = c\boldsymbol{T}_{\mathrm{slave}}\boldsymbol{L}. \qquad (4)$$

Here c is a constant that depends only on the distance between the probe tip and the surface of the tile.

From the same measurement we find $\boldsymbol{T}_{\mathrm{master}}\boldsymbol{L}$ through the equality

$$\boldsymbol{I}_{\mathrm{WS2}} - \boldsymbol{I}_n = c\boldsymbol{T}_{\mathrm{master}}\boldsymbol{L}, \qquad (5)$$

where it is implicitly assumed that the distance between the probe tip and the surface of the diffusely reflecting tile is large enough that the constant c has the same value for both fibers.

Thus we have

$$\boldsymbol{R}_{\mathrm{ms}} + \boldsymbol{R}_{\mathrm{ss}}^{\mathrm{deep}} = c\,\frac{\boldsymbol{J}}{\boldsymbol{J}_{\mathrm{WS2}}},$$

$$\boldsymbol{R}_{\mathrm{ss}}^{\mathrm{shal}} + \boldsymbol{R}_{\mathrm{ss}}^{\mathrm{deep}} + \boldsymbol{R}_{\mathrm{ms}} = c\,\frac{\boldsymbol{I} - \boldsymbol{I}_n}{\boldsymbol{I}_{\mathrm{WS2}} - \boldsymbol{I}_n}. \qquad (6)$$

The reflection coefficient for singly scattered light originating from the region close to the collection-and-delivery fiber is then obtained by

$$\boldsymbol{R}_{\mathrm{ss}}^{\mathrm{shal}} = c\left(\frac{\boldsymbol{I} - \boldsymbol{I}_n}{\boldsymbol{I}_{\mathrm{WS2}} - \boldsymbol{I}_n} - \frac{\boldsymbol{J}}{\boldsymbol{J}_{\mathrm{WS2}}}\right) = c(\boldsymbol{I}_{\mathrm{dc}} - \boldsymbol{J}_{\mathrm{col}}), \qquad (7)$$

where we have defined $\boldsymbol{I}_{\mathrm{dc}} = \boldsymbol{I} - \boldsymbol{I}_n/\boldsymbol{I}_{\mathrm{WS2}} - \boldsymbol{I}_n$ and $\boldsymbol{J}_{\mathrm{col}} = \boldsymbol{J}/\boldsymbol{J}_{\mathrm{WS2}}$.

C. Phantoms

The performance of our setup was tested with several phantoms. In all but one case the phantoms consisted of one or two layers of suspensions of monodisperse polystyrene spheres (Polysciences, Inc.) with diameters of 4.5 ± 0.2 μm and 9.4 ± 0.6 μm, which are typical sizes for epithelial nuclei.[3] The refractive index of the polystyrene spheres is 1.6, which is considerably larger than the refractive index of epithelial nuclei. For these phantoms the anisotropy is $g \approx 0.9$. In the other case the phantom consisted of a bulk layer of Intralipid-20% and a top layer of a suspension of 4.5-μm polystyrene spheres.

3. Results

A. One-Layer Phantoms

Figure 2(a) shows the signals $\boldsymbol{I}_{\mathrm{dc}}$ and $\boldsymbol{J}_{\mathrm{col}}$ when the probe is placed in a container with an aqueous suspension of 9.4-μm polystyrene spheres (with refractive index $n = 1.6$). A clear oscillatory pattern is observed in both channels, which is evidence for single Mie scattering from monodisperse particles. Note the different scales for the signals $\boldsymbol{I}_{\mathrm{dc}}$ and $\boldsymbol{J}_{\mathrm{col}}$; the signal from the delivery-and-collection fiber is more than an order of magnitude larger than the signal from the collection fiber. The figure shows that the period of the oscillations increases with increasing wavelength. When the signals are plotted versus wave number, a constant oscillation period is observed [Fig. 2(b)]. The Fourier transform of this periodic signal depends on the size distribution of the polystyrene spheres and on the relative refractive index of the spheres in the aqueous medium. Figure 2(c) shows the power spectrum of the measured signals, with the horizontal axis calculated according to
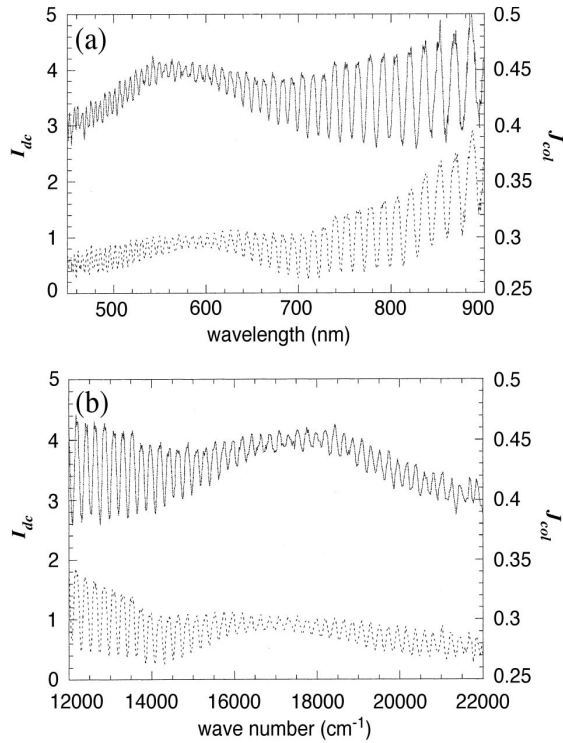
Fig. 2. (a) Signals I_{dc} (from the delivery-and-collection fiber, solid curve) and J_{col} (from the collection fiber, dashed curve) with the probe placed in a container with an aqueous suspension of 9.4-μm polystyrene spheres. (b) The same signals plotted versus wave number. (c) The power spectrum from (b) with the horizontal axis calculated according to the refractive-index specifications of the supplier ($n = 1.6$).

Fig. 3. Delivery-and-collection fiber signals I_{dc} for suspensions of (a) 4.5-μm polystyrene spheres, (b) 9.4-μm polystyrene spheres, and (c) a mixture of 9.4- and 4.5-μm polystyrene spheres in equal amounts.

the supplier's refractive-index specifications. The vertical scales are different (by more than an order of magnitude) for the signals I_{dc} and J_{col} in order to show both signals in the same graph. A single peak at 9.4 μm is observed in both signals, which is in agreement with the size specified by the supplier.

Figure 3 shows the delivery-and-collection fiber signals I_{dc} for suspensions of (a) 4.5-μm polystyrene spheres, (b) 9.4-μm polystyrene spheres, and (c) a mixture of 9.4- and 4.5-μm polystyrene spheres in equal amounts. The power spectrum of these signals is plotted in Fig. 4. Figure 4(a) shows a single
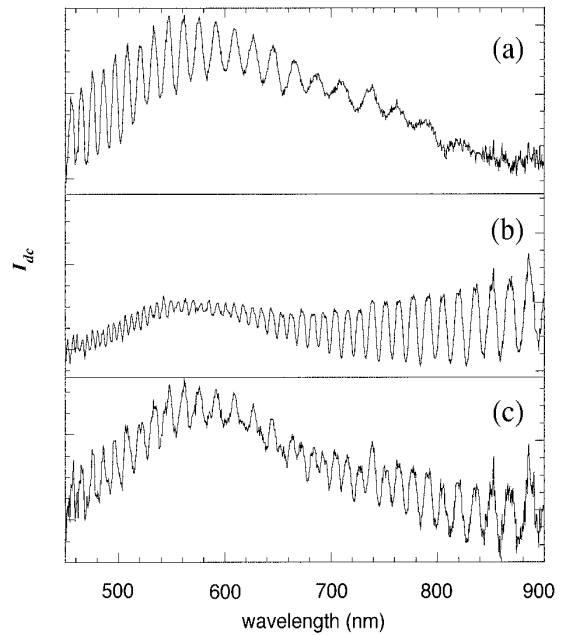
peak at 4.5 μm, Fig. 4(b) shows a single peak at 9.4 μm, and Fig. 4(c) shows the two peaks simultaneously. Thus by using Fourier transform single-
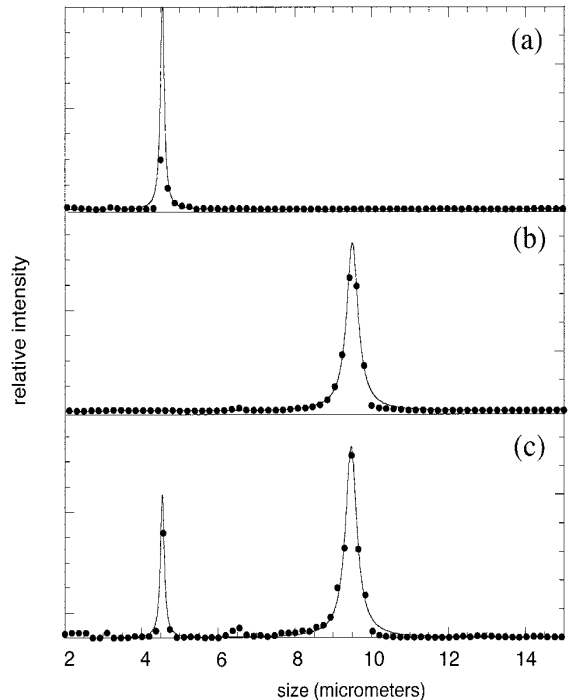

Fig. 4. Power spectra of the delivery-and-collection fiber signals I_{dc} for suspensions of (a) 4.5-μm polystyrene spheres, (b) 9.4-μm polystyrene spheres, and (c) a mixture of 9.4- and 4.5-μm polystyrene spheres in equal amounts.
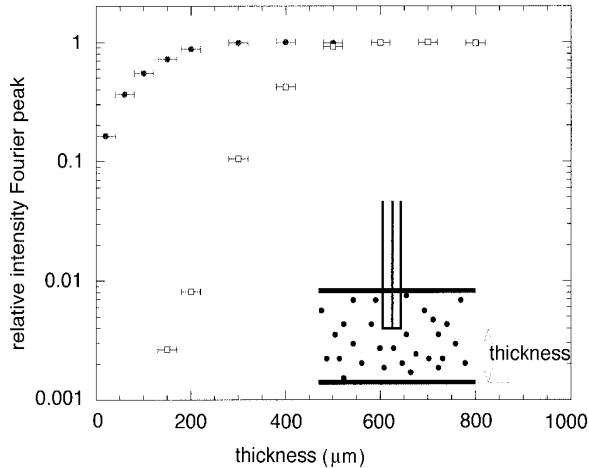
Fig. 5. Area under the FTSSS peak for both signals I_{dc} (filled circles) and J_{col} (open squares) for various distances of the probe tip from the bottom of the container, plotted on a logarithmic scale.
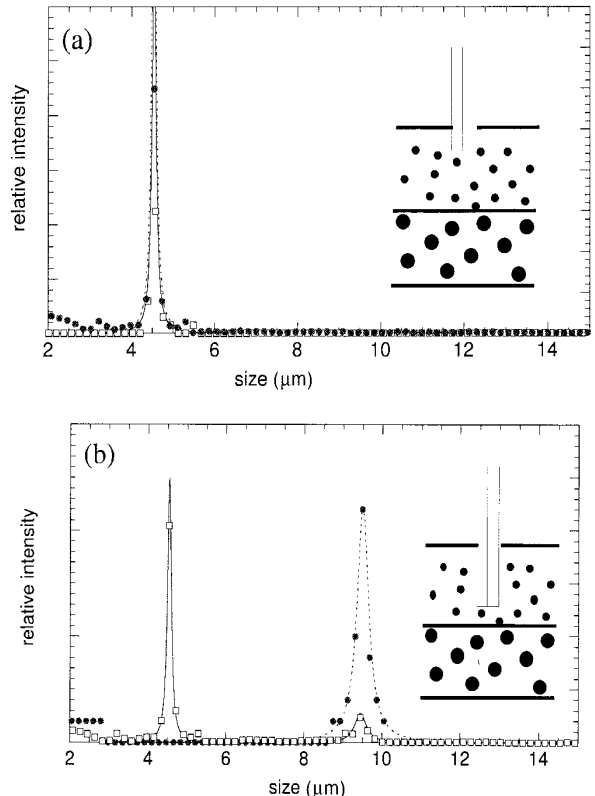

Fig. 6. (a) Power spectrum of the signals I_{dc} (filled circles, solid curve) and J_{col} (open squares, dotted curve) for a two-layer phantom (bottom layer: suspension of 9.4-μm particles, top layer: suspension of 4.5-μm particles) with the probe at a large distance (>1 mm) from the bottom layer. (b) Power spectrum of the signals I_{dc} and J_{col} for the same two-layer phantom with the probe at a small distance (<150 μm) from the bottom layer.

scattering spectroscopy (FTSSS), i.e., by plotting the power spectrum of the wave-number-dependent single-scattering reflection coefficient (Eq. 7), we can easily extract the size distribution of particles in a suspension.

To measure the sensitivity of our fiber-optic probe for single scattering close to the probe tip, we placed our fiber-optic probe in a container with a suspension of 4.5-μm particles with the reduced scattering coefficient $\mu_s' \approx 1400$ m^{-1} and anisotropy $g \approx 0.9$ and varied the distance z from the probe tip to the bottom of the container. In Fig. 5 the area under the FTSSS peak is plotted for both signals I_{dc} and J_{col} for various distances. Both signals are normalized to unity at infinite depth to show them in the same graph; in fact $I_{dc} \gg J_{col}$. This figure clearly shows that the collection fiber starts to collect singly scattered photons from depths greater than 150 μm, whereas the delivery-and-collection fiber already picks up a substantial amount of singly scattered photons from a very small layer (approximately 20 μm) of particles. Figure 5 shows that ~90% of the signal collected by the delivery-and-collection fiber originates from within $z = 200$ μm (corresponding to an optical thickness of $\tau = \mu_s z \approx 3$) of the probe tip. In contrast only 1% of the signal collected by the collection fiber originates from within 200 μm of the probe tip.

B. Two-Layer Phantoms

To further explore the sensitivity of our fiber-optic probe to shallow single scattering we conducted experiments on two-layer phantoms. The first phantom consisted of a bulk suspension of 9.4-μm latex particles with a top layer of 4.5-μm spheres (with a 10 times higher concentration), separated by a very thin plastic wrap, which we verified to have no effect on the measurements. Figure 6(a) shows the power spectrum of the signals I_{dc} and J_{col} (at different vertical scales to display them in the same graph) with the probe at a large distance (>1 mm) from the sec-

ond layer. This figure shows a lack of signal from the second layer of 9.4-μm particles in both fibers. In contrast Fig. 6(b) shows the power spectrum of the signals I_{dc} and J_{col} with the fiber-optic probe at a small distance (<150 μm) from the second layer. This figure clearly illustrates that the collection fiber is sensitive only to single scattering from the deeper, 9.4-μm-particle suspension, whereas the delivery-and-collection fiber receives mostly singly scattered photons from the (highly concentrated) 4.5-μm-particle suspension layer of less than 150-μm thickness. This demonstrates that our delivery-and-collection measurement geometry optimally detects singly scattered photons from a close distance from the fiber tip.

Finally a phantom consisting of Intralipid-20% and Evans Blue with reduced scattering and absorption coefficients of 1000 m^{-1} and 200 m^{-1} at 600 nm (which are typical values for biological tissue[10]), respectively, was used. On top of this bulk layer was a thin water layer, separated from the bulk layer by a thin plastic wrap. Figure 7(a) shows the signals I_{dc} and J_{col} and the resulting shallow single-scattering coefficient R_{ss}^{shal} [Eq. (7)]. Clearly no periodicity is observed, which is explained by the broad
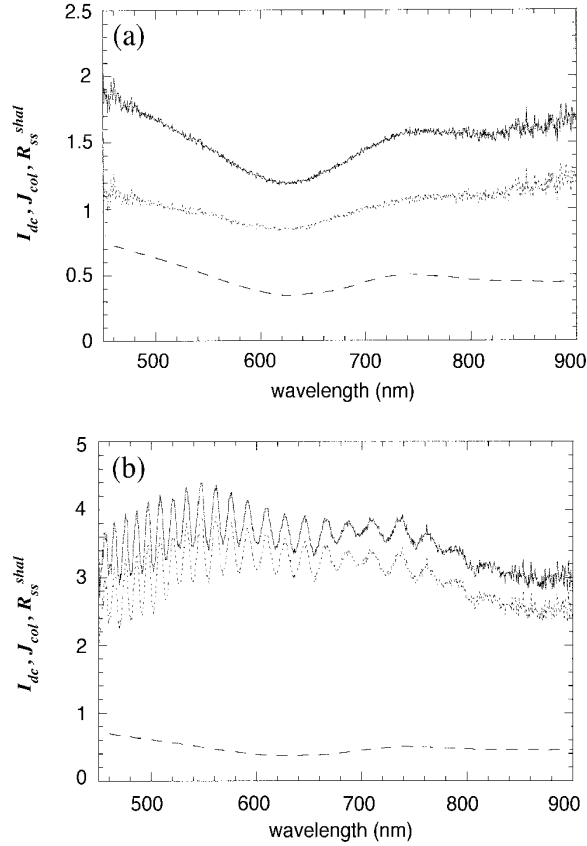
Fig. 7. (a) Signals I_{dc} (solid curve), J_{col} (dashed curve) and the resulting shallow single-scattering coefficient R_{ss}^{shal} (dotted curve) for a two-layer phantom (bottom layer: Intralipid-20% and Evans Blue, top layer: water). (b) Signals I_{dc} and J_{col} and the resulting superficial single-scattering coefficient R_{ss}^{shal} for the same two-layer phantom with 4.5-μm polystyrene spheres added to the top layer.

particle-size distribution of Intralipid (in the nanometer range).[11] Figure 7(b) shows the signals I_{dc} and J_{col} and R_{ss}^{shal} with the water layer replaced by a thin layer of a suspension of 4.5-μm polystyrene spheres (reduced scattering coefficient $\mu_s' \approx 1400$ m^{-1}) to mimic the epithelial nuclei. The signal J_{col} in the collection fiber does not change, which is in agreement with our previous findings that the collection fiber collects only singly scattered photons from depths greater than 150 μm. However, the signal I_{dc} is greatly enhanced and shows the telltale Mie-scattering periodicity, which is also reflected in the single-scattering coefficient R_{ss}^{shal}. This measurement proves that our fiber probe is capable of determining the size distribution of particles in a very thin layer close to the fiber tip, which is essential for the *in vivo* diagnosis of superficial epithelial lesions.

4. Discussion and Conclusions

We developed a fiber-based diagnostic tool that is sensitive to single-scattering events close to the probe tip. By using a single fiber to deliver and detect light we optimized the detection probability of singly scattered photons from small depths. A second fiber spaced close to the first fiber detects singly scattered photons from large depths as well as multiply scattered photons and thus gives complementary information about the optical properties of the tissue under examination.

The use of light-scattering spectroscopy as a noninvasive diagnostic tool for early epithelial malignancies requires that the signal due to (multiple) scattering from the subepithelium is significantly smaller than the signal due to scattering from the epithelium. This can be accomplished by using a measurement geometry that is sensitive to superficial scattering. Canpolat and Mourant[9] have shown that a single-fiber measurement geometry maximizes the probability of collecting singly scattered light. However, they only estimated the contribution of multiply scattered light in their setup. We adapted their approach and measured the amount of multiply scattered light collected by the delivery-and-collection fiber by using an additional fiber. Additionally, they only simulated the depth probed by their fiber with a Monte Carlo simulation, whereas we directly measured the depth probed by both of our fibers.

We analysed our data by taking the Fourier transform of the wave-number-dependent single-scattering signal. Figure 4 shows that this type of analysis is ideally suited for the visualization of the distribution of scatterers present in a suspension. Whether this approach is suitable for *in vivo* applications as well depends on the size distribution of biological backscatterers. Recently Mourant *et al.*[12] showed that biological cells and the nuclei within them are very heterogeneous and that light scattering is likely sensitive to very small subcellular structures with a broad size distribution. In this case it is not expected that *in vivo* single-scattering measurements will yield a Fourier-transformable wavelength periodicity, as was the case with our phantoms containing monodisperse polystyrene spheres. Furthermore, the relative refractive index of the scatterers in biological tissue is much smaller and less uniquely defined than in our phantoms, which also complicates the interpretation of an *in vivo* backscatter signal in terms of scatter size.

To investigate the depth probed by our fibers we measured the area under the peaks of the power spectra taken with the probe tip at various distances from the bottom of a container filled with 4.5-μm polystyrene spheres (reduced scattering coefficient $\mu_s' = 1400$ m^{-1}). Figure 5 shows that ~90% of the single-scattering signal in the delivery-and-collection fiber originates from less than 200 μm (optical thickness $\tau \approx 1$) from the fiber tip, whereas the collection fiber starts to collect singly scattered photons substantially from depths greater than 200 μm. This proves that our single-fiber approach is indeed sensitive to single scattering close to the fiber tip, which is indispensible if scattering from an epithelial layer is to be observed. Note that the probed depth depends on the reduced scattering and absorption coefficients of the sample under examination, and the

43

absolute values shown here may deviate for biological tissue.

Our two-layer phantom experiments demonstrate the sensitivity of our delivery-and-collection fiber to single-scattering events close to the fiber tip. In all our phantoms (including the tissuelike Intralipid phantom) the contribution of multiply scattered light in the delivery-and-collection fiber is very small compared with the single-scattering contribution. We therefore conclude that it is not necessary to subtract the diffuse reflectance from the signal of the delivery-and-collection fiber to obtain the signal due to single scattering close to the fiber tip. However, the diffuse component may be relatively larger when measuring biological tissue, which would make it desirable to subtract it in such cases. In any case we have proven that the collection fiber probes a different depth than the delivery-and-collection fiber and thus gives additional, complementary information about the scatterers in the tissue. We therefore recommend the use of a second fiber to obtain as much information about the optical properties of the tissue under investigation as possible.

References

1. T. Naruke, R. Tsuchiya, H. Kondo, H. Asamura, and H. Nakayama, "Implications of staging in lung cancer," Chest **112,** 242S–248S (1997).
2. B. J. Venmans, T. J. van Boxem, E. F. Smit, P. E. Postmus, and T. G. Sutedja, "Outcome of bronchial carcinoma *in situ,*" Chest **117,** 1572–1576 (2000).
3. R. S. Cotran, V. Kumar, and S. L. Robbins, *Pathological Basis of Disease* (Saunders, Philadelphia, Pa., 1994).
4. L. T. Perelman, V. Backman, M. Wallace, G. Zonios, R. Manoharan, A. Nusrat, S. Shields, M. Seiler, C. Lima, T. Hamano, I. Itzkan, J. Van Dam, J. M. Crawford, and M. S. Feld, "Observation of periodic fine structure in reflectance from biological tissue: a new technique for measuring nuclear size distribution," Phys. Rev. Lett. **80,** 627–630 (1998).
5. M. B. Wallace, L. T. Perelman, V. Backman, J. M. Crawford, M. Fitzmaurice, M. Seiler, K. Badizadegan, S. J. Shields, I. Itzkan, R. R. Dasari, J. Van Dam, and M. S. Feld, "Endoscopic detection of dysplasia in patients with Barrett's esophagus using light-scattering spectroscopy," Gastroenterology **119,** 677–682 (2000).
6. I. Georgakoudi, E. E. Sheets, M. G. Muller, V. Backman, C. P. Crum, K. Badizadegan, R. R. Dasari, and M. S. Feld, "Trimodal spectroscopy for the detection and characterization of cervical precancers *in vivo,*" Am. J. Obstet. Gynecol. **186,** 374–382 (2001).
7. V. Backman, R. Gurjar, K. Badizadegan, I. Itzkan, R. R. Dasari, L. T. Perelman, and M. S. Feld, "Polarized light scattering spectroscopy for quantitative measurement of epithelial cellular structures *in situ,*" IEEE J. Sel. Top. Quantum Electron. **5,** 1019–1026 (1999).
8. H. C. van de Hulst, *Light Scattering by Small Particles* (Wiley, New York, 1957).
9. M. Canpolat and J. R. Mourant, "Particle size analysis of turbid media with a single optical fiber in contact with the medium to deliver and detect white light," Appl. Opt. **40,** 3792–3799 (2001).
10. W. F. Cheong, S. A. Prahl, and A. J. Welch, "A review of the optical properties of biological tissues," IEEE J. Quantum Electron. **26,** 2166–2185 (1990).
11. H. J. van Staveren, C. J. M. Moes, J. van Marle, S. A. Prahl, and M. J. C. van Gemert, "Light scattering in Intralipid-10% in the wavelength range of 400–1100 nm," Appl. Opt. **31,** 4507–4514 (1991).
12. J. R. Mourant, T. M. Johnson, S. Carpenter, A. Guerra, T. Aida, and J. P. Freyer, "Polarized angular dependent spectroscopy of epithelial cells and epithelial cell nuclei to determine the size scale of scattering structures," J. Biomed. Opt. **7,** 378–387 (2002).

CHAPTER 3

In vivo measurement of the local optical properties of tissue by use of differential path-length spectroscopy

Amelink A., H.J.C.M. Sterenborg, M.P.L. Bard, S.A. Burgers

In vivo measurement of the local optical properties of tissue by use of differential path-length spectroscopy

Arjen Amelink and Henricus J. C. M. Sterenborg

Department of Radiation Oncology, Erasmus Medical Centre, P.O. Box 5201, 3008 AE Rotterdam, The Netherlands

Martin P. L. Bard and Sjaak A. Burgers

Department of Pulmonary Diseases, Erasmus Medical Centre, P.O. Box 5201, 3008 AE Rotterdam, The Netherlands

We demonstrate the capability of differential path-length spectroscopy (DPS) to determine the local optical properties of tissue *in vivo*. DPS measurements on bronchial mucosa are analyzed and yield information on the local blood oxygenation, blood content, average microvessel diameter, and wavelength dependence of the reduced scattering coefficient. Our data collected to date show that cancerous bronchial mucosa has a lower capillary oxygenation and a larger average capillary diameter than normal bronchial mucosa. © 2004 Optical Society of America

OCIS codes: 170.6510, 170.7050, 170.3660, 170.4580, 170.3890.

In situ measurement of the optical properties of tissue is an important challenge in biomedical science. Changes in the optical properties of tissue may reflect interesting morphological and physiological changes, such as those that occur in the (pre)cancerous transformation of normal epithelial tissue. Several methods exist to determine the optical properties of tissuelike turbid media, including time-resolved,[1] frequency-domain,[2,3] and spatially resolved continuous-wave[4–6] systems. These systems require large source–detector separations to satisfy the validity of the diffusion approximation. As a consequence, the detected photons have traveled a long distance through the sample, and the extracted optical properties represent average values over a relatively large tissue volume. However, an important aspect in the detection of precancerous lesions is the fact that the relevant morphological and physiological changes typically occur in or just below the mucosa, a superficial tissue layer with a thickness of only a few hundred micrometers. To facilitate the determination of biologically relevant parameters, such as neovascularization with formation of abnormal vessels[7] and microvascular oxygenation, a diagnostic tool that is sensitive to the optical properties of the most superficial layer of tissue is required. Even when small source–detector separations are used,[8,9] the average path length of the detected photons depends on the optical properties of the sample, which complicates the interpretation of the measured spectra and allows the interrogation depth to extend beyond the mucosal layer.

We recently developed a novel diagnostic technique, differential path-length spectroscopy (DPS), that is sensitive to the optical properties in the most superficial layer of tissue.[10,11] A schematic diagram of the setup is shown in Fig. 1. The setup consists of two optical fibers for the delivery and detection of light to and from the tissue. Light from a tungsten halogen lamp (Avantes HL-2000) is led through one arm of a 200-μm bifurcated optical fiber, which is coupled at its distal end to one arm [the delivery-and-collection (dc) fiber] of a 400-μm bifurcated optical fiber probe.

The distal end of this fiber is polished at an angle of 15° to minimize the collection of specularly reflected light at the probe–medium interface, and it contacts the sample under investigation. Light reflected into the dc fiber is coupled back into the 200-μm bifurcated fiber and analyzed with a dual-channel spectrometer (Avantes SD2000). Light reflected back from the sample into the other arm of the 400-μm bifurcated fiber-optic probe [the collection (c) fiber] is led directly into the second channel of the dual-channel spectrometer. Both signals are divided by spectra recorded with the probe at a distance from a diffuse reflecting white reflectance standard (Labsphere SRS-99). The difference of the dc- and c-fiber collection signals [$I(\lambda)$ and $J(\lambda)$, respectively] is the differential reflectance signal $R(\lambda) = I(\lambda) - J(\lambda)$. It was shown in another paper[11] that, in the range of parameters relevant for biological tissue, the differential signal can be modeled by

$$R(\lambda) = C_1 \mu_s{}'(\lambda)\exp[-\tau\mu_a(\lambda)]$$
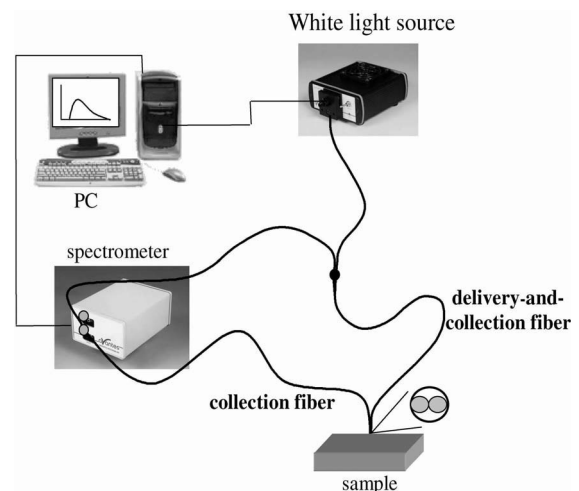$$= C_1 \mu_s{}'(\lambda)\exp[-C_2 d_{\text{fiber}}\mu_a(\lambda)], \qquad (1)$$

Fig. 1. Schematic diagram of the experimental setup.

where $\mu_s'(\lambda)$ is the reduced scattering coefficient, $\mu_a(\lambda)$ is the absorption coefficient, τ is the apparent differential path length, d_{fiber} is the diameter of the dc and c fibers, and C_1 and C_2 are proportionality constants. Equation (1) was determined from Monte Carlo simulations and was validated experimentally with tissue phantoms. We found that the apparent differential path length is independent of the optical properties of the tissue and depends on the fiber diameter only: $\tau = C_2 d_{\text{fiber}}$, with $C_2 = 0.80 \pm 0.03$. As a consequence, the depth of tissue probed by our instrument is small and depends on only the diameter of the probe fibers. For the experiments described in this Letter we used fibers with a diameter of 400 μm, which results in an apparent differential path length of 320 μm.[11]

We have applied the DPS technique to measure normal and malignant bronchial mucosa as an extension to a pilot study designed to distinguish malignant from nonmalignant bronchial mucosa by use of a combination of autofluorescence bronchoscopy, autofluorescence spectroscopy, and diffuse reflectance spectroscopy.[12] The results for DPS, which was developed during the pilot study, are presented in this Letter. Patients with a medical indication for a bronchoscopy were invited to participate in this study. All patients were older than 18 years and signed informed consent. The study was approved by the Medical Ethics Review Board of the Erasmus Medical Centre in Rotterdam. After screening the bronchial tree for suspicious lesions with autofluorescence imaging, our fiber-optic probe was placed in gentle contact with all suspicious areas and differential path-length spectra were obtained with the endoscopic light source turned off. Bronchial biopsies were obtained at all locations that were spectroscopically measured. Local pathologists evaluated hematoxylin-eosin-stained slides and the pathological diagnoses were coded referring to the World Health Organization Lung Cancer classification.[13] For this preliminary *in vivo* evaluation of the DPS technique we included 9 patients and obtained 27 spectra representing healthy tissue and 4 spectra representing malignant lesions.

For analysis of the spectra we assumed Lorentz–Mie scattering, i.e., $\mu_s'(\lambda) = a\lambda^{-b}$, where b is a constant related to the size of the scattering particles.[14,15] Furthermore, the main absorber in the measured wavelength range (350–1000 nm) is blood. Since blood is not distributed homogeneously throughout the tissue but concentrated in blood vessels, a correction must be made to Eq. (1) in accordance with Van Veen *et al.*[16] The complete model to which the differential path-length spectra are fitted is given by

$$R(\lambda) = C_1 \mu_s'(\lambda)\exp[-0.32\mu_a(\lambda)]$$
$$= C_1'\lambda^{-b} \exp\{-0.32 C_{\text{cor}}(\lambda)$$
$$\times \rho[\text{StO}_2\mu_a^{\text{HbO2}}(\lambda) + (1 - \text{StO}_2)\mu_a^{\text{Hb}}(\lambda)]\},$$

(2)

where ρ is the blood volume fraction, StO_2 is the microvascular blood oxygenation, $\mu_a^{\text{HbO2}}(\lambda)$ is the

absorption coefficient of fully oxygenated whole blood, $\mu_a^{\text{Hb}}(\lambda)$ is the absorption coefficient of fully deoxygenated whole blood, C_1' is a proportionality constant, and C_{cor} is the correction factor that accounts for the inhomogeneous distribution of blood in tissue. Since the apparent differential path length is 320 μm and the only blood vessels located within 160 μm from the surface of the bronchial wall are the capillaries and the venules, the extracted StO_2 represents the microvascular oxygenation. For whole blood contained in an infinitely long cylinder, the correction factor is given by $C_{\text{cor}} = \{1 - \exp[\mu_a^{\text{bl}}(\lambda)D_{\text{vessel}}]\}/[\mu_a^{\text{bl}}(\lambda)D_{\text{vessel}}]$, where $\mu_a^{\text{bl}}(\lambda)$ is the absorption coefficient of whole blood and D_{vessel} is the vessel diameter.[16] However, this may not be an appropriate geometric description for blood contained in the capillary network. Additionally, because of the Fahraeus effect, the hematocrit of blood in the capillaries is lower than the hematocrit of whole blood and may be different for malignant and normal bronchial tissue as well. Since the absolute values of blood volume fraction ρ and microvessel diameter D_{vessel} in Eq. (2) are determined assuming a blood hemoglobin content of 150 g/l, which is typical for whole blood, the fitted values for these parameters may actually deviate from their absolute values.

Fitting the data to Eq. (2) yields values for StO_2, ρ, D_{vessel}, and b. In situations in which the distance from the surface of the bronchial wall to the microvascular network is larger than 160 μm, only a small amount of blood will be present in the detection volume ($\rho < 0.01$) and StO_2 and D_{vessel} cannot be fitted accurately. This was actually the case in nine spectra representing healthy tissue and one spectrum representing malignant tissue. Therefore the values for StO_2 and D_{vessel} were obtained from 18 spectra representing healthy tissue and 3 spectra representing malignant lesions with enough blood present in the detection volume to ensure a stable fit for these parameters.

Figure 2 shows examples of spectra and fits for normal and malignant bronchial mucosa. The noise at $\lambda = 940$ nm is caused by strong absorption in the fibers. Striking differences are observed between the
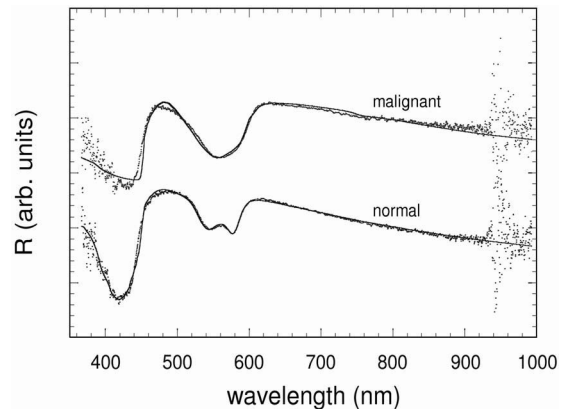

Fig. 2. Examples of spectra and fits of normal bronchial mucosa (lower spectrum) and malignant bronchial mucosa (upper spectrum, displaced vertically to show both spectra in the same graph).

47

Table 1. Fit Results

Parameter	Normal Mucosa[a]	Malignant Mucosa[b]
StO_2	92 ± 9	49 ± 36[c]
D_{vessel} (μm)	15 ± 10	29 ± 5[c]
ρ (%)	3.5 ± 6	8 ± 6
b	-0.97 ± 0.24	-1.09 ± 0.14

[a]For StO_2 and D_{vessel}, $n = 18$; for ρ and b, $n = 27$.
[b]For StO_2 and D_{vessel}, $n = 3$; for ρ and b, $n = 4$.
[c]$p < 0.05$.

two spectra in the wavelength range 500–600 nm. In this wavelength region blood absorption dominates the spectral shape of the differential reflectance signal. Comparing the spectra of Fig. 2 with the absorption spectra of Hb and HbO_2,[17] it is clear that the malignant lesion has a much lower saturation than the normal bronchial mucosa. Table 1 shows the average values and standard deviations for blood volume fraction ρ, Mie slope b, blood oxygenation StO_2, and average blood vessel diameter D_{vessel} derived by fitting Eq. (2) to the data with a least-squares fit. The fitted values for blood volume fractions ρ are in agreement with previous observations.[7] The differences in both microvascular oxygenation StO_2 and average blood vessel diameter D_{vessel} between malignant tissue and normal tissue are statistically significant according to a Mann–Whitney test ($p < 0.05$). The low capillary oxygenation combined with large variations is typical for malignant tissue,[18] as is the increased microvessel diameter.[18–20] The large standard deviations of the microvessel diameter and microvascular blood content of normal tissue are not unnatural[7] but may be induced in part by probe pressure variations during the endoscopic examinations as well. If the probe is pressed too hard against the tissue, the tissue will be compressed, leading to a decrease in blood content, vessel diameter, and blood saturation. Although an attempt was always made to measure the spectra with as little pressure as possible, it cannot be completely ruled out that part of the variations in the fitted blood parameters is due to pressure variations.

Other studies have revealed that the formation of a pathological vessel network is an early phenomenon in the oncogenesis of endobronchial tumors.[21,22] Therefore we think that, although the data set for cancerous lesions is limited, the observed differences justify a study of a larger patient group to assess the capability of DPS to distinguish premalignant from normal bronchial mucosa.

In conclusion, we have shown the feasibility of DPS to determine the local capillary oxygenation, blood volume fraction, blood vessel size, and wavelength dependence of the scattering coefficient *in vivo*. Since all these parameters may be related to local morphological and physiological changes occurring during malignant transformations, DPS may be used as a tool to discriminate premalignant lesions from normal mucosa. Our results to date show a lower oxygenation, larger vessel size, and larger blood volume fraction for malignant lesions compared with normal bronchial tis-

sue. A prospective study using the same methodology in a larger patient group is under way.

References

1. M. S. Patterson, B. Chance, and B. C. Wilson, Appl. Opt. **28**, 2331 (1989).
2. M. Gerken and G. W. Faris, Opt. Lett. **24**, 1726 (1992).
3. J. B. Fishkin, O. Coquoz, E. R. Anderson, M. Brenner, and B. J. Tromberg, Appl. Opt. **36**, 10 (1997).
4. T. J. Farrell, M. S. Patterson, and B. C. Wilson, Med. Phys. **19**, 879 (1992).
5. M. G. Nichols, E. L. Hull, and T. H. Foster, Appl. Opt. **36**, 93 (1997).
6. R. M. P. Doornbos, R. Lang, M. C. Aalders, F. W. Cross, and H. J. C. M. Sterenborg, Phys. Med. Biol. **44**, 967 (1999).
7. K. Shibuya, H. Hoshino, M. Chiyo, K. Yasufuku, T. Iizasa, Y. Saitoh, M. Baba, K. Hiroshima, H. Ohwada, and T. Fujisawa, Thorax **57**, 902 (2002).
8. F. Bevilacqua, D. Piguet, P. Marquet, J. D. Gross, B. J. Tromberg, and C. Depeursinge, Appl. Opt. **38**, 4939 (1999).
9. G. Zonios, L. T. Perelman, V. Backman, R. Manoharan, M. Fitzmaurice, J. Van Dam, and M. S. Feld, Appl. Opt. **38**, 6628 (1999).
10. A. Amelink, M. P. L. Bard, J. A. Burgers, and H. J. C. M. Sterenborg, Appl. Opt. **42**, 4095 (2003).
11. A. Amelink and H. J. C. M. Sterenborg, "Measurement of the local optical properties of turbid media using differential path-length spectroscopy," Appl. Opt. (to be published).
12. M. P. L. Bard, A. Amelink, M. Skurichina, M. den Bakker, J. A. Burgers, H. C. Hoogsteden, and H. J. C. M. Sterenborg, "Improving the specificity of fluorescence bronchoscopy for the analysis of neoplastic lesions of the bronchial tree by combination with optical spectroscopy," submitted to Lung Cancer.
13. E. Brambilla, W. D. Travis, T. V. Colby, B. Corrin, and Y. Shimosato, Eur. Respir. J. **18**, 1059 (2001).
14. J. R. Mourant, T. Fuselier, J. Boyer, T. M. Johnson, and I. J. Bigio, Appl. Opt. **36**, 949 (1997).
15. A. M. K. Nilsson, C. Sturesson, D. L. Liu, and S. Andersson-Engels, Appl. Opt. **37**, 1256 (1998).
16. R. L. P. van Veen, W. Verkruysse, and H. J. C. M. Sterenborg, Opt. Lett. **27**, 246 (2002).
17. S. Prahl, "Optical absorption of hemoglobin" (Oregon Medical Laser Center, Portland, Oreg., December 15, 1999), http://omlc.ogi.edu/spectra/hemoglobin/.
18. P. Vaupel, F. Kallinowski, and P. Okunieff, Cancer Res. **49**, 6449 (1989).
19. B. A. Warren, in *Tumor Blood Circulation: Angiogenesis, Vascular Morphology and Blood Flow of Experimental Human Tumors*, H.-I. Peterson, ed. (CRC Press, Boca Raton, Fla., 1979).
20. J. R. Less, T. C. Skalak, E. M. Sevick, and R. K. Jain, Cancer Res. **51**, 265 (1991).
21. R. L. Keith, Y. E. Miller, R. M. Gemmill, H. A. Drabkin, E. C. Dempsey, T. C. Kennedy, S. Prindiville, and W. A. Franklin, Clin. Cancer Res. **6**, 1616 (2000).
22. K. Hiroshima, A. Iyoda, K. Shibuya, H. Hoshino, Y. Haga, T. Toyozaki, M. Shiba, M. Baba, T. Fujisawa, and H. Ohwada, Cancer **95**, 1539 (2002).

CHAPTER 4

Measurement of hypoxia-related parameters in bronchial mucosa by use of optical spectroscopy

Bard M.P.L., A. Amelink, V. Noordhoek Hegt, W. Graveland, H.J.C.M. Sterenborg, H.C. Hoogsteden, J.G.J.V. Aerts

Measurement of Hypoxia-related Parameters in Bronchial Mucosa by Use of Optical Spectroscopy

Martin P. L. Bard, Arjen Amelink, Vincent Noordhoek Hegt, Wilfried J. Graveland, Henricus J. C. M. Sterenborg, Henk C. Hoogsteden, and Joachim G. J. V. Aerts

Department of Respiratory Diseases, Center for Optical Diagnostics and Therapy; Departments of Radiation Oncology and Statistics, Erasmus Medical Centre Rotterdam; and Departments of Pathology and Respiratory Diseases, Sint Franciscus Hospital, Rotterdam, the Netherlands

Rationale: Tumor hypoxia has both prognostic and therapeutic consequences for solid tumors. We developed a novel noninvasive technique, differential path-length spectroscopy (DPS), which allows the measurement of hypoxia-related parameters in the superficial microvasculature of tissue. *Objectives:* The aim of this study was to measure the microvascular oxygenation of histologically normal endobronchial mucosa and of neoplastic lesions during bronchoscopy using DPS. *Methods:* Sixty-four patients with known or suspected malignancies of the lung were studied. One hundred and five endobronchial lesions (38 histologically normal, 37 metaplastic/ mild dysplastic lesions, and 30 invasive carcinomas) were detected by white and/or autofluorescence bronchoscopy and measured using DPS. *Results:* We observed that bronchial tumors are characterized by a lower blood oxygen saturation and a higher blood content than normal mucosa. No differences were observed between normal and metaplastic/mild dysplastic mucosa. *Conclusion:* DPS is a new optical technique allowing the noninvasive study of endobronchial tumor hypoxia.

Keywords: cancer; hypoxia; lung; optical spectroscopy; premalignant

Tumor hypoxia has been associated with a lower survival rate, a higher degree of invasiveness, and a higher risk of regional and distant metastases in uterine cervical carcinoma (1–4), head and neck carcinoma (5, 6), and soft tissue sarcoma (7). In addition, hypoxia limits the response of tumor cells to ionizing radiation and to some chemotherapies (8, 9). Therefore, tumor hypoxia has both prognostic and therapeutic consequences, indicating the importance of its measurement (8).

In vivo measurement of tissue oxygenation is challenging in the lung. Invasive techniques, such as polarographic oxygen microelectrodes, cannot be used in the lung because of the inaccessibility of the bronchial tree. Histologic techniques, such as the study of exogeneous (pimonidazole) and endogeneous (hypoxia inducible factor, carbonic anhydrase IX, vascular endothelial growth factors) hypoxic factors, or the measurement of tissue microvessel density (MVD), are indirect methods that can only be used *ex vivo* on biopsy specimens (9). Functional imaging techniques, such as magnetic resonance imaging, positron emission tomography, and single photon emission computed tomography, are noninvasive techniques that have the advantage to investigate nonaccessible organs such as the lungs and to give information about the metabolic activity, the blood flow, and the microcirculation of tumors (10–13). However, these techniques are expensive, are limited by their spatial resolution hampering their use in case of tumors of size less than 1 cm, and are not sensitive to the early changes associated with cancerous transformations occurring in the epithelium of mucosa.

Noninvasive measurement of relevant parameters in the superficial layer of bronchial mucosa would be particularly interesting because the majority of lung cancers arise in the epithelium and are preceded by precancerous changes that affect only the surface epithelium. Previous authors have reported that both the expression of hypoxic factors and an increased tumor MVD are related to a poor prognosis in lung cancer (14, 15). Interestingly, it was also reported that these hypoxia-related changes could be observed in cases of early-stage (intraepithelial) bronchial carcinomas (16, 17) and in cases of premalignant lesions, such as dysplasia. These results suggest that the modifications of the bronchial mucosal oxygenation occur early during oncogenesis. An *in vivo* confirmation of these findings requires the development of an original technique sensitive to the oxygenation changes occurring in the bronchial epithelium.

White-light reflectance spectroscopy is a noninvasive technique that allows the analysis of tissue optical properties. Because blood is the dominant light absorber in the visible wavelength range, both the local blood content and the blood oxygen saturation can be extracted from reflected light signal. Visible and near-infrared diffuse reflectance spectroscopy has been used in animal models and in humans to analyze the oxygenation of tumoral tissues (18–22). However, the reflectance spectroscopic techniques used by these authors were characterized by large source-detector separations and a relatively long path length. As a consequence, the detected photons have traveled a long distance through the tissue, and the extracted optical properties represent average values over a relatively large tissue volume. This results in a decreased sensitivity of these optical techniques to changes in the epithelial tissue layer. We recently developed a novel spectroscopic technique, differential path-length spectroscopy (DPS), that allows the *in vivo* measurement of blood oxygenation, blood volume, and vessel diameter in the most superficial layer of tissue (23). This fiber-based technique can be used during an endoscopic procedure, and preliminary data in the bronchial tree have shown that cancerous bronchial mucosa has a lower capillary oxygenation, a higher blood volume fraction, and a larger average capillary diameter than normal bronchial mucosa (24).

The aim of this study was to measure the oxygenation of histologically normal bronchial mucosa and of endobronchial neoplastic lesions during bronchoscopy in a large population of patients to confirm our preliminary results for a larger variety of histologic tissue types.

METHODS

Study Population

Patients with known or suspected malignancies of the lung and with a medical indication for a bronchoscopy were invited to participate. All patients were older than 18 years and provided signed informed consent.

The study was approved by the Medical Ethics Review Board of the Erasmus Medical Center Rotterdam, the Netherlands.

Reflectance Probe

Spectra were measured using a custom-made instrument using a fiber-optic probe small enough to be led through the 2.8-mm working channel of the bronchoscope (Figure 1). The fiber probe consisted of two 400-μm-diameter optical fibers fitted into a small metal tube. The two fibers touch one another to minimize the distance between them. One fiber (delivery and collection dc-fiber) is used for both delivery and detection of light. The second fiber (collection c-fiber) is used for only detection of reflected light from the tissue. A tungsten-halogen lamp (Model HL-2000-FHSA; Ocean Optics, Duiven, the Netherlands) is used to light up the bronchial mucosa through the dc-fiber, and the remitted light collected in the dc- and c-fiber is analyzed in a dual-channel spectrometer (SD2000; Ocean Optics). The data presented in this article are part of a larger study using a combination of reflectance and autofluorescence spectroscopy during bronchoscopy for the detection of bronchial (preneoplastic) lesions (25). The autofluorescence of the bronchial lesions is induced by a blue-violet light source, and the autofluorescence spectra are collected through the c-fiber. To attenuate the short-wavelength background caused by the blue-violet light source, the autofluorescence spectra are filtered through a long-pass glass filter (GG435; Schott, Tiel, the Netherlands). As a consequence, the white-light reflectance spectra measured by the c-fiber are very noisy below 435 nm.

The difference of the dc- and c-fiber collection signals is the differential reflectance signal $R(\lambda)$. In the range of parameters relevant for biological tissue, we have previously reported that the differential reflectance signal $R(\lambda)$ can be simply modeled by the following equation: $R(\lambda) = C_1\mu_s'(\lambda)exp[-\tau\mu_a(\lambda)]$, where $\mu_s'(\lambda)$ is the reduced scattering coefficient, $\mu_a(\lambda)$ is the absorption coefficient, τ is the apparent differential path length, and C_1 is a proportionality constant (23). We have
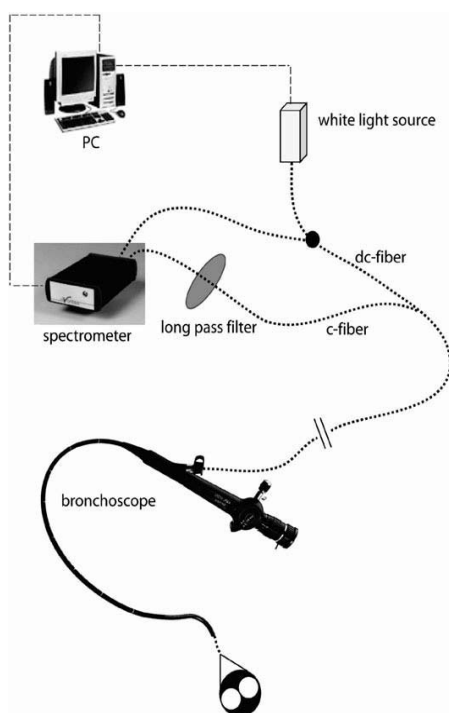

Figure 1. Setup used for the differential path-length spectroscopy (DPS) measurement in the bronchial tree. The bifurcated optical fiber probe is small enough to be led through the working channel of the bronchoscope. A tungsten-halogen lamp is used to light up the bronchial mucosa through the dc-fiber, and the remitted light collected in the dc- and c-fiber is analyzed in a dual-channel spectrometer.

previously demonstrated that the apparent differential path length (τ) is independent of the optical properties of the tissue and depends on the fiber diameter only. For fibers with a diameter of 400 μm, the apparent differential path length is only 320 μm, allowing the analysis of photons reflected in the most superficial layer of tissue (within $\sim$ 160 μm of the surface).

Examination Procedure

The endoscopic examination of the bronchial tree was performed with a commercially available flexible fluorescence bronchoscope (11004BI; Karl Storz, Tuttlingen, Germany). All lesions that appeared abnormal at blue- and/or white-light imaging were measured. The probe was led through the working channel of the bronchoscope and placed in gentle contact with the bronchial mucosa (Figure 2). The duration of reflectance spectral acquisition was less than 1 second during which the light source of the bronchoscope was switched off. An average of three measurements was done on each location to take into account the tissue heterogeneity. Finally, bronchial biopsies of the lesions were obtained. Biopsy specimens were transported in formaldehyde and fixed in paraffin. Hematoxylin-eosin–stained slides were evaluated without knowledge of the bronchoscopic and spectroscopic findings. The pathologic diagnoses were coded referring to the World Health Organization lung cancer classification (26).

Analysis of Spectra

In accordance with Lorentz-Mie scattering theory, we assumed that $\mu_s'(\lambda) = \alpha\lambda^{-b}$, where the Mie parameter (b) is a constant related to the size of the scattering particles (27). Furthermore, the main absorber in the measured wavelength range (350–1,000 nm) is blood. The complete model to which the differential path-length spectra are fitted is given by the following equation (24):

$$R(\lambda) = C_1\mu_s'(\lambda)exp[-0.32\ \mu_a(\lambda)] \qquad (1)$$
$$= C_1'\lambda^{-b}\ exp\{-0.32C_{cor}(\lambda)\ \rho[StO_2\mu_a^{HbO2}(\lambda)$$
$$+ (1 - StO_2)\ \mu_a^{Hb}(\lambda)]\},$$

where ρ is the blood volume fraction, StO_2 is the microvascular blood oxygenation, $\mu_a^{HbO2}(\lambda)$ is the absorption coefficient of fully oxygenated whole blood, $\mu_a^{Hb}(\lambda)$ is the absorption coefficient of fully deoxygenated whole blood, C_1' is a proportionality constant, and C_{cor} is the correction factor that accounts for the inhomogeneous distribution of blood in tissue (28). For whole blood contained in infinitely long cylindric vessels, the correction factor is given by $C_{cor} = \{1 - exp[\mu_a^{bl}(\lambda)D_{vessel}]\}/[\mu_a^{bl}(\lambda)D_{vessel}]$, where $\mu_a^{bl}(\lambda)$ is the absorption coefficient of whole blood and D_{vessel} is the vessel diameter. Blood volume fraction (ρ) and microvessel diameter (D_{vessel}) are extracted from Equation 1 assuming cylindric vessels and a blood hemoglobin content of 150 g/L, which is typical for whole blood. However, the size and shape of capillaries vary in the microvasculature, and the hematocrit of blood in the capillaries is lower than the hematocrit of whole blood and may vary between normal and cancerous tissue. As a consequence, the fitted values for these parameters may actually deviate from their absolute values. An additional difficulty for proper analysis of the vessel diameter arises from the large noise observed in the reflectance spectra below 435 nm caused by the presence of the long-pass glass filter. The measured reflectance signal is affected by the size of the blood vessels most notably around 420 nm; the large noise in that wavelength region reduces the accuracy in the fit of the vessel diameter considerably.

Fitting the data to our equation yields values for the local blood oxygenation (StO_2), local blood volume fraction (ρ), apparent average vessel diameter (D_{vessel}), and the Mie parameter (b). An additional parameter was chosen to appreciate the amplitude of the scattering signal. This scattering amplitude parameter (a) corresponds to the amplitude of the scattering signal measured at 800-nm wavelength, where blood absorption is minimal.

Statistical Analysis

The difference of optical parameters between the normal, metaplastic/mild dysplastic, and cancerous lesions were evaluated with a Kruskal-Wallis test (29). We have chosen this test because some optical parameters have a skewed distribution, which makes the Student *t* test inappropriate. p values less than 0.05 were regarded as significant.
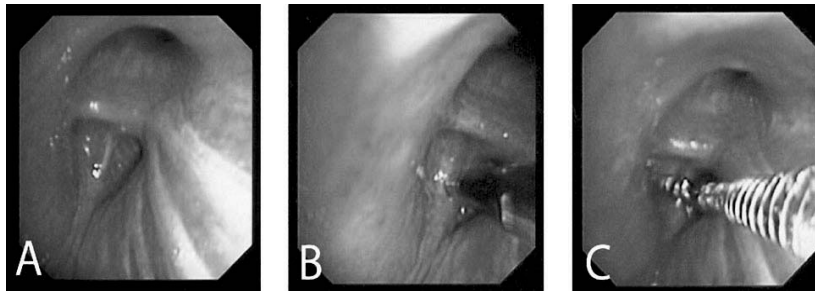
Figure 2. Three-stage examination procedure for DPS measurements in the bronchial tree. (*A*) Lesions of the bronchial mucosa are detected with a flexible fluorescence bronchoscope (white light image). (*B*) The probe is led through the working channel of the bronchoscope and placed in gentle contact with the bronchial mucosa. (*C*) Bronchial biopsies of the bronchial lesion are obtained.

RESULTS

Endobronchial Lesions

Sixty-four patients (39 men and 25 women with a median age of 65 ± 12 years) were studied during a 1-year period. One hundred and ten endobronchial lesions were detected by white and/or autofluorescence bronchoscopy and measured using DPS. An adequate amount of lesions was obtained in three histologic types: normal mucosa (38 lesions), metaplastic/mild dysplastic mucosa (37 lesions), and invasive carcinoma (30 lesions). The histologic repartition of the invasive carcinomas were as follows: 10 squamous cell, 9 adenocarcinomas, 5 large cell carcinomas, and 6 non–small cell carcinomas. In addition, two severe dysplastic/carcinoma in situ (CIS) lesions and three necrotic lesions were measured, but because of their low numbers, no statistical analysis was performed on these types of lesions.

Reflectance Spectra

Figure 3 illustrates four examples of DPS spectra measured in normal bronchial mucosa with increasing local blood volume fractions (ρ). The blood volume fraction (ρ) is proportional to the depth of the signal dips observed below 600 nm corresponding to the absorption of light by hemoglobin (Figure 3). Figure 4 illustrates examples of DPS spectra, fits, and residues measured in normal (Figure 4, *upper panel*) and cancerous (Figure 4, *lower panel*) mucosa, respectively. Note the difference in the shape of the blood absorption signals for wavelengths below 600 nm caused by a difference in microvascular saturations (StO_2). A high StO_2 (100%) is measured for the normal mucosa (Figure 4, *upper panel*), and a low StO_2 (45%) is measured for the cancerous lesion (Figure 4, *lower panel*).

Because both the StO_2 and the apparent average vessel diameter (D_{vessel}) are related to the shape of the blood absorption dips below 600 nm, the accuracy of the fits for these two parameters is limited in case of small blood volumes (*see*, e.g., Figure 3A). Therefore, we decided to restrain the calculation of these two parameters to spectra for which the blood volume fraction (ρ) was higher than 1% (24). As a consequence, these parameters were calculated for 25, 27, and 28 normal, metaplastic/mild dysplastic, and invasive carcinomas, respectively. In addition, Figure 5 illustrates an example of a DPS spectrum measured in necrotic cancerous tissue. Compared with spectra measured in normal mucosa or nonnecrotic cancerous mucosa, an additional absorption dip is visible in the 600- to 650-nm wavelength range. This additional absorption dip is related to an (as yet unidentified) additional absorber present in the necrotic tissue that is not accounted for in Equation 1 but should be incorporated for adequate fitting.

Two parameters extracted from the spectra contain information about the scattering properties of the tissue: the Mie parameter (b), which corresponds to the slope of the DPS spectra, and the
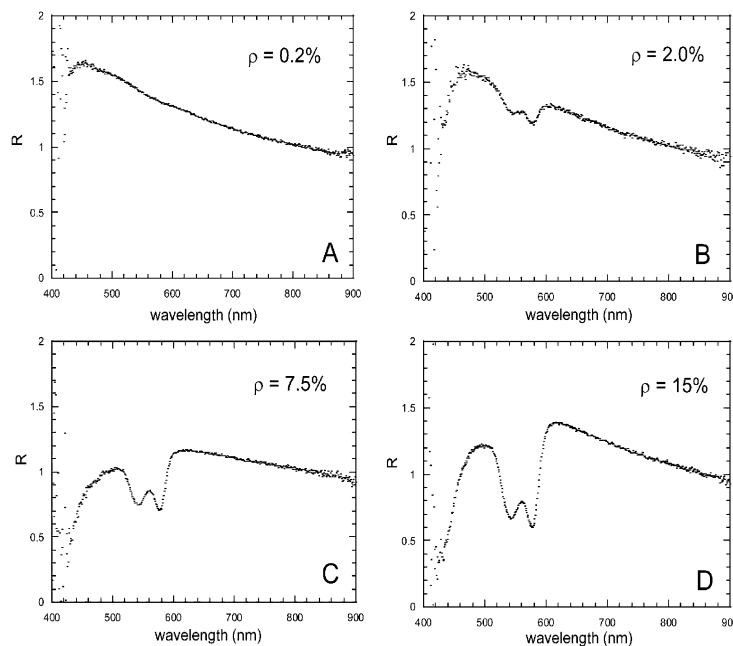

Figure 3. Illustration of four DPS spectra (*A–D*) with increasing local blood volume fraction (ρ) measured in normal bronchial mucosa. The signal dips observed below 600 nm are caused by the absorption of blood.
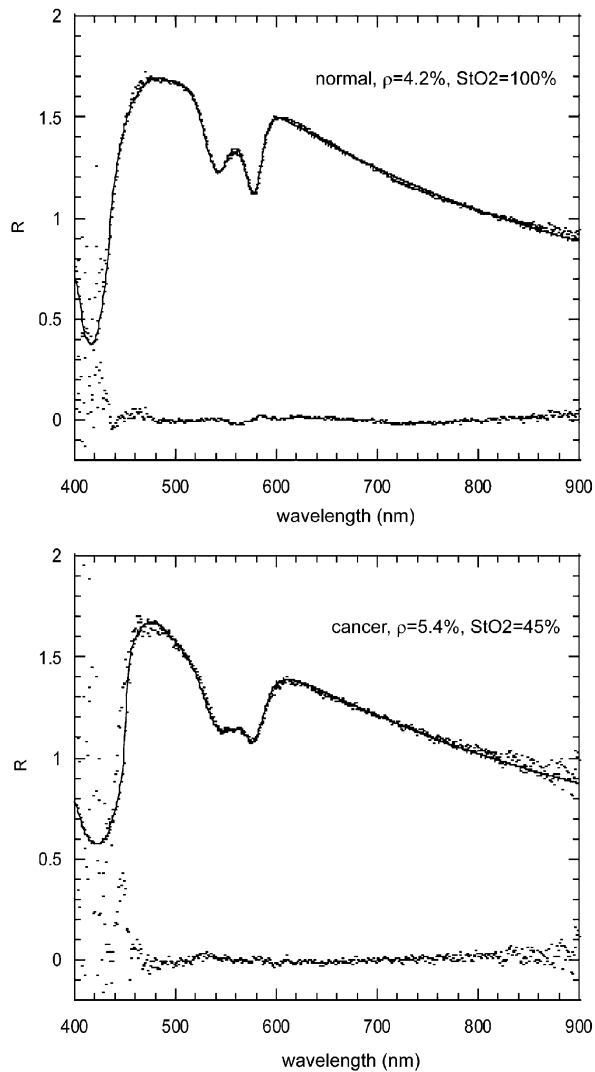
52

Figure 4. Illustration of DPS spectra, fits, and residues (= spectrum − fit) measured on normal (*upper panel*) mucosa and on a cancerous (*lower panel*) lesion. A difference in oxygen blood saturation (StO₂) is observable through a difference in the shape of the blood absorption dips below 600 nm.

scattering amplitude parameter (a), which corresponds to the amplitude of the scattering signal at 800 nm. Both the slope (b) and amplitude (a) are not affected by the local blood volume fraction (ρ) because they are measured in a wavelength range where the absorption of blood is negligible.

Optical Parameters

Multiple measurements were systematically done on each bronchial lesion to take into account the intralesion heterogeneity. The optical parameters extracted from all the spectra measured on the same lesion were averaged, and these averaged values were used to optically characterize each bronchial lesion. The bronchial lesions were clustered into three histologic groups: normal mucosa, metaplastic/mild dysplastic mucosa, and invasive carcinoma. Table 1 summarizes the average values and standard deviations of the optical parameters in each of these three histologic groups. Invasive carcinomas were characterized by a
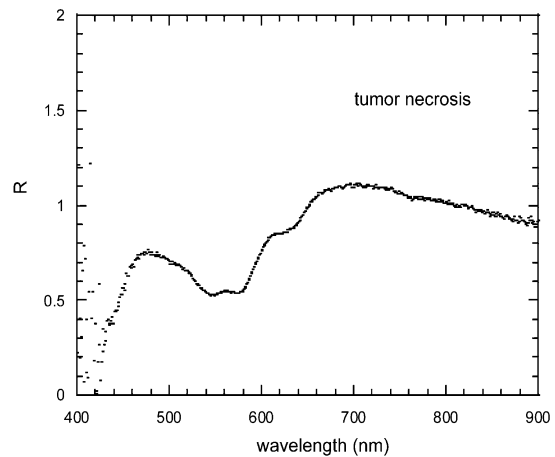

Figure 5. Illustration of a DPS spectrum measured in necrotic cancerous tissue showing an additional absorption dip in the 600–650-nm wavelength range.

lower oxygen saturation, a higher blood volume, and a larger average vessel diameter compared with normal or metaplastic/mild dysplastic mucosa (statistically significant for blood saturation and blood volume, $p < 0.001$ using a Kruskal-Wallis test; not significant for the vessel diameter). The scattering amplitude parameter (a) was significantly lower in cancer ($p < 0.001$ using a Kruskal-Wallis test), but no significant difference in the scattering slope (b) was observed between invasive carcinoma and both normal and metaplastic/mild dysplastic mucosa. Furthermore, no significant difference in any of the parameters was observed between normal and metaplastic/mild dysplastic lesions.

DISCUSSION

We used DPS to study the oxygenation and the microvasculature of bronchial lesions *in vivo*. This is to our knowledge the first report of an optical analysis of human bronchial mucosa during bronchoscopy. DPS allows a real-time and noninvasive measurement of tissue hypoxia–related parameters, such as the blood oxygenation, the blood content, and the microvessel size. Moreover, DPS informs about the scattering properties of the bronchial mucosa. We observed that endobronchial tumors are characterized by a lower blood oxygenation, a higher blood content, and a smaller scattering amplitude than normal or metaplastic/mild dysplastic bronchial mucosa.

Bronchial epithelium is the location of premalignant lesions and *in situ* carcinomas, which are precursors of the majority of lung cancers. The development of an instrument allowing the *in vivo* analysis of this superficial layer would help to better understand the pathophysiology of these early lesions and possibly improve their detection. Because DPS uses a fiber-optic probe that is guided through the working channel of a bronchoscope, the technique is limited to lesions of the proximal bronchial tree. We have demonstrated in tissue phantoms that DPS using 400-µm fibers is sensitive to the light scattered in approximately the first 150 µm of the tissue surface (30). Such depth corresponds to the epithelium thickness encountered in cases of metaplastic/dysplastic lesions or *in situ* carcinomas. In cases of invasive carcinomas, the tumor thickness can attain several centimeters, and DPS informs only about the most superficial layer of these larger tumors. At this point, we must emphasize that DPS was developed with the intention to study the microvasculature

53

TABLE 1. AVERAGE VALUES AND SDs OF BLOOD OXYGENATION, VESSEL DIAMETER, BLOOD VOLUME, MIE PARAMETER, AND SCATTERING AMPLITUDE PARAMETER MEASURED IN NORMAL MUCOSA, METAPLASTIC/MILD DYSPLASTIC MUCOSA, AND INVASIVE CARCINOMA OF THE BRONCHIAL TREE

	StO_2 (%)	D_{vessel} (μm)	ρ (%)	b	a
Normal	(n = 25)	(n = 25)	(n = 38)	(n = 38)	(n = 38)
	76.1 ± 15.8	14.2 ± 9.2	3.6 ± 6.0	-1.01 ± 0.18	2.38 ± 0.75
Metaplasia/mild dysplasia	(n = 27)	(n = 27)	(n = 37)	(n = 37)	(n = 37)
	82.1 ± 21.0	14.5 ± 8.3	3.8 ± 5.0	-1.02 ± 0.17	2.13 ± 0.76
Cancer	(n = 28)	(n = 28)	(n = 30)	(n = 30)	(n = 30)
	$56.3 \pm 26.1^*$	23.1 ± 16.9	$11.8 \pm 14.4^*$	-0.99 ± 0.22	$1.67 \pm 0.80^*$

Definition of abbreviations: a = scattering amplitude; b = Mie parameter; D_{vessel} = vessel diameter; ρ = blood volume; StO_2 = microvascular blood saturation.

The number of lesions in each group is indicated in parentheses.

* $p < 0.001$, Kruskal-Wallis test.

and the scattering properties of the most superficial layer of bronchial tissue only. Little is known about the relation between the vasculature at the bronchial epithelial surface and at the center of larger tumors. The use of an animal lung cancer model would allow the study of the correlation between the superficial and deep bronchial tumor oxygenation, but this is beyond the scope of this article.

Tumor hypoxia is a heterogeneous process that depends on several factors, including an increased consumption of oxygen related to the high metabolism and high proliferation rate of the cancerous cells, a lower quality of the tumoral microcirculation related to architectural and functional abnormalities of the tumor microvessels, a decreased capacity of oxygen to diffuse to the cells because of the increased distance between the microvessels and the cancerous cells, and a sluggish blood flow in the tumor microcirculation as a consequence of the increased resistance in the microvessels and the increased viscosity of the blood (8, 9). A correct description of the oxygenation of solid tumors requires the concomitant study of these various parameters (31). It must be noted that DPS measures only a part of these hypoxia-related parameters—that is, blood oxygenation, blood volume, and microvessel size. DPS does not measure blood flow, nor does it measure the MVD. An increased MVD would result in an increased blood volume fraction (ρ), but an increased blood volume fraction may also be caused by an increase in the microvessel size. As a consequence, we cannot simply relate our parameters to commonly used parameters such as MVD. However, alternative techniques for the *in vivo* assessment of hypoxia-related parameters, such as tissue oxygenation, MVD or blood flow in bronchial mucosa, do not exist to our knowledge. Moreover, exogeneous hypoxia markers, such as pimonidazole, are hard to measure in the small-size bronchial biopsies obtained during bronchoscopy, and large tumor samples are generally not available in the majority of patients suffering from lung cancer.

Tumor hypoxia has previously been reported in various kinds of solid cancers (2, 4, 5, 32). Oxygenation of tumors is facilitated by the creation of new blood vessels by the tumor itself (neoangiogenesis). This process is regulated depending on a balance of angiogenic and angiostatic factors (33). In response to hypoxemia, tumors secrete angiogenic cytokines, such as vascular endothelial growth factor, inducing the formation of microvessels from the surrounding host vasculature. However, the delivery of oxygen to the neoplastic and stromal cells is frequently altered by structural abnormalities of the microcirculation. We observed that hypoxia is a common event in the mucosal capillary blood of bronchial tumors. In addition to the measurement of capillary blood oxygenation, DPS allows us to study the microvascular geometry of the superficial layer of bronchial mucosa.

An increased blood content and enlarged microvessel diameters were observed in bronchial tumors in comparison with normal mucosa, although the latter was not significant. The fact that no significant differences were observed in microvessel size may at least in part be explained by the low signal-to-noise ratio below 435 nm, as explained in METHODS. Lung tumors are known to be characterized by an increase in microvessel count (33). An increase in the size of microvessels is also characteristic of the tumoral microvasculature. Tumor blood vessels are commonly tortuous and irregular, have venous shunts and blind ends, and lack smooth muscles and innervation (34). This increase in vessel size, associated with a decrease of local blood pressure and an increase of blood viscosity, induces tumor blood flow alterations leading to hypoxia (35).

The development of hypoxia and microvasculature alterations during oncogenesis is poorly known. Neoangiogenesis has been reported to be increased in smokers and in bronchial preneoplastic lesions with the expression of angiogenic and proliferation markers and an increase of the MVD (36–38). Moreover, the increased microvascular density observed in solid cancer is directly linked to the angiogenesis process, and previous authors have reported a correlation between increased vessel density and tumor stage (39, 40). A direct visualization of the microvasculature in bronchial mucosa has recently been reported using high-magnification bronchovideoscopy (41, 42). These authors have shown that larger blood vessels were present in dysplastic lesions of the bronchial mucosa. We observed no significant change in oxygenation, blood content, and microvessel size in the metaplastic/mild dysplastic mucosa in comparison with normal mucosa. However, these alterations of the bronchial mucosa are frequent (particularly in smokers), tiny, and mostly spontaneously reversible, and are not considered to be premalignant. Our data show that the onset of macroscopic changes in the microvasculature of bronchial mucosa must occur at a later stage than metaplasia/mild dysplasia. Unfortunately, concerning the alterations occurring in more advanced mucosal lesions, such as severe dysplasia and carcinoma *in situ*, no conclusion can be drawn from the very small number of these types of lesions measured in our study. The use of DPS during high-magnification bronchoscopy would be particularly interesting, allowing a comparison of these two different techniques for the study of the bronchial microvasculature.

When light enters tissue it is scattered whenever it encounters refractive index variations. The fact that membranes, nuclei, mitochondria, and other organelles all have a different refractive index from the surrounding cytoplasm makes tissue a highly scattering medium. Although the detailed dependence of the scattering signal on the tissue composition is not completely

understood, most experimental evidence suggests that the mito-chondria contribute most to the light scattering in the backward directions (43–46). In our study, the Mie parameter (b) was not modified in cancerous tissue compared with normal or metaplas-tic tissue, suggesting that the size of the light scatterers in the cancerous epithelium are not significantly modified. The de-creased amplitude of the scattering signal observed in bronchial tumors may be related to a decrease in the mitochondrial content of tumors (44) or to changes in the refractive index of the cyto-plasm because of an increased protein and enzyme content, but this is highly speculative and requires further investigation into the microscopic origins of light scattering in tissue.

Recent improvements in the endoscopic technology, such as fluorescence endoscopy and high-magnification videoscopy, have allowed the development of highly sensitive bronchoscopes for the detection of bronchial mucosal lesions. However, these bronchoscopic techniques are characterized by a low specificity (i.e., a lot of false-positives), inducing unnecessary biopsies at greater costs and a longer duration of the endoscopic examina-tion. The concomitant use of DPS during bronchoscopy may be helpful to increase the specificity of bronchoscopy. However, it must be emphasized that the objective of the present study was to measure the oxygenation and the microvasculature in the most superficial layer of tissue noninvasively during routine bronchoscopy for various histologic tissue types. The fact that statistically significant differences are found between the microvas-cular saturations of normal and cancerous tissue does not imply that it is possible to use the measured saturation for classification purposes. The classification of lesions based on saturation mea-surements alone requires not only a statistically significant differ-ence in the mean values of the groups but a relatively small standard deviation within each group as well. The latter condition is clearly not fulfilled for our data, and any attempt to classify the lesions using the extracted saturation parameter (StO_2) alone will be futile. The question of whether DPS can be used to classify lesions using more advanced statistical techniques (e.g., using combined classifiers and linear discriminant analysis) will be answered in a separate study.

In conclusion, DPS allows a real-time, noninvasive analysis of the oxygenation, the microvasculature, and the scattering properties in the most superficial layer of tissue. This technique is particularly interesting for the analysis of cancer developing in superficial tissues, such as epithelium. Its use during an endo-scopic procedure is easy and well tolerated, and opens up a wide field of investigation in various organs. Potentially, DPS can be used for a better understanding of the oxygenation alterations that occur during the bronchial oncogenesis, an improvement of our capacity to detect the preneoplastic and intraepithelial cancers, the analysis of the prognostic significance of endobronchial tumor oxygenation, the survey of antihypoxia or antiangiogenesis thera-pies, and the real-time monitoring of oxygen-dependent therapies, such as radiotherapy or photodynamic therapy.

References

1. Fyles AW, Milosevic M, Wong R, Kavanagh M-C, Pintilie M, Sun A, Chapman W, Levin W, Manchul L, Keane TJ, *et al.* Oxygenation predicts radiation response and survival in patients with cervix cancer. *Radiother Oncol* 1998;48:149–156.
2. Höckel M, Schlenger K, Aral B, Mitze M, Schaffer U, Vaupel P. Associa-tion between tumor hypoxia and malignant progression in advanced cancer of the uterine cervix. *Cancer Res* 1996;19:4509–4515.
3. Sundfor K, Lyng H, Rofstad EK. Tumor hypoxia and vascular density as predictors of metastasis in squamous cell carcinoma of the uterine cervix. *Br J Cancer* 1998;78:822–827.
4. Höckel M, Knoop C, Schlenger K, Vorndran B, Baussmann E, Mitze M, Knapstein PG, Vaupel P. Intratumoral pO2 predicts survival in advanced cancer of the uterine cervix. *Radiother Oncol* 1993;26:45–50.
5. Brizel DM, Sibley GS, Prosnitz LR, Scher RL, Dewhirst MW. Tumor hypoxia adversely affects the prognosis of carcinoma of the head and neck. *Int J Radiat Oncol Biol Phys* 1997;38:285–289.
6. Nordsmark M, Overgaard M, Overgaard J. Pretreatment oxygenation predicts radiation response in advanced cell carcinoma of the head and neck. *Radiother Oncol* 1996;41:31–39.
7. Brizel DM, Scully SP, Harrelson JM, Layfield LJ, Bean JM, Prosnitz LR, Dewhirst MW. Tumor oxygenation predicts for the likehood of distant metastases in human soft tissue sarcoma. *Cancer Res* 1996;56:941–943.
8. Evans SM, Koch CJ. Prognostic significance of tumor oxygenations in humans. *Cancer Lett* 2003;195:1–16.
9. Höckel M, Vaupel P. Tumor hypoxia: definitions and current clinical biologic, and molecular aspects. *J Natl Cancer Inst* 2001;93:266–276.
10. Foo SS, Abbott DF, Lawrentschuk N, Scott AM. Functional imaging of intratumoral hypoxia. *Mol Imaging Biol* 2004;6:291–305.
11. McCoy CL, McIntyre DJ, Robinson SP, Aboagye EO, Griffiths JR. Magnetic resonnance spectroscopy and imaging methods for measur-ing tumour and tissue oxygenation. *Br J Cancer* 1996;27:S226–S231.
12. Halpern HJ, Yu C, Peric M, Barth E, Grdina DJ, Teicher BA. Oxymetry deep in tissues with low-frequency electron paramagnetic resonance. *Proc Natl Acad Sci USA* 1994;91:13047–13051.
13. Rasey JS, Koh W-J, Evans ML, Peterson LM, Lewellen TK, Graham MM, Krohn KA. Quantifying regional hypoxia in human tumors with positron emission tomography of [18F]fluoromisonidazole: a prether-apy study of 37 patients. *Int J Radiat Oncol Biol Phys* 1996;36:417–428.
14. Swinson DEB, Jones JL, Richardson D, Wykoff C, Turley H, Pastorek J, Taub N, Harris AL, O'Byrne KJ. Carbonic anhydrase IX expression, a novel surrogate marker of tumor hypoxia, is asssociated with a poor prognosis in non-small-cell lung cancer. *J Clin Oncol* 2003;21:473–482.
15. Giatromanolaki A, Koukourakis MI, Sivridis E, Turley H, Talks K, Pez-zela F, Gatter KC, Harris AL. Relation of hypoxia inducible factor 1a and 2a in operable non-small cell lung cancer to angiogenic/molecular profile of tumours and survival. *Br J Cancer* 2001;85:881–890.
16. Kim SJ, Rabbani ZN, Vollmer RT, Schreiber E-G, Oosterwijk E, Dewhirst MW, Vujaskovic Z, Kelley MJ. Carbonic anhydrase IX in early-stage non-small cell lung cancer. *Clin Cancer Res* 2004;10:7925–7933.
17. Vermylen P, Roufosse C, Burny A, Verhest A, Bosschaerts T, Pastore-kova S, Ninane V, Sculier J-P. Carbonic anhydrase IX antigen differen-tiates between preneoplastic malignant lesions in non-small cell lung carcinoma. *Eur Respir J* 1999;14:806–811.
18. Knoefel WT, Kollias N, Rattner DW, Nishioka NS, Warshaw AL. Reflec-tance spectroscopy of pancreatic microcirculation. *J Appl Physiol* 1996;80:116–123.
19. Zonios G, Perelman LT, Backman V, Manoharan R, Fitzmaurice M, Van Dam J, Feld MS. Diffuse reflectance spectroscopy of human adenomatous colon polyps in vivo. *Appl Opt* 1999;38:6628–6637.
20. Hornung R, Pham TH, Keefe KA, Berns MW, Tadir Y, Tromberg BJ. Quantitative near-infrared spectroscopy of cervical dysplasia in vivo. *Hum Reprod* 1999;14:2908–2916.
21. Hull EL, Conover DL, Foster TH. Carbogen-induced changes in rat mammary tumour oxygenation reported by near infrared spectroscopy. *Br J Cancer* 1999;79:1709–1716.
22. Sevick EM, Chance B, Leigh J, Nioka S, Maris M. Quantitation of time- and frequency-resolved optical spectra for the determination of tissue oxygenation. *Ann Biochem* 1991;195:330–351.
23. Amelink A, Sterenborg HJCM. Measurement of the local optical proper-ties of turbid media by differential path-lenght spectroscopy. *Appl Opt* 2004;43:3048–3054.
24. Amelink A, Sterenborg HJCM, Bard MPL, Burgers SA. In vivo measure-ment of the local optical properties of tissue by use of differential path-length spectroscopy. *Opt Lett* 2004;29:1087–1089.

25. Bard MPL, Amelink A, Skurichina M, den Bakker M, Burgers SA, van Meerbeeck JP, Duin RPW, Aerts JGJV, Hoogsteden HC, Sterenborg HJCM. Improving the specificity of fluorescence bronchoscopy for the analysis of neoplastic lesions of the bronchial tree by combination with optical spectroscopy: preliminary communication. *Lung Cancer* 2005;47:41–47.

26. Brambilla E, Travis WD, Colby TV, Corrinz B, Shimosato Y. The new World Health Association classification of lung cancer. *Eur Respir J* 2001;18:1059–1068.

27. Mourant JR, Fuselier T, Boyer J, Johnson TM, Bigio IJ. Prediction and measurements of scattering and absorption over broad wavelength ranges in tissue phantoms. *Appl Opt* 1997;36:949–957.

28. van Veen RLP, Verkruysse W, Sterenborg HJCM. Diffuse-reflectance spectroscopy from 500 to 1060 nm by correction for inhomogeneously distributed absorbers. *Opt Lett* 2002;27:246–248.

29. Kruskal WH, Wallis WA. Use of ranks in one-criterion variance analysis. *J Am Stat Assoc* 1952;47:583–621.

30. Amelink A, Bard MPL, Burgers SA, Sterenborg HJCM. Single-scattering spectroscopy for the endoscopic analysis of particle size in superficial layers of turbid media. *Appl Opt* 2003;42:4095–4101.

31. Menon C, Polin GM, Prabakaran I, Hsi A, Cheug C, Culver JP, Pingpank JF, Sehgal CS, Yodh AG, Buerk DG, *et al.* An integrated approach to measuring tumor oxygen status using human melanoma xenografts as a model. *Cancer Res* 2003;63:7232–7240.

32. Evans SM, Judy KD, Dunphy I, Jenkins WT, Nelson PT, Collins R, Wileyto EP, Jenkins K, Hahn SM, Stevens CW, *et al.* Comparative measurement of hypoxia in human brain tumors using needle electrodes and EF5 binding. *Cancer Res* 2004;64:1886–1892.

33. Shijubo N, Kojima H, Nagata M, Ohchi T, Suzuki A, Abe S, Sato N. Tumor angiogenesis of non–small cell lung cancer. *Microsc Res Tech* 2003;60:186–198.

34. Brown JM. The hypoxic cell: a target for selective therapy: eighteenth Bruce F. Cain memorial award lecture. *Cancer Res* 1999;59:5863–5870.

35. Jain RK. Determinant of tumor blood flow: a review. *Cancer Res* 1988; 48:2641–2658.

36. Hiroshima K, Iyoda A, Shibuya K, Hoshino H, Haga Y, Toyozaki T, Shiba M, Baba M, Fujisawa T, Ohwada H. Evidence of neoangiogenesis and an increase in the number of proliferating cells within the bronchial epithelium of smokers. *Cancer* 2002;95:1539–1545.

37. Fontanini G, Calcinai A, Boldrini L, Lucchi M, Mussi A, Angeletti C, Cagno C, Tognetti MA, Basolo F. Modulation of neoangiogenesis in bronchial preneoplastic lesions. *Oncol Respir* 1999;6:813–817.

38. Keith RL, Miller YE, Gemmill RM, Drabkin HA, Dempsey EC, Kennedy TC, Prindiville S, Franklin WA. Angiogenic squamous dysplasia in bronchi of individuals at high risk for lung cancer. *Clin Cancer Res* 2000;6:1616–1625.

39. Pazouki S, Chisholm DM, Carmichael AG, Farquharson M, Ogden GR, Schor SL, Schor AM. The association between tumor progression and vascularity in the oral mucosa. *J Pathol* 1997;183:39–43.

40. Kayser G, Baumhäkel JD, Szöke T, Trojan I, Riede U, Werner M, Kayser K. Vascular diffusion density and survival of patients with primary lung carcinomas. *Virchows Arch* 2003;442:462–467.

41. Shibuya K, Hoshino H, Chiyo M, Iyoda A, Yoshida S, Sekine Y, Lizasa T, Saitoh Y, Baba M, Hiroshima K, *et al.* High magnification bronchovideoscopy combined with narrow band imaging could detect capillary loops of angiogenic squamous dysplasia in heavy smokers at high risk for lung cancer. *Thorax* 2003;58:989–995.

42. Shibuya K, Hoshino H, Chiyo M, Yasufuku K, Lizasa T, Saitoh Y, Baba M, Hiroshima K, Ohwada H, Fujisawa T. Subepithelial vascular patterns in bronchial dysplasias using a high magnification bronchovideoscope. *Thorax* 2002;57:902–907.

43. Bartlett M, Huang G, Larcom L, Jiang H. Measurement of particle size distribution in mammalian cells in vitro by use of polarized light spectroscopy. *Appl Opt* 2004;43:1296–1307.

44. Beauvoit B, Chance B. Time-resolved spectroscopy of mitochondria, cells and tissue under normal and pathological conditions. *Mol Cell Biochem* 1998;184:445–455.

45. Mourant JR, Johnson TM, Carpenter S, Guera A, Aida T, Freyer JP. Polarized angular dependent spectroscopy of epithelial cells and epithelial cell nuclei to determine the size scale of scattering structures. *J Biomed Opt* 2002;7:378–387.

46. Mourant JR, Johnson TM, Freyer JP. Characterizing mammalian cells and cell phantoms by polarized backscattering fiber-optic measurement. *Appl Opt* 2001;40:5114–5123.

CHAPTER 5

Relation of lung cancer histology to hypoxia measured using optical spectrosopy

Bard M.P.L., A. Amelink, V. Noordhoek Hegt, W. Graveland, H.J.C.M. Sterenborg, H.C. Hoogsteden, J.G.J.V. Aerts

RELATION OF LUNG CANCER HISTOLOGY TO HYPOXIA MEASURED USING OPTICAL SPECTROSCOPY

Short title: relation of lung cancer histology to hypoxia

Martin P.L. Bard[1], Arjen Amelink[2], Vincent Noordhoek Hegt[4], Wilfried J. Graveland[3], Henricus J.C.M. Sterenborg[2], Henk C. Hoogsteden[1], Joachim G.J.V. Aerts[1,5]

[1]Department of Respiratory Diseases, [2]Center for Optical Diagnostics and Therapy, Department of Radiation Oncology, [3]Department of Statistics, Erasmus Medical Centre Rotterdam, [4]Department of Pathology, [5]Department of Respiratory Diseases, Sint Franciscus Hospital, Rotterdam, The Netherlands

Address for correspondence:

Joachim Aerts, M.D., PhD.

Department of Respiratory Diseases, Sint Franciscus Hospital

Kleiweg 500, 3045 PM, Rotterdam, The Netherlands,

Phone: +31 10 4616149, Fax : +31 10 4612692, e-mail: j.aerts@sfg.nl

ABSTRACT

Tumor hypoxia is known to correlate with a poor prognosis in solid cancers. We developed a novel non-invasive optical technique, differential path-length spectroscopy (DPS), which allows the *in vivo* measurement of hypoxia-related parameters in bronchial mucosa. Our aim was to investigate the association between the hypoxia-related parameters measured *in vivo* in endobronchial tumors and the histopathological diagnosis of lung cancers.

Forty-seven endobronchial tumors were measured using DPS in 37 patients suffering from lung cancer. DPS spectra were measured during bronchoscopy using a custom-made fiberoptic instrument. Tumor histological diagnoses were defined using bronchoscopic biopsies.

Blood oxygen saturation (StO2) and blood volume fraction (ρ) were lower (average $\pm$ standard deviations) in small-cell carcinomas (StO2 = 38.3 $\pm$ 22.7%, ρ = 6.3 $\pm$ 4.9%) and poorly differentiated large-cell carcinomas (StO2 = 39.6 $\pm$ 23.4%, ρ = 5.7 $\pm$ 6.4%) in comparison with squamous cell carcinomas (StO2 = 64.6 $\pm$ 21.3%, ρ = 15.9 $\pm$ 19.2%) and adenocarcinomas (StO2 = 55.9 $\pm$ 23.8%, ρ = 11.7 $\pm$ 8.6%).

Hypoxia-related parameters measured using DPS are related to the histological type of lung cancer.

Key words: Hypoxia, Lung Cancer, Spectroscopy

INTRODUCTION

Tumor hypoxia is a bad prognostic indicator of solid cancers (1). Using polarographic oxygen electrodes, previous authors have reported an association between tumor hypoxia and a low survival rate in uterine cervical (2-5) and head-and-neck (6, 7) carcinomas. Moreover, a higher invasiveness and a lower sensitivity to ionising radiation have been reported in cases of hypoxic tumors (1, 8), indicating the clinical relevance for measurement of oxygen saturation in tumors.

In lung cancer, the *ex vivo* measurement of hypoxic factors (hypoxia inducible factor, carbonic anhydrase IX, vascular endothelial growth factors) or tissue micro vessel density (MVD) has been related to a poor prognosis (9-14). Few *in vivo* data are available due to the inaccessibility of the lungs for tumor oxygenation measurement. Indeed, the use of oxygen polarographic electrodes is not possible in the bronchial tree. Using functional imaging techniques, such as [18][F]fluoromisonidazole proton emission tomography (PET) or single-photon emission computed tomography (SPECT), previous authors have reported a low oxygen saturation both in small- and non small-cell lung carcinomas (15, 16). Although these imaging techniques are promising, they are expensive and of limited use in case of small size tumors (less than 1 cm) and cancer confined to the bronchial mucosa. We recently developed a novel spectroscopic technique, differential path-length spectroscopy (DPS), that allows the *in vivo* measurement of hypoxia-related parameters such as blood oxygenation, blood content, and microvessel size in the most superficial layer of tissue (17, 18). We recently used DPS during bronchoscopy to study endobronchial mucosa in patients known or suspected to be suffering from lung cancer (19). We observed that endobronchial tumors are characterized by a lower blood oxygenation and a higher blood content in comparison with normal or metaplastic/mild dysplastic lesions.

The histological diagnosis is one of the most important prognostic factors in lung cancer (20, 21). Small cell carcinomas are highly aggressive tumors mostly associated with distant metastases and a poor survival (22). Within non small-cell lung cancers, prognosis of undifferentiated large cell carcinomas is generally worse than that of squamous cell carcinomas or adenocarcinomas (21). To investigate whether DPS can be used as a non-invasive, real-time tool to e.g. predict the aggressiveness of lung tumors and better define their treatments, we will here examine the correlation between the hypoxia-related parameters measured in endobronchial tumors using DPS and the cancer cell type.

MATERIAL & METHODS

Patients

Patients with known or suspected malignancies of the lung and with a medical indication for a bronchoscopy were invited to participate. All patients were more than 18 years old and signed informed consent. The study was approved by the Medical Ethics Review Board of the Erasmus Medical Centre Rotterdam, The Netherlands.

Examination procedure

The endoscopic examination of the bronchial tree was performed with a commercially available flexible fluorescence bronchoscope (Karl Storz® 11004BI, Germany). All lesions that appeared abnormal at blue and/or white light imaging were measured. The DPS fiber-probe was led through the working channel of the bronchoscope and placed in gentle contact with the bronchial mucosa. The duration of reflectance spectral acquisition was less than one second during which the light source of the bronchoscope was switched off. An average of three measurements was done on each location in order to take into account the tissue heterogeneity. Finally, bronchial biopsies of the lesions were obtained. Biopsy specimens were transported in formaldehyde and fixed in paraffin. Hematoxylin-eosin stained slides were evaluated without knowledge of the bronchoscopic and spectroscopic findings. The pathological diagnosis were coded referring to the World Health Organisation Lung Cancer classification (23). For the visualization of microvessels, the histological slides were stained with a commercially available monoclonal antibody against CD34 (Neomarkers, Fremont USA, dilution 1:400).

Differential path-length spectroscopy

The DPS technique has been previously described in great detail (18, 19). In short, spectra are measured using a custom-made instrument using a fiberoptic probe small enough to be led through the working channel of a flexible bronchoscope (Fig. 1). One fiber (delivery-and-collection (dc)-fiber) is used for both delivery and detection of light. The second fiber (collection (c)-fiber) is used for only detection of reflected light from the tissue. A tungsten-halogen lamp (Ocean Optics HL-2000-FHSA, Duiven, The Netherlands) is used to light up the bronchial mucosa through the dc-fiber and the remitted light collected in the dc- and c-fiber is analysed in a dual channel spectrometer (Ocean Optics, SD2000, Duiven, The Netherlands). The data presented in this article are part of a larger study using a combination of reflectance and autofluorescence spectroscopy during bronchoscopy for the diagnosis of bronchial (pre-)neoplastic lesions (24). The autofluorescence of the bronchial lesions is induced by a blue-violet light source and the autofluorescence spectra are collected through the c-fiber. In order to attenuate the short wavelength background due to the blue-violet light source, the autofluorescence spectra are filtered through a long pass glass filter (Schott GG435, Tiel, The Netherlands). As a consequence, the white-light reflectance spectra measured by the c-fiber are very noisy below 435 nm.

The difference of the dc- and c-fiber collection signals is the differential reflectance signal $R(\lambda)$. In the range of parameters relevant for biological tissue, we have previously reported that the differential reflectance signal $R(\lambda)$ can be modelled by (19):

$$R(\lambda) = C_1 \lambda^{-b} \exp\{-0.32 C_{cor}(\lambda) \, \rho [StO_2 \mu_a^{HbO2}(\lambda) + (1 - StO_2) \, \mu_a^{Hb}(\lambda)]\}, \tag{1}$$

where C_1 is a proportionality constant, b is a parameter related to the size of the scattering particles, C_{cor} is a correction factor that accounts for the inhomogeneous distribution of blood in tissue (25) and is related to the vessel diameter D_{vessel}, ρ is the blood volume fraction, StO_2 is the microvascular blood oxygenation, $\mu_a^{HbO2}(\lambda)$ is the absorption coefficient of fully

oxygenated whole blood, and $\mu_a^{Hb}(\lambda)$ is the absorption coefficient of fully deoxygenated whole blood.

Fitting the data to our equation yields values for the local blood oxygenation (StO_2), local blood volume fraction (ρ), apparent average vessel diameter (D_{vessel}), and the Mie parameter (b). An additional parameter was chosen to appreciate the intensity of the scattering signal. This scattering amplitude parameter (a) corresponds to the amplitude of the scattering signal measured at 800nm wavelength, where blood absorption is minimal. Since the path length of the photons which have travelled through the tissue is short (apparent differential path length = 320 μm), the optical properties extracted from the differential reflectance signal characterize the most superficial layer of the tissue (roughly within 160 μm of the tissue surface).

Statistical analysis

The difference of optical parameters between the histological type of cancer were evaluated with a Kruskal-Wallis test (26). We chosen this test because of the small amount of data and because some optical parameters have a skewed distribution which makes the student t-test inappropriate. P-values less than 0.05 were regarded as significant.

RESULTS

Patients and bronchial lesions

Thirty-seven patients (27 men, 10 women with a median age of 68 ± 10 years) suffering from lung cancer were studied. In this patient population, a total of 47 endobronchial tumors were found by bronchoscopy and measured using DPS.

Reflectance spectra

Figure 2 illustrates an example of a DPS spectrum measured with the fiberoptic probe in contact with an endobronchial tumor. The parameters extracted from fitting Eq. (1) to the data are related to the spectral characteristics in the following way. The blood volume fraction (ρ) is proportional to the depth of the signal dips observed below 600nm corresponding to the absorption of light by haemoglobin. Both the local blood oxygenation (StO_2) and the apparent average vessel diameter (D_{vessel}) are related to the shape of the blood absorption dips below 600 nm. The accuracy of the fits for these two parameters is limited in case of small blood volumes. Therefore, we decided to restrain the calculation of these two parameters to spectra for which the blood volume fraction (ρ) was higher than 1% (18). Two parameters extracted from the spectra contain information about the scattering properties of the tissue, the Mie parameter (b) which corresponds to the slope of the DPS spectra, and the scattering amplitude parameter (a) which corresponds to the amplitude of the scattering signal at 800 nm. Both the slope (b) and amplitude (a) are hardly affected by the local blood volume fraction, blood saturation and vessel diameter since they are measured in a wavelength range where the absorption of blood is negligible.

Global results in lung cancer

Multiple measurements were systematically done on each bronchial tumor in order to take into account the intra-lesion heterogeneity. The optical parameters extracted from all the spectra measured on the same lesion were averaged and these averaged values were used to optically characterise each bronchial lesion.

In comparison with values measured in normal bronchial mucosa (19), lung tumors are characterized (average ± standard deviations) by a low blood oxygen saturation ($StO_2 = 49.8 \pm 24.8\%$, n=43 lesions), a large average vessel diameter ($D_{vessel} = 22.3 \pm 14.7\mu m$, n=43 lesions), a high blood volume fraction ($\rho = 9.8 \pm 12.2\%$, n=47 lesions), a low scattering amplitude (a = 1.64 ± 0.88, n=47 lesions), and an unchanged scattering Mie parameter (b = -1.00 ± 0.19, n=47 lesions).

Results as a function of lung cancer histology

Table 1 shows average values and standard deviations of the 5 parameters measured in squamous cell carcinomas, adenocarcinomas, large cell undifferentiated carcinomas, and small cell carcinomas of the bronchial tree. The relatively high proportion of undifferentiated large cell carcinomas observed in our patient population may be explained by the limitation of our analysis to the proximal bronchial tree and by the use of bronchoscopic biopsies for the histological diagnosis. It is observed that, according to the cancer histological type, small cell and poorly differentiated large cell carcinomas are characterized by the lowest blood oxygenation (StO_2) (p=0.07 and p=0.05, respectively, in comparison with squamous cell carcinomas, using a Kruskall-Wallis test). No significant differences are observed between small cell and non-small cell carcinomas concerning the average vessel diameter (D_{vessel}). Blood volume fraction (ρ) trended lower in small cell carcinomas and undifferentiated large cell carcinomas, although this did not reach statistical significance. A higher Mie scattering

parameter (b) was observed in cases of small cell carcinomas (p=0.01 in comparison with both large cell and squamous cell carcinomas, using a Kruskall-Wallis test) but no difference in the scattering amplitude (a) was observed between the different histological types.

DISCUSSION

We studied hypoxia-related parameters using DPS technology in various types of lung cancer during bronchoscopy. Small-cell and poorly differentiated large cell carcinomas are associated with the lowest blood oxygenation and the lowest blood content in comparison with other lung cancer cell types. No difference in microvessel size is observed between the different types of carcinoma. These results may increase our knowledge of the oxygenation alterations occurring in lung cancer and may help to better define the prognosis and the therapeutic options of this disease.

The oxygenation of microvascular blood (StO_2) was lower in cases of small-cell carcinomas and undifferentiated large cell carcinomas in comparison with squamous cell carcinomas and adenocarcinomas. Small-cell carcinomas represent one of the more aggressive types of lung cancer (22). On a cellular level, small-cell carcinomas are characterized by a high proliferation rate with a high mitotic count (27). Such a rapid cell division rate is associated with an increase in cell metabolism and consequently an increase in oxygen consumption (8). Because the oxygenation of blood in the tissues microcirculation is related to the consumption of oxygen by cells, the low blood oxygenation measured in small cell carcinomas may be explained by a higher cell metabolism and oxygen consumption of these kinds of tumor cells.

Concerning the organisation of the tumor microcirculation, small cell carcinomas and undifferentiated large cell carcinomas were associated with the lowest blood volume fraction (although this difference did not reach statistical significance) but no difference in microvessel diameters was observed. However, the latter may at least in part be caused by the low signal-to-noise ratio below 435 nm. The measured reflectance signal is affected by the size of the blood vessels most notably around 420 nm; the large noise in that wavelength region reduces the accuracy in the fit of the vessel diameter considerably. Tissue blood

68

content depends on both the size and the density of microvessels. Although DPS does not provide a direct measure of the microvessel density (MVD), the lack of differences observed in the microvessel size between the different lung cancer cell types argues for a smaller density of microvessels in cases of tumors with a low blood volume fraction. Such results suggest a poorer organisation of the microcirculation in cases of small-cell carcinomas. This is in agreement with our histological findings. Figure 3 illustrates typical sections of bronchial biopsies obtained from different lung cancer cell types, stained with anti-CD34 to highlight the status of their vasculature. Small-cell carcinoma (Fig. 3A) is characterized by a small number of microvessels, often squeezed by the high amount of surrounding tumor cells. Squamous cell carcinoma, on the other hand, shows more abundant and less squeezed microvessels (Fig. 3B). Unfortunately, a direct comparison between our measured parameters (blood volume fraction and microvessel diameter) and the histology of all lesions was technically not possible due to the small size of most of the bronchoscopic biopsies and the frequent modification of the tissue architecture induced by the biopsy forceps.

Concerning the scattering properties of the lung tumors, we observe that the scattering Mie parameter (b) was significantly smaller in cases of small-cell carcinomas in comparison with non small-cell lung carcinomas. Moreover, the lowest value of the scattering amplitude parameter (a) was also observed in cases of small cell carcinomas, although this difference did not reach a statistical significance. These results suggest that, in cases of small-cell carcinomas, several changes occur in both the size (related to the (b) parameter) and the concentration (related to the (a) parameter) of cellular light scatterers. The exact dependence of the scattered signal on the intracellular composition is only partially understood. Suspected cellular scatterers include the cytoplasmic membrane, the nucleus, and intra-cytosolic organelles. Recent reports suggest that intracellular particles of sizes smaller than 2μm, such as mitochondria, may contribute mostly to the backscattering of light (28-31). Small-cell

carcinoma is a malignant epithelial tumor with the cytologic features of scant cytoplasm, finely granular chromatin, absent nucleoli, and frequent mitosis. These round-to-oval cells have a high nucleus-to-cytoplasm ratio (27). Therefore, the changes in the scattering properties observed in small-cell carcinomas could be related to the changes occurring in their cytosolic organisation and especially in their mitochondrial content. However, further research into the scattering properties of tissue is required in order to confirm the relation between the optical properties of lung cancer cells and their cytosolic content.

We observed that lung cancer types with a poor prognosis, i.e. small-cell and undifferentiated large cell carcinomas, are characterised by the lowest blood oxygenation and the lowest blood content. A relation between tumor hypoxia and some prognostic factors of solid cancers has already been reported in various kinds of tumors. Tumor hypoxia has been associated with a lower survival, a higher invasiveness and a higher risk of regional and distant metastases in cervical carcinoma (2-5), head and neck carcinoma (6, 7) and soft-tissue sarcoma (32). The association of tumor hypoxia with a bad prognosis has been related to cell phenotype modifications induced by hypoxia (1). Indeed, hypoxia modifies both the genomic and the proteomic content of cancerous cells (8, 33). These molecular changes modify the expression of proteins involved in the regulation of tumor growth such as pro-apoptotic, pro-angiogenic, and growth factors, but also of proteins influencing the invasiveness and metastatic spread capacity of tumors (33-35). It would therefore be interesting to correlate our measurements not only with histology, but also with patient survival. Unfortunately, the short follow-up in our patient population does not allow us to conclude on the impact of bronchial tumor hypoxia on patient prognosis at this point. The relation between the DPS measurements, the patient survival, and possibly the sensitivity of tumors to therapy will be reported in a separate paper.

Tumor hypoxia arises due to a heterogeneous process that depends on several factors such as the structure of the tumor microcirculation, the quality of the blood flow in the microcirculation, the capacity of oxygen to diffuse from the microvessels to the cancerous cells, and the oxygen consumption rate of the cancerous cells (1, 8). The blood oxygenation (StO_2) extracted from our spectra is different from the tissue tumor oxygenation (tPO_2) measured with chemical techniques such as polarographic electrodes. However, previous authors have reported, in a human tumor xenograph model, that a low tissue tumor oxygenation was associated with a low blood content and a low blood oxygenation (36). Moreover, the hypoxia measured in endobronchial tumors using DPS is in agreement with the hypoxia measured in lung tumors using PET and SPECT technology (15, 16). Finally, DPS studies the most superficial layer (first 150 μm) of the bronchial mucosa allowing the analysis of localized intra-epithelial carcinomas. In case of larger tumors, DPS informs only about the superficial layer of the endobronchial extension of the lung cancer. The relation between the microvascular oxygenation of the tumor periphery and of the centre of solid tumor is poorly known. The combination of DPS and functional imaging technology may be a suitable way to study this relation *in vivo*.

In conclusion, the hypoxia-related parameters measured in endobronchial tumors using DPS are related to the cancer cell types. Poor prognosis tumors such as small-cell carcinomas are characterized by a low blood oxygenation and a low blood volume. These results may be explained by the higher proliferation rate characterizing this kind of tumor. Potential applications of DPS could be to characterize these aggressive tumors non-invasively during bronchoscopy, in order to determine the optimal therapeutic strategy. Oxygen-dependent therapies such as radiotherapy and photodynamic therapy, but also more recently developed hypoxia- or angiogenesis-targeted therapies may benefit greatly from this new technology. Finally, DPS is not restricted to measure hypoxia-related parameters in superficial tissues

such as bronchial mucosa only, but was recently succesfully applied on breast tissue using a modified fiberoptic needle-probe as well (37). Therefore, DPS technology opens up a wide field of *in vivo* investigation into hypoxia-related parameters in various organs.

LEGENDS OF THE FIGURES

Figure 1: Set-up used for the DPS-measurement in the bronchial tree. The bifurcated optical fiber-probe is small enough to be led through the working channel of the bronchoscope. A tungsten-halogen lamp is used to light up the bronchial mucosa through the dc-fiber and the remitted light collected in the dc- and c- fiber is analysed in a dual channel spectrometer.

Figure 2: Illustration of DPS spectra, fits, and residues (= spectrum minus fit) measured on a cancerous bronchial tumor. The blood volume fraction (ρ) is proportional to the depth of the signal dips observed below 600nm corresponding to the absorption of light by haemoglobin. Both the local blood oxygenation (StO_2) and the apparent average vessel diameter (D_{vessel}) are related to the shape of the blood absorption dips below 600 nm. Two scattering parameters are the Mie parameter (b) which corresponds to the slope of the DPS spectra, and the scattering amplitude parameter (a) which corresponds to the amplitude of the scattering signal at 800 nm.

Figure 3: Histological sections of bronchial biopsies obtained from different types of lung cancer. The slides were stained with a monoclonal antibody against CD34 to highlight the vasculature and counterstained with Harris' hematoxylin. Small-cell carcinoma (Fig.3A) is characterized by rare and squeezed microvessels in comparison with squamous cell carcinoma (Fig.3B) showing more abundant and less squeezed microvessels (original magnification x 400).

REFERENCES

1. Evans SM, Koch CJ. Prognostic significance of tumor oxygenations in humans. Cancer Lett 2003;195:1-16.

2. Fyles AW, Milosevic M, Wong R, Kavanagh M-C, Pintilie M, Sun A, et al. Oxygenation predict radiation response and survival in patients with cervix cancer. Radiother Oncol 1998;48:149-156.

3. Höckel M, Schlenger K, Aral B, Mitze M, Schaffer U, Vaupel P. Association between tumor hypoxia and malignant progression in advanced cancer of the uterine cervix. Cancer Res 1996;19:4509-4515.

4. Höckel M, Knoop C, Schlenger K, Vorndran B, Baussmann E, Mitze M, et al. Intratumoral pO2 predicts survival in advanced cancer of the uterine cervix. Radiother Oncol 1993;26:45-50.

5. Sundfor K, Lyng H, Rofstad EK. Tumor hypoxia and vascular density as predictors of metastasis in squamous cell carcinoma of the uterine cervix. Br J Cancer 1998;78:822-827.

6. Brizel DM, Sibley GS, Prosnitz LR, Scher RL, Dewhirst MW. Tumor hypoxia adversely affects the prognosis of carcinoma of the head and neck. Int J Radiat Oncol Biol Phys 1997;38:285-289.

7. Nordsmark M, Overgaard M, Overgaard J. Pretreatment oxygenation predicts radiation response in advanced cell carcinoma of the head and neck. Radiother Oncol 1996;41:31-39.

8. Höckel M, Vaupel P. Tumor hypoxia: definitions and current clinical biologic, and molecular aspects. J Natl Cancer Inst 2001;93:266-276.

9. Kayser G, Baumhakel JD, Szoke T, ITrojan I, Riede U, Werner M, et al. Vascular diffusion density and survival of patients with primary lung carcinomas. Virchows Arch 2003;442:462-467.

10. Fontanini G, Faviana P, Lucchi M, Boldrini L, M, A., Camacci T, et al. A high vascular count and overexpression of vascular endothelial growth factor are associated with unfavourable prognosis in operated small cell lung carcinoma. Br J Cancer 2002;86:558-563.

11. Meert A-P, Paesmans M, Martin B, Delmotte P, Berghmans T, Verdebout J-M, et al. The role of microvessel density on the survival of patients with lung cancer: a systematic review of the literature with meta-analysis. Br J Cancer 2002;87:694-701.

12. Giatromanolaki A, Koukourakis MI, Sivridis E, Turley H, Talks K, Pezzela F, et al. Relation of hypoxia inducible factor 1a and 2a in operable non-small cell lung cancer to angiogenic/molecular profile of tumours and survival. Br J Cancer 2001;85:881-890.

13. Swinson DEB, Jones JL, Richardson D, Wykoff C, Turley H, Pastorek J, et al. Carbonic anhydrase IX expression, a novel surrogate marker of tumor hypoxia, is asssociated with a poor prognosis in non-small-cell lung cancer. J Clin Oncol 2003;21:473-482.

14. Kim SJ, Rabbani ZN, Vollmer RT, Schreiber E-G, Oosterwijk E, Dewhirst MW, et al. Carbonic anhydrase IX in early-stage non-small cell lung cancer. Clin Cancer Res 2004;10:7925-7933.

15. Urtasun RC, Parliament MB, McEwan AJ, Mercer JR, Manan RH, Wiebe LI, et al. Measurement of hypoxia in human tumours by non-invasive spect imaging of iodoazomycin arabinoside. Br J Cancer 1996;27:S209-S212.

16. Rasey JS, Koh W-J, Evans ML, Peterson LM, Lewellen TK, Graham MM, et al. Quantifying regional hypoxia in human tumors with positron emission tomography of [18F]fluoromisonidazole: a pretherapy study of 37 patients. Int J Radiat Oncol Biol Phys 1996;36:417-428.

17. Amelink A, Sterenborg HJCM. Measurement of the local optical properties of turbid media by differential path-lenght spectroscopy. Appl Optics 2004;43:3048-3054.

18. Amelink A, Sterenborg HJCM, Bard MPL, Burgers SA. In vivo measurement of the local optical properties of tissue by use of differential path-length spectroscopy. Opt Lett 2004;29:1087-1089.

19. Bard MPL, Amelink A, Noordhoek-Hegt V, Graveland WJ, Sterenborg HJCM, Hoogsteden HC, et al. Measurement of hypoxia-related parameters in bronchial mucosa by use of optical spectroscopy. Am J Resp Crit Care Med 2005;February 11, as doi:10.1164/rccm.200501-046OC.

20. Beadsmoore CJ, Screaton NJ. Classification, staging and prognosis of lung cancer. Eur J Radiol 2003;45:8-17.

21. Janssen-Heijnen MLG, Coebergh J-WW. Trends in incidence and prognosis of the histological subtypes of lung cancer in North America, Australia, New Zealand and Europe. Lung Cancer 2001;31:123-137.

22. Simon GR, Wagner H, Physicians American College of Chest Physicians. Small cell lung cancer. Chest 2003;123(1 suppl):259S-271S.

23. Brambilla E, Travis WD, Colby TV, Corrinz B, Shimosato Y. The new World Health Association classification of lung cancer. Eur Respir J 2001;18:1059-1068.

24. Bard MPL, Amelink A, Skurichina M, den Bakkerd M, Burgers SA, van Meerbeeck JP, et al. Improving the specificity of fluorescence bronchoscopy for the analysis of neoplastic lesions of the bronchial tree by combination with optical spectroscopy: preliminary communication. Lung Cancer 2005;47:41-47.

25. van Veen RLP, Verkruysse W, Sterenborg HJCM. Diffuse-reflectance spectroscopy from 500 to 1060 nm by correction for inhomogeneously distributed absorbers. Opt Lett 2002;27:246-248.

26. Kruskal WH, Wallis WA. Use of ranks in one-criterion variance analysis. Journal Am Stat Assoc 1952;47:583-621.

27. Colby TV, Koss MN, Travis WD. Tumors of the Lower Respiratory Tract. In: Atlas of Tumor Pathology. Washington (DC): American Registry of Pathology; 1995.

28. Bartlett M, Huang G, Larcom L, Jiang H. Measurement of particle size distribution in mammalian cells in vitro by use of polarized light spectroscopy. Appl Optics 2004;43:1296-1307.

29. Beauvoit B, Chance B. Time-resolved spectroscopy of mitochondria, cells and tissue under normal and pathological conditions. Mol Cell Bioch 1998;184:445-455.

30. Mourant JR, Johnson TM, Carpenter S, Guera A, Aida T, Freyer JP. Polarized angular dependent spectroscopy of epithelial cells and epithelial cell nuclei to detremine the size scale of scattering structures. J Biomed Opt 2002;7:378-387.

31. Mourant JR, Johnson TM, Freyer JP. Characterizing mammalian cells and cell phantoms by polarized backscattering fiber-optic measurement. Appl Opt 2001;40:5114-5123.

32. Brizel DM, Scully SP, Harrelson JM, Layfield LJ, Bean JM, Prosnitz LR, et al. Tumor oxygenation predicts for the likehood of distant metastases in human soft tissue sarcoma. Cancer Res 1996;56:941-943.

33. Vaupel P, Kelleher DK, Höckel M. Oxygen status of malignant tumors: pathogenesis of hypoxia and significance for tumor therapy. Semin Oncol 2001;28:29-35.

34. Brown JM. The hypoxic cell: a target for selective therapy-eighteenth Bruce F. Cain memorial award lecture. Cancer Res 1999;59:5863-5870.

35. Chapman JD, Engelhardt EL, Stobbe CC, Schneider RF, Hanks GE. Measuring hypoxia and predicting tumor radioresistance with nuclear medicine assays. Radiother Oncol 1998;46:229-237.

36. Menon C, Polin GM, Prabakaran I, Hsi A, Cheung C, Culver JP, et al. An integrated approach to measuring tumor oxygen status using human melanoma xenografts as a model. Cancer Res 2003;63:7232-7240.

37. van Veen RLP, Amelink A, Menke-Pluymers M, van der Pol C, Sterenborg HJCM. Optical biopsy of breast tissue using differential path-length spectroscopy. Phys Med Biol 2005:in press.

Table 1: Average values and standard deviations of blood oxygenation (StO_2), vessel diameter (D_{vessel}), blood volume fraction (ρ), the Mie parameter (b), and the scattering amplitude parameter (a) measured in squamous cell carcinomas, adenocarcinomas, large cell undifferentiated carcinomas, and small cell carcinomas of the bronchial tree. The amount of lesions in each group is indicated in brackets.

	StO_2(%)	D_{vessel} (µm)	ρ(%)	b	a
Squamous cell carcinoma	(n=12) 64.6 ± 21.3	(n=12) 29.2± 20.7	(n=13) 15.9 ± 19.2	(n=13) -0.92 ± 0.22	(n=13) 1.71 ± 0.98
Adenocarcinoma	(n=9) 55.9 ± 23.8	(n=9) 21.1± 11.2	(n=9) 11.7 ± 8.6	(n=9) -1.00 ± 0.24	(n=9) 1.52 ± 0.69
Large cell undifferentiated carcinoma	(n=17) 39.6 ± 23.4§	(n=17) 18.3 ± 10.4	(n=19) 5.7 ± 6.4	(n=19) -1.00 ± 0.13*	(n=19) 1.70 ± 1.01
Small cell carcinoma	(n=5) 38.3 ± 22.7	(n=5) 21.8 ± 14.5	(n=6) 6.3 ± 4.9	(n=6) -1.16 ± 0.05*	(n=6) 1.49 ± 0.56

StO_2;microvascular blood saturation, D_{vessel}; vessel diameter, ρ; blood volume, b; Mie parameter, a; scattering amplitude. §p= 0.05, * p=0.001, Kruskall-Wallis test.
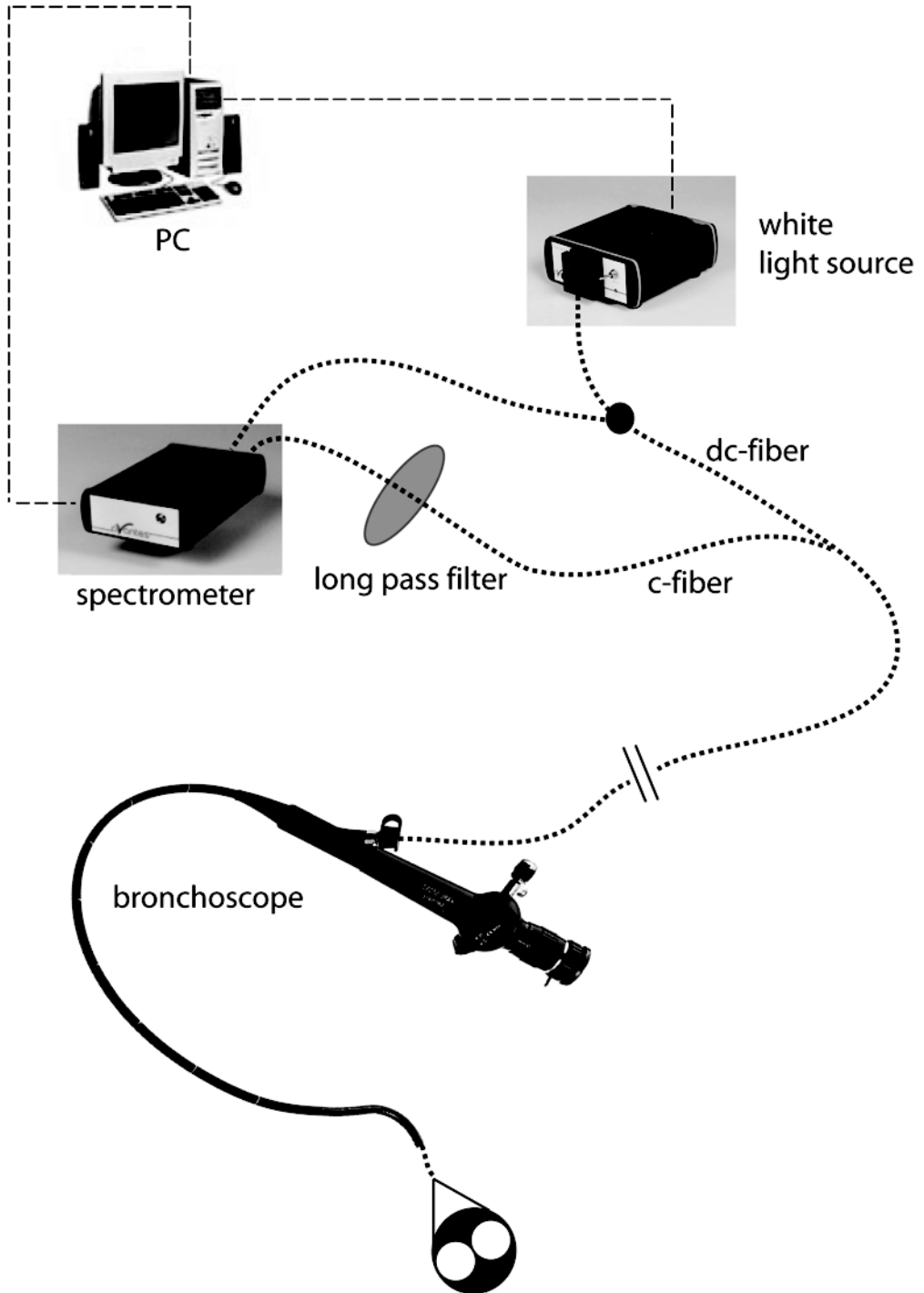
Figure 1

Figure 2

Figure 3

CHAPTER 6

Improving the specificity of fluorescence bronchoscopy for the analysis of neoplastic lesions of the bronchial tree by combination with optical spectroscopy: preliminary communication

Bard M.P.L., A. Amelink, M. Skurichina, M. den Bakker, S.A. Burgers, J.P. van Meerbeeck, R.P.W. Duin, J.G.J.V. Aerts, H.C. Hoogsteden, H.J.C.M. Sterenborg
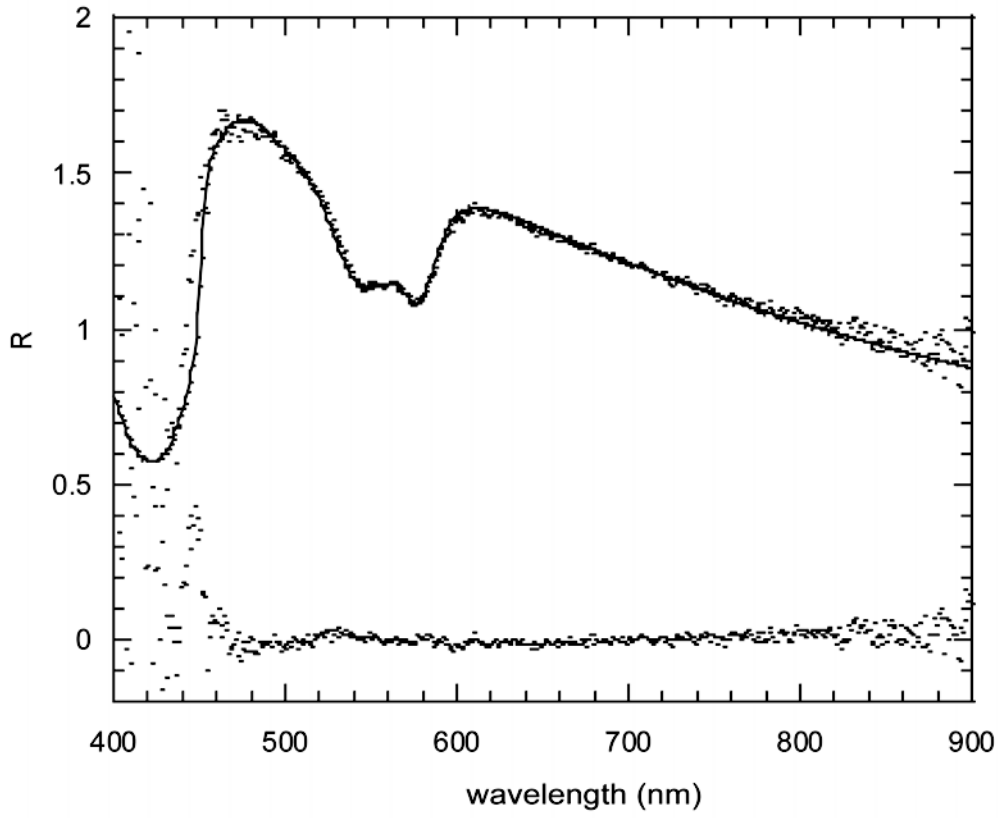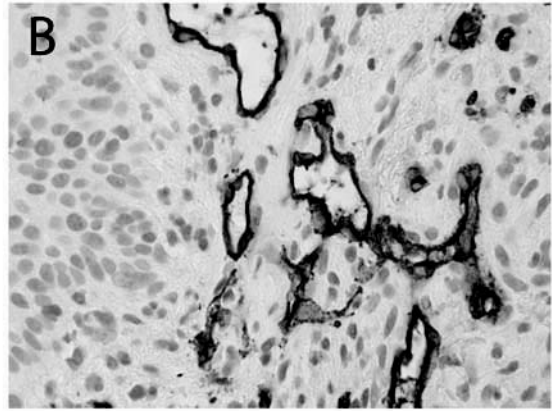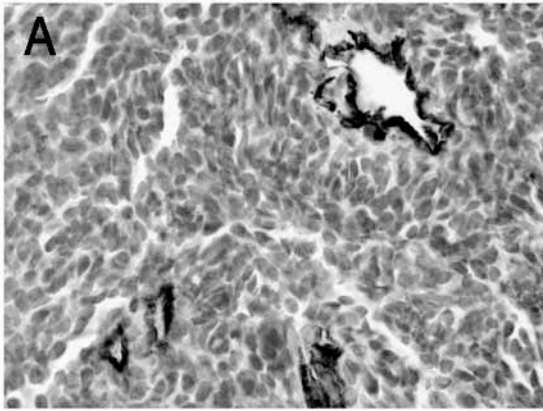
Improving the specificity of fluorescence bronchoscopy for the analysis of neoplastic lesions of the bronchial tree by combination with optical spectroscopy: preliminary communication

Martin P.L. Bard[a,*], Arjen Amelink[b], Marina Skurichina[c],
Michael den Bakker[d], Sjaak A. Burgers[a,1], Jan P. van Meerbeeck[a,2],
Robert P.W. Duin[c], Joachim G.J.V. Aerts[a,e], Henk C. Hoogsteden[a],
Henricus J.C.M. Sterenborg[b]

[a] *Department of Respiratory Diseases, Erasmus Medical Center, H-Ee2253a, P.O. Box 1738,
3000 DR Rotterdam, The Netherlands*
[b] *Photodynamic Therapy and Optical Spectroscopy Research Program, Department of Radiation Oncology,
Erasmus Medical Center, Rotterdam, The Netherlands*
[c] *Faculty of Electrical Engineering, Mathematics and Computer Science, Delft University of Technology,
The Netherlands*
[d] *Department of Pathology, Erasmus Medical Center, Rotterdam, The Netherlands*
[e] *Department of Respiratory Diseases, Sint Franciscus Hospital, Rotterdam, The Netherlands*

Summary Detection of malignancies of the bronchial tree in an early stage, such as carcinoma in situ (CIS), augments the cure rate considerably. It has been shown that the sensitivity of autofluorescence bronchoscopy is better than white light bronchoscopy for the detection of CIS and dysplastic lesions. Autofluorescence bronchoscopy is, however, characterized by a low specificity with a high rate of false positive findings. In the present paper we propose to combine autofluorescence bronchoscopy with optical spectroscopy to improve the specificity of autofluorescence imaging, while maintaining the high sensitivity. Standard autofluorescence bronchoscopy was used to find suspect lesions in the upper bronchial tree, and these lesions were

* Corresponding author. Tel.: +31 10 408 7697; fax: +31 10 408 9453.
  E-mail address: m.bard@erasmusmc.nl (M.P.L. Bard).
[1] Present address: Department of Respiratory Diseases, Netherlands Cancer Institute, Amsterdam, Netherlands.
[2] Present address: Department of Respiratory Diseases, University Hospital Gent, Belgium.

subsequently characterized spectroscopically using a custom made fiberoptic probe. Autofluorescence spectra of the lesions as well as reflectance spectra were measured. We will show in this preliminary report that the addition of either of these spectroscopic techniques decreases the rate of false positives findings, with the best results obtained when both spectroscopic modalities are combined.

1. Introduction

White light and fluorescence endoscopic imaging are commonly used for the detection of proximal endobronchial lesions. The sensitivity of autofluorescence bronchoscopy has shown to be better than white light bronchoscopy for the detection of carcinoma in situ (CIS) and dysplastic lesions [1—4]. Fluorescence bronchoscopy is, however, characterized by a low specificity with a high rate of false positive findings. This induces unnecessary biopsies at greater costs and longer duration of the examination. Additional techniques are therefore needed to improve the specificity of autofluorescence imaging.

Light induced spectroscopic techniques are potential tools for differentiation of pathological from normal tissue [5—17]. After illumination of the tissue with a light source, the photons diffuse in the tissue and a fraction of the photons is re-emitted from the tissue surface, enabling non-invasive spectroscopic measurements. Autofluorescence spectra are primarily determined by the fluorescent chromophores naturally present in the tissue (NADH, collagen, elastin and keratin) and hence reflect the chemical composition of the tissue. However, the fluorescence spectra are reshaped by absorption and scattering of light in the tissue. These optical artefacts greatly influence the shape of the measured autofluorescence spectra and it is still not determined which of the tissue properties actually contain the information relevant to cancer diagnostics. Diffuse reflectance spectroscopy does not employ fluorescent chromophores, but directly measures how the spectral composition of white light changes on its path through tissue by scattering and absorption events. In the present paper we evaluate whether the addition of either of these spectroscopic techniques can improve the specificity of autofluorescence bronchoscopy for the detection of endobronchial lesions.

2. Materials and methods

2.1. Study population

Patients with known or suspected malignancies of the lung and with a medical indication for a bronchoscopy were invited to participate in this study. All patient were more than 18 years old and signed informed consent. The study was approved by the Medical Ethics Review Board of the Erasmus Medical Center Rotterdam.

2.2. Examination procedure

White light and autofluorescence imaging of the bronchial tree was performed with a commercially available flexible fluorescence bronchoscope (Karl Storz 11004BI, Germany). All lesions that appeared abnormal at blue and/or white imaging were measured and additionally some spectra of macroscopically normal bronchial mucosa were taken. The probe was led through the working channel of the bronchoscope and placed in gentle contact with the bronchial mucosa. The duration of autofluorescence and reflectance spectral acquisition was less than one second during which the light source of the bronchoscope was switched off. Biopsy specimens of the measured areas were transported in formaldehyde and fixed in paraffin. Hematoxylin—eosin stained slides were evaluated without knowledge of the spectroscopic results. The pathological diagnoses were coded referring to the World Health Organization Lung Cancer classification [18].

2.3. Autofluorescence and diffuse reflectance probe

Spectra were measured using a custom-made instrument using a fiberoptic probe small enough to be led through the 2.8 mm working channel of the bronchoscope (Fig. 1). The fiber-probe consisted of three identical fibers, 440 μm in diameter with a core of 400 μm, fitted into a small metal tube. One fiber was used for blue light illumination, one for white light illumination and the third one for the detection of both autofluorescence and reflectance emission (Fig. 1). An ultraviolet/blue laser (407 nm, Nichia, Tokio, Japan) and a tungsten-halogen lamp (Avantes HL-2000-FHSA, Eerbeek, The Netherlands) were used to light up the bronchial mucosa through the probe and the reflected light from the bronchial mucosa was analyzed in one channel of a dual-
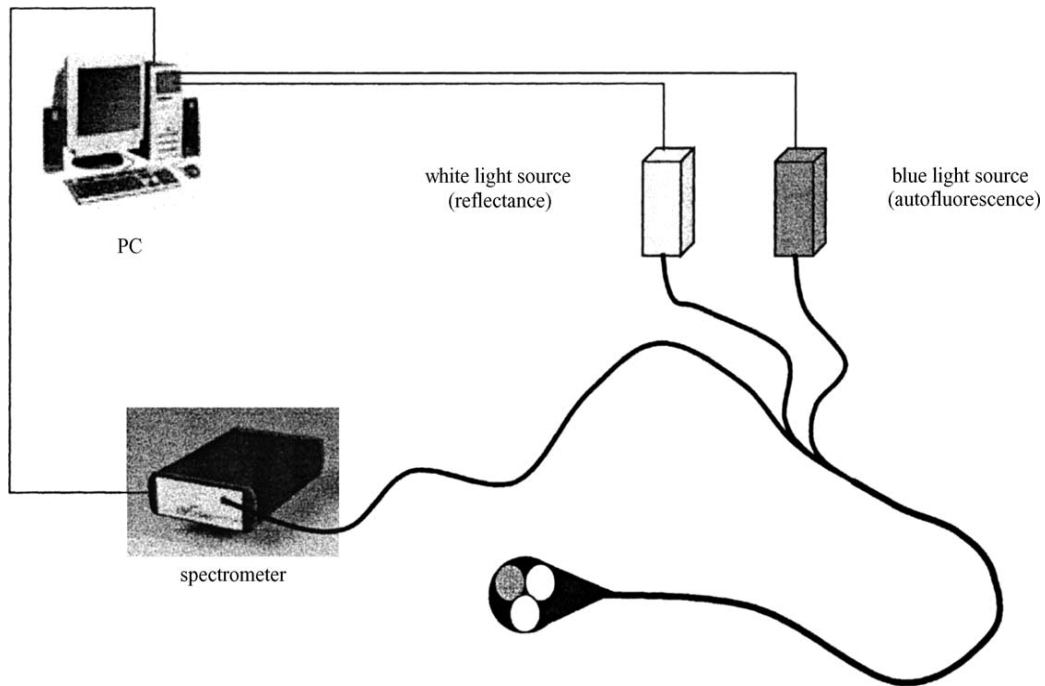
Fig. 1. Schematic diagram of the experimental set-up. Spectra were measured with a custom-made instrument using a fiberoptic probe small enough to be led through the 2.8 mm working channel of the bronchoscope.

channel spectrometer (Avantes, SD2000, Eerbeek, The Netherlands).

2.4. Data analysis

Reflectance spectra were pre-processed by dividing the spectra by the spectrum of a white reflective tile (Avantes WS-2, Eerbeek, The Netherlands) with reflection coefficient >99% over the measured wavelength range and normalizing the spectra to unity at 800 nm. At this wavelength, blood absorption plays only a minor role and the spectra in this wavelength region are generally smooth.

To analyze the signals principal component analysis was applied on all 85 spectra [19]. We retained 10 leading principal components that describe 99.99% of the total variation of data. To evaluate the quality of discrimination between healthy and malignant tissues, linear discriminant analysis was applied. Specifically, we used the Karhunen—Loeve Linear Classifier also known as the regularized linear discriminant function. For both spectroscopic modalities the sensitivity and the specificity of the classifier was calculated using the leave-one-out method with different threshold (cut-off) values to distinguish healthy from malignant tissue. The sensitivity and specificity can be represented as receiver—operator characteristics (ROC) curves by plotting (1-specificity) values against corresponding values of sensitivity. The areas under different

ROC curves were then compared in order to make a fair judgment of the effectiveness of different methods without being constricted to single values of sensitivity and specificity, which largely depend on the cut-off value chosen to distinguish normal from malignant tissue. Next, the cut-off value with smallest classification error (corresponding to the highest combined sensitivity and specificity) was chosen for each spectroscopic modality, and the classification of the subset of spectra measured on lesions observed by autofluorescence bronchoscopy was evaluated.

3. Results

3.1. Bronchoscopic examination and spectral measurements

Measurements were performed in 21 patients (13 men and 8 women with a median age of 60 years). For all patients, tolerance was excellent and no adverse events were reported. A total of 21 bronchial areas of abnormal fluorescence were found using autofluorescence bronchoscopy. Due to the relatively small data set we decided to cluster the lesions into two groups: the ''high-grade lesion'' group ($n = 7$) including invasive carcinoma ($n = 6$), and carcinoma in situ/severe dysplastic mucosa (n

86
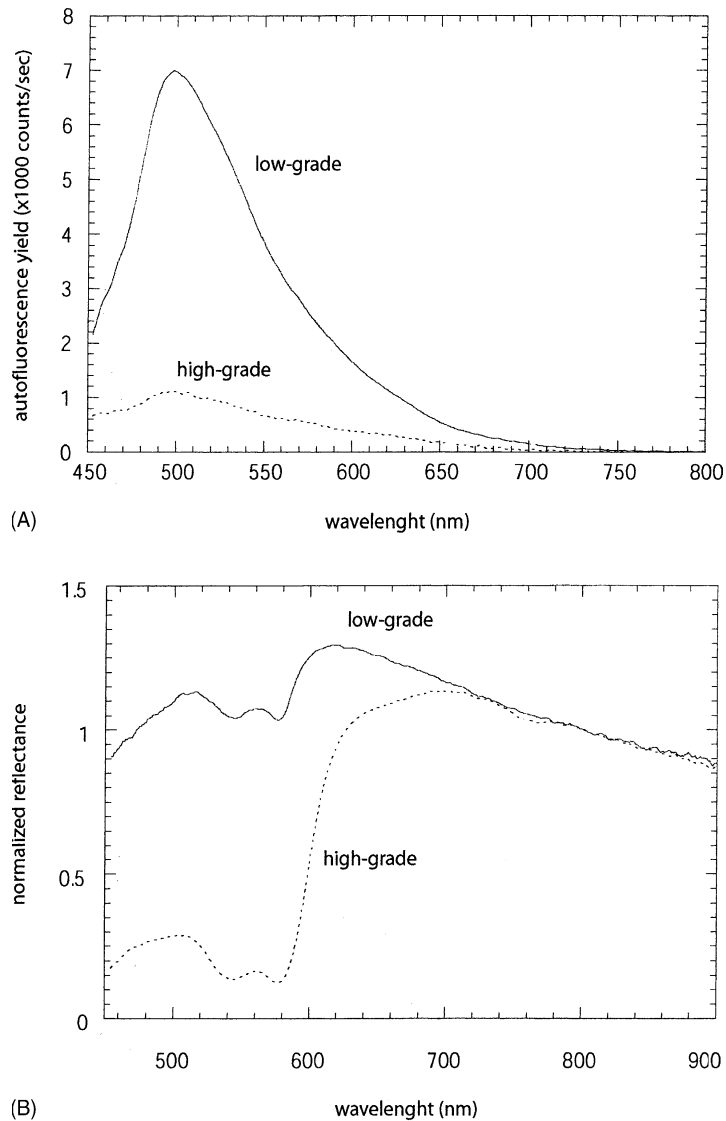
Fig. 2. Typical spectra of low-grade (solid line) and high-grade (dotted line) lesions of the bronchial mucosa for autofluorescence (A) and diffuse reflectance (B) spectroscopy.

= 1), and the "low-grade lesion" group ($n = 14$) including normal ($n = 7$) and metaplastic/low grade dysplastic mucosa ($n = 7$).

One single paired (autofluorescence spectroscopy (AFS) and diffuse reflectance spectroscopy (DRS)) measurement was mostly done on each suspicious endobronchial location. In five locations (four normal, one invasive carcinoma) spectra were measured twice and in two locations (one normal, one invasive carcinoma) three times. To increase the number of spectra for the training set for the linear classifier, 54 additional spectra of normal bronchial epithelium and one additional spectrum of an invasive carcinoma (observed using white light imaging) measured in the same 21 patients were used. Thus, for both AFS and DRS, 74 and 11 spectra were obtained from low-grade and high-grade lesions, respectively.

3.2. Data analysis

Typical autofluorescence and reflectance spectra are illustrated in Fig. 2A and B, respectively. For AFS, the average intensity of the spectra of low-grade tissue was larger than of high-grade tissue (Fig. 2A). For DRS, the spectra of low-grade tissue generally have a higher intensity in the left part (lowest wavelengths) of the spectra compared to high-grade tissue (Fig. 2B).

For both spectroscopic modalities the ROC curves were calculated for the Karhunen–Loeve

Fig. 3. Receiver—operator characteristics curves for the two different spectroscopic modalities. Circles and solid line: autofluorescence spectroscopy, squares and dotted line: diffuse reflectance spectroscopy.
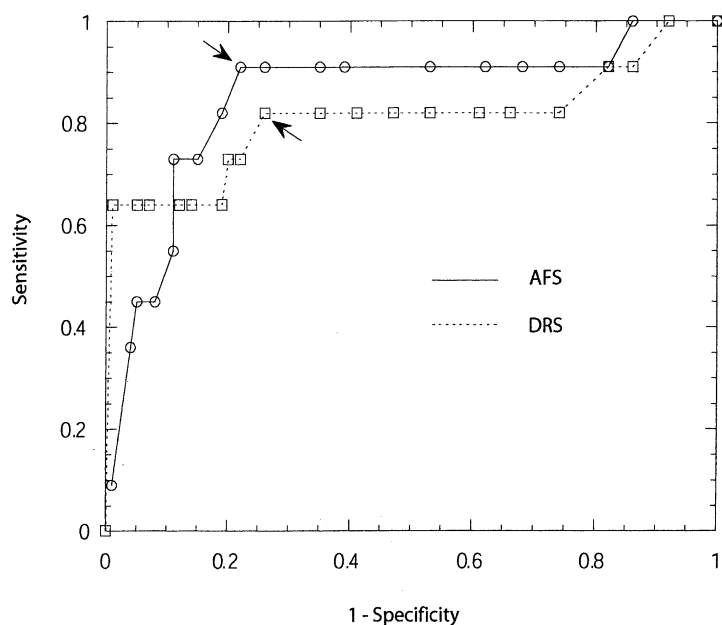
Table 1   Classification results of the test set (21 bronchial areas of abnormal fluorescence)

		AF-imaging		AFS		DRS		AFS + DRS	
		Normal	Abnal.	Normal	Abnal.	Normal	Abnal.	Normal	Abnal.
Path.	Low-grade	—	14	9	5	10	4	10	4
	High-grade	—	7	1	6	2	5	0	7
PPV (%)			33		55		55		64[a]

AF: autofluorescence, AFS: autofluorescence spectroscopy, DRS: diffuse reflectance spectroscopy, path.: pathology, PPV: positive predictive value, abnal.: abnormal.
[a] $P < 0.005$ (Fischer exact test).

Linear Classifier using the leave-one-out approach. These curves are presented in Fig. 3. The areas under the ROC curves are 0.85 for AFS and 0.80 for DRS. The highest combined sensitivity and specificity (indicated by the arrows in Fig. 3) are 91% and 78%, respectively, for AFS and 82% and 74%, respectively, for DRS. However, these numbers include the 54 spectra of visually normal tissue that have been used for the training set. The clinically relevant data set consists only of spectra measured on the 21 lesions found by autofluorescence imaging. When only the classification results of this subset of spectra are analyzed, we obtain the results shown in Table 1. For AFS and DRS separately, the classification of each lesion was established following the principle of simple majority voting, i.e., for each lesion with a single spectral measurement the lesion was classified accordingly, for each lesion with two spectral measurements the lesion was classified as low-grade when both spectra were classified as low-

grade and classified as high-grade when at least one of the spectra was classified as high-grade, and for each lesion with three measurements the majority of spectral classifications determined the classification of the lesion. For the combination of AFS and DRS, the same principles applied based on the separate spectral classifications, e.g., for a lesion with 2 AFS and 2 DRS spectra the majority of four spectral classifications determined the classification of the lesion, and in the absence of a majority a lesion was classified as high-grade.

4. Discussion

Autofluorescence bronchoscopy is at the moment the screening technique with the best sensitivity for detection of superficial bronchial carcinoma but is characterized by a low specificity with a high

88

rate of false positive findings. This paper builds on these previous findings as we set out to improve the specificity of autofluorescence imaging by combining it with optical spectroscopy. The performance of autofluorescence spectroscopy, diffuse reflectance spectroscopy as well as the combination of both has been analyzed.

Autofluorescence spectroscopy sacrifices the spatial resolution of the autofluorescence signal but allows the examination of fluorescence spectra on a large wavelength range. Analysis of the intensity, shape, and time-resolved dynamics of autofluorescence spectra gives additional information on the morphological and chemical changes occurring in tissues [20]. AFS has already been studied both ex vivo and in vivo in several optically accessible organs as the gut [7,8], mouth [10], bronchial tree [11–13], bladder [17] and skin [15]. Most of these studies reported a decrease of autofluorescence intensity in unhealthy tissue. Our data confirm these previous reports. The average intensity of the autofluorescence spectra was markedly decreased in high-grade mucosa compared to low-grade mucosa.

In addition to autofluorescence spectra, our instrument was able to measure reflectance spectra. These spectra corresponded to the light re-emitted from the tissue surface after illumination with a white light source. The reflectance spectra are sensitive to the absorption and scattering coefficients of tissue and particularly allow us to evaluate the influence of absorbers in the autofluorescence signal. In our preliminary analysis, we find that the area under the ROC curves for AFS and DRS are approximately equal with good classification results. This suggests that the optical properties of tissue are the most important parameters for distinguishing low-grade from high-grade mucosa, although the intrinsic fluorescence (=fluorescence corrected for spectral changes induced by the optical properties of the tissue) must contain some information as well given the slightly higher ROC area under the AFS curve. Most likely, these results are a consequence of the blood content of the different tissue types. Tumors are generally more vascularized than healthy tissue. Analysis of the absorption properties of blood shows that it is the dominant absorber in the wavelength range 350–600 nm. Since the autofluorescence excitation wavelength, 407 nm, and the autofluorescence emission peak wavelength, 500 nm, are both well within the wavelength region where blood absorbs strongly, the autofluorescence spectra are strongly affected by the presence of blood. Similarly, the left part (wavelengths < 600 nm) of the diffuse reflectance spectra is also strongly domi-

nated by blood absorption. It is therefore reasonable that the high-grade spectra are characterized by small AFS intensities and low DRS intensities at small wavelengths. The fact that the classification results of both AFS and DRS are good is therefore strong evidence that blood content plays an important role in the distinction between low-grade and high-grade tissue. Whether this is also the case for the distinction between normal and premalignant tissue must be investigated in a larger patient group.

When we study the subset of spectral data corresponding to the spectra of lesions found by autofluorescence bronchoscopy, we confirm what others have previously found, i.e., a large rate of false-positives and a small positive predictive value (PPV = 33%). Autofluorescence spectroscopy alone was able to improve the PPV to 55% but resulted in one false negative finding (out of seven high-grade lesions), while diffuse reflectance spectroscopy alone improved the PPV to 55% as well but at the cost of two false negative findings. Interestingly, the combination of AFS and DRS resulted in a significant ($P <$ 0.005, Fischer exact test) increase of the PPV to 64% without sacrificing the high sensitivity of autofluorescence imaging. This suggests that the spectroscopic techniques are to some degree complementary and that information regarding tissue pathology may be found in both the chemistry (AFS) and morphology (DRS) of the tissue.

5. Conclusion

We developed an easy-to-use and well-tolerated tool allowing the measurement of autofluorescence and reflectance spectra during a standard bronchoscopy procedure. A preliminary evaluation of the techniques shows that the combination of autofluorescence spectroscopy and diffuse reflectance spectroscopy significantly improves the positive predictive value of autofluorescence imaging without sacrificing its sensitivity. However, the analysis of more spectra is needed to draw conclusions on the application of AFS and DRS in the detection of premalignant endobronchial lesions. A prospective study using the same methodology in a larger patient group is therefore currently under way.

Acknowledgements

References

[1] Hirsch FR, Prindiville SA, Miller YE, et al. Fluorescence versus white-light bronchoscopy for detection of preneoplastic lesions: a randomized study. J Natl Cancer Inst 2001;93:1385—91.

[2] Kurie JM, Lee JS, Morice RC, et al. Autofluorescence bronchoscopy in the detection of squamous metaplasia and dysplasia in current and former smokers. J Natl Cancer Inst 1998;90:991—5.

[3] Lam S, Kennedy T, Unger M, et al. Localization of bronchial intraepithelial neoplastic lesions by fluorescence bronchoscopy. Chest 1998;113:696—702.

[4] Sutedja TG, Venmans BJ, Smit EF, et al. Fluorescence bronchoscopy for early detection of lung cancer. A clinical perspective. Lung Cancer 2001;34:157—68.

[5] Wagnières GA, Star WM, Wilson BC. In vivo fluorescence spectroscopy and imaging for oncological applications. Photochem Photobiol 1998;68:603—32.

[6] Wang C-Y, Chiang HK, Chen C-T, et al. Diagnosis of oral cancer by light induced autofluorescence spectroscopy using double excitation wavelengths. Oral Oncol 1999;35:144—50.

[7] Mayinger B, Horner P, Jordan M, et al. Endoscopic fluorescence spectroscopy in the upper GI tract for the detection of GI cancer: initial experience. Am J Gastroenterol 2001;96:2616—21.

[8] Mycek M-A, Schomacker KT, Nishioka NS. Colonic polyp differentiation using time-resolved autofluorescence spectroscopy. Gastrointest Endosc 1998;48:390—4.

[9] Georgakoudi I, Jacobson BC, van dam J, et al. Fluorescence, reflectance, and light-scattering spectroscopy for evaluating dysplasia in patient with Barrett's esophagus. Gastroenterology 2001;120:1620—9.

[10] van Staveren HJ, van Veen RLP, Speelman OC, et al. Classification of clinical autofluorescence spectra of oral leukoplakia using an artificial neural network: a pilot study. Oral Oncol 2000;36:286—93.

[11] Hung J, Lam S, LeRiche JC, et al. Autofluorescence of normal and malignant bronchial tissue. Lasers Surg Med 1991;11:99—105.

[12] Kusunoki Y, Imamura F, Uda H, et al. Early detection of lung cancer with laser-induced fluorescence endoscopy and spectrofluorometry. Chest 2000;118:1776—82.

[13] Zellweger M, Grosjean P, Goujon D, et al. In vivo autofluorescence spectroscopy of human bronchial tissue to optimize the detection and imaging of early cancers. J Biomed Opt 2001;6:41—51.

[14] Zonios G, Bykowski J, Kollias N. Skin melanin, hemoglobin, and light scattering properties can be quantitatively assessed in vivo using diffuse reflectance spectroscopy. J Invest Dermatol 2001;117:1452—7.

[15] Brancaleon L, Durkin AJ, Tu JH, et al. In vivo fluorescence spectroscopy of nonmelanoma skin cancer. Photochem Photobiol 2001;73:178—83.

[16] Georgakoudi I, Sheets EE, Müller MG, et al. Trimodal spectroscopy for the detection and characterization of cervical precancers in vivo. Am J Obstet Gynecol 2002;186:374—82.

[17] Koenig F, McGovern FJ, Enquist H, et al. Autofluorescence guided biopsy for the early diagnosis of bladder carcinoma. J Urol 1998;159:1871—5.

[18] Brambilla E, Travis WD, Colby TV, et al. The new World Health Association classification of lung cancer. Eur Respir J 2001;18:1059—68.

[19] Jain AK, Duin RPW, Mao J. Statistical pattern recognition: a review. IEEE Trans Pattern Anal Machine Intell 2000;22:4—37.

[20] Ramanujam N. Fluorescence spectroscopy of neoplastic and non-neoplastic tissues. Neoplasia 2000;2:89—117.

CHAPTER 7

Combination of optical spectroscopy and autofluorescence bronchoscopy for the detection of malignant lesions of the bronchial tree: final report

Bard M.P.L., A. Amelink, M. Skurichina, V. Noordhoek Hegt, R.P.W. Duin, H.C. Hoogsteden, H.J.C.M. Sterenborg, J.G.J.V. Aerts
submitted

COMBINATION OF AUTOFLUORESCENCE BRONCHOSCOPY AND OPTICAL SPECTROSCOPY FOR THE DETECTION OF MALIGNANT LESIONS OF THE BRONCHIAL TREE: FINAL REPORT

Martin P.L. Bard[1], Arjen Amelink[2], Marina Skurichina[3], Vincent Noordhoek Hegt[4], Robert P.W. Duin[3], Henricus J.C.M. Sterenborg[2], Henk C. Hoogsteden[1], Joachim G.J.V. Aerts[1,5]

[1]Department of Respiratory Diseases, [2]Center for Optical Diagnostics and Therapy, Department of Radiation Oncology, Erasmus MC, Rotterdam, [3]Faculty of Electrical Engineering, Mathematics and Computer Science, Delft University of Technology, [4]Department of Pathology, [5]Department of Respiratory Diseases, Sint Franciscus Hospital, Rotterdam, The Netherlands

Address for correspondence:

Joachim Aerts, M.D., Ph.D.

Department of Respiratory Diseases, Sint Franciscus Hospital

Kleiweg 500, 3045 PM, Rotterdam, The Netherlands,

Phone: +31 10 4616149, Fax : +31 10 4612692, e-mail: j.aerts@sfg.nl

ABSTRACT

Autofluorescence bronchoscopy is characterized by a high sensitivity but a low specificity for the detection of malignant lesions of the bronchial tree. The aim of our study was to combine autofluorescence bronchoscopy with optical spectroscopy in order to improve the specificity of autofluorescence imaging.

We developed a fiberoptic instrument allowing the measurement of autofluorescence (AFS), diffuse reflectance (DRS) and differential path length (DPS) spectroscopy during bronchoscopy. Spectroscopic measurements were obtained from 191 different endobronchial lesions (63 "high grade" and 128 "low grade lesions") in 107 patients.

The positive predictive value (PPV) of autofluorescence imaging was 34.7% for 101 bronchial lesions showing abnormal fluorescence. Combining autofluorescence imaging with the three spectroscopic techniques improved the PPV to 69.4%, 78.6%, and 76.9% for AFS, DPS and DRS, respectively. Even better results were obtained when the three spectroscopic techniques were combined yielding a PPV of 83.3%, indicating that optical spectroscopy improves the specificity of autofluorescence bronchoscopy for the detection of bronchial tumors.

Key words: lung cancer, bronchoscopy, spectroscopy, autofluorescence, reflectance

INTRODUCTION

Lung cancer is the leading cause of cancer death worldwide. Bronchoscopy is, along with thoracic imaging, the cornerstone technique for both diagnosis and staging of lung cancer. Autofluorescence bronchoscopy (AFB) has been reported to have a higher sensitivity than white light bronchoscopy (WLB) for the detection of endobronchial (pre-)malignant lesions [1-3]. However, AFB is characterized by a low specificity with a high rate of false positive findings, inducing unnecessary biopsies at a greater cost and a longer examination duration [4, 5].

Optical spectroscopic techniques explore the optical phenomena resulting from the interaction of light with biological tissue. Autofluorescence spectroscopy (AFS) investigates the fluorescence of the endogeneous fluorophores present in the tissue, but the autofluorescence spectra are also affected by the optical properties (i.e. scattering and absorption) of the tissue [6]. White light reflectance spectroscopy does not employ fluorophores but directly studies the optical properties of tissue. Reflectance spectra depend on the presence of light absorbers such as haemoglobin, and light scatterers. The nature of these scatterers is still a mater of scientific debate, but most probably several membrane-bound cellular organelles are involved [7, 8]. Optical spectroscopy may be particularly useful for the analysis of differences in normal and cancerous tissue because major scattering, absorption, and fluorescence changes are known to occur during the development of cancer [6, 9]. Therefore, these non-invasive optical spectroscopic techniques may allow a real-time, *in vivo* analysis of bronchial tissue and may help to distinguish healthy from cancerous tissue based on their optical differences.

Our approach was to combine a very sensitive (but non-specific) imaging technique, i.e. autofluorescence bronchoscopy, with optical spectroscopy to improve the specificity. The spectroscopic measurements were performed during bronchoscopy using a custom-made fiberoptic probe. The feasibility of the technique was demonstrated in a pilot study and the

preliminary data suggested that the addition of AFS and DRS may improve the specificity of AFB for the detection of endobronchial cancers [10]. For this final study, we improved our fiberoptic instrument allowing the measurement of autofluorescence (AFS), diffuse reflectance (DRS) and differential path length (DPS) spectroscopy during bronchoscopy. DPS is a new spectroscopic technique developed in our group for the purpose of studying the optical properties of the most superficial layer of the bronchial mucosa, i.e. the epithelium [11-13]. These three spectroscopic techniques were used in a large group of patients in order to examine their diagnostic accuracies. The capacity to decrease the rate of false positive findings of autofluorescence bronchoscopy was studied for each spectroscopic technique separately and for their combination.

Material & Methods

Study population

Patients with known or suspected malignancies of the lung and with a medical indication for a bronchoscopy were invited to participate in the study. All patients were more than 18 years old and signed informed consent. The study was approved by the Medical Ethics Review Board of the Erasmus Medical Centre Rotterdam. Spectroscopic measurements were performed on 191 different endobronchial lesions in 107 patients, studied during a 18 month period. For the classification analysis, the endobronchial lesions were divided into two histological groups: a "*high-grade lesion*" group (n= 63 lesions) including invasive carcinoma (n=57) and carcinoma in situ/severe dysplastic (n=6) lesions, and a "*low-grade lesion*" group (n= 128 lesions) including the normal (n=54), metaplastic (n=67) and mild grade dysplastic (n=7) lesions.

Examination procedure

The endoscopic examination of the bronchial tree was performed using a commercially available flexible fluorescence bronchoscope (Karl Storz® 11004BI, Germany) or a flexible white light video-bronchoscope (Olympus, BF-T160, The Netherlands). All lesions that appeared abnormal at blue and/or white light imaging were measured. Additionally, some spectra of macroscopically normal bronchial mucosa (corresponding to healthy carina systematically biopted for preoperative staging purposes) were taken. An average of three measurements was performed on slighly different locations within each lesion in order to take into account possible tissue heterogeneity. During the spectral acquisition, the light source of the bronchoscope was switched off. Biopsy specimens were taken from all measured lesions, transported in formaldehyde and fixed in paraffin. Hematoxylin-eosin stained slides were

evaluated without knowledge of the bronchoscopic findings. The pathological diagnoses were coded referring to the World Health Organisation Lung Cancer classification [14].

Optical probe

Spectra were acquired with a custom-made instrument using a fiberoptic probe small enough to be led through the working channel of the bronchoscope (Fig. 1). The fiber-probe consisted of three identical 400 μm fibers fitted into a small metal tube. The first fiber was used for delivery of blue light to the tissue (delivery (d)-fiber), the second fiber was used for both delivery of white light and detection of reflected white light from the tissue (delivery and collection (dc)-fiber), and the third fiber was used for the detection of both autofluorescence and reflected white light (collection (c)-fiber). A blue diode laser (407 nm, Nichia, Tokio, Japan) and a tungsten-halogen lamp (Ocean Optics, HL-2000-FHSA, Duiven, The Netherlands) were used as excitation sources. The reflected light from the bronchial mucosa was analyzed in a dual-channel spectrometer (Ocean Optics, SD2000, Duiven, The Netherlands). In order to attenuate the strong 407 nm background due to the blue-violet light source, light collected in the c-fiber was filtered through a long pass glass filter (Schott GG435, Tiel, The Netherlands).

As discussed above, two different white light reflection signals were collected: reflected light collected by the c-fiber (J_c) and reflected light collected by the dc-fiber (I_{dc}). The difference between these signals is called the differential reflectance signal ($R = I_{dc} - J_c$) and has been investigated in detail previously [11-13]. This J_c signal, which we have termed "diffuse reflectance" (but has been referred to by others as "elastic-scattering" signal as well [15]) corresponds to photons multiply ("diffusely") scattered in the tissue. The interrogation depth of diffuse reflectance spectroscopy (DRS) depends on the optical properties of the tissue under investigation, and is typically of the order of 1 mm [15]. We have previously

reported that the apparent path length (τ) of photons contributing to the differential reflectance signal R is independent of the optical properties of the sample under investigation and is approximately equal to the diameter of the fibers (d_{fiber}) used ($\tau = 0.8d_{fiber}$), as long as the fiber diameter is larger than the mean free path of the photons [11]. Thus the depth probed by DPS is roughly equal to $1/2\ \tau = 0.4d_{fiber} \sim 160\mu m$ for fiber diameters of 400 μm. Such a tissue depth corresponds to the most superficial layer of the bronchial mucosa.

Spectral analysis

Autofluorescence and reflectance spectra were analyzed in a range of 435nm to 700nm and 435nm to 900nm, respectively. Autofluorescence spectra were preprocessed by dividing the spectrum by the maximum intensity of a fluorescence measurement with the probe at a specific distance (roughly 7 mm) from a fluorescence calibration standard (Labsphere USFS-200), to correct for day-to-day variations in laser-output. Diffuse reflectance spectra were preprocessed by dividing the raw spectrum by a reference spectrum measured with the probe subsequently at a specific distance (roughly 7 mm) from a diffuse reflecting white reflectance standard (Labsphere SRS-99) and from a diffuse reflecting black reflectance standard (Labsphere SRS-02):

$$J_c = \left(\frac{J}{\left(J_{white} - J_{black} \right)} \right) \tag{1}$$

Here J is the raw signal from the collection fiber in contact with the sample, J_{white} is the signal from the c-fiber with the probe-tip at the previously mentioned distance from the white reflectance standard and J_{black} is the signal from the c-fiber with the probe-tip at the previously mentioned distance from the black reflectance standard. Similarly, the differential path-length spectra are preprocessed by [11]:

$$R = \left(\frac{\left(I - I_n \right)}{\left(I_{white} - I_{black} \right)} - \frac{J}{\left(J_{white} - J_{black} \right)} \right) \equiv \left(I_{dc} - J_c \right) \tag{2}$$

Here I is the raw signal from the delivery-and-collection fiber in contact with the sample, I_n is the signal from the dc-fiber submersed in a fluid with an appropriate refractive index (for tissue: water would be appropriate), I_{white} is the signal from the dc-fiber with the probe-tip at the previously mentioned distance from the white reflectance standard and I_{black} is the signal from the dc-fiber with the probe-tip at that same distance from the black reflectance standard.

The variability of all the spectra was decreased by normalization to Unit Area and the median intensity of the spectra was used as an additional feature in order to take into account the information related to the intensity of the spectra. To analyze the spectra, principal component analysis was applied [16]. In order to determine the optimal amount of leading principal components used to describe the spectra, we studied the classification accuracy of all spectroscopic modalities, i.e. AFS, DRS and DPS, in a range of leading principal components from 1 to 20. As explained below in more detail, the classification accuracy of each spectroscopic modality can be expressed in terms of an area under a Receiver Operating Characteristic (ROC) curve. The largest areas under the ROC curves were found using 15, 20, and 15 leading principal components for AFS, DRS and DPS, respectively.

To evaluate the quality of discrimination between the "low grade" and "high grade" lesions, linear discriminant analysis was applied. Specifically, we used the Karhunen-Loeve Linear Classifier also known as the regularized linear discriminant function. For all spectroscopic modalities, the classifier was constructed using the leave-one-person-out approach, for which the classifier is constructed on a training set containing all spectra except the spectra measured in one particular patient. Compared to leave-one-spectrum-out or leave-one-lesion-out methods, the leave-one-patient-out method improves the independence of the lesion classification since this approach prevents that spectra belonging to the same patient (which might not be considered to be completely independent) will be used both in the

training data set (used to construct the classifier) and in the independent test set (used to test the goodness of the classification rule). Using the classifier, we obtain for all spectra a classification label, i.e. "low grade" or "high grade", and two posterior class probabilities (p1 and p2) which correspond to the confidence (from 0 to 1) of the classification rule about the membership of a certain spectrum to the "low grade" or "high grade" lesion classes. When multiple measurements were made on the same lesion, the final decision of the classifier for this lesion was obtained using the "mean fusion" approach. In the mean fusion approach, the posterior class probabilities obtained for all spectra measured on the same lesion were averaged and the maximum value of these means of p1's and p2's were retained for the final decision of the classifier. The advantage of this approach is that the final decision on a lesion measured multiple times is an average between decisions made for each measurement separately.

For all spectroscopic modalities, i.e. AFS, DRS and DPS, the sensitivity and the specificity of the classifier were calculated with different threshold values to distinguish the "low grade" and "high grade" tissue. Based on these calculations for different thresholds, Receiver Operator Characteristics (ROC) curves are constructed by plotting (1-specificity) values against corresponding values of sensitivity. We calculate for each spectroscopic modalitiy the mean and the standard deviation of the area under the ROC curve using the leave-one-lesion-out method. Using this method, an area under the ROC curve was calculated 191 times for 190 lesions (each time one lesion was left out) and the 191 ROC curves were used to calculated the mean and the standard deviation of the area under the ROC curve for a given spectroscopic technique.

RESULTS

Typical AFS, DRS and DPS spectra measured in "low grade" and "high grade" bronchial lesions are illustrated in figures 2A, 2B and 2C, respectively. The average intensity of the autofluorescence spectra (Fig. 2A) is higher in "low grade" lesions than in "high grade" lesions. For diffuse reflectance spectra (Fig. 2B) and differential path length spectra (Fig. 2C) the decrease in signal intensity observed in the wavelength range 500-600nm corresponds to the light absorption of blood and was generally higher on "high grade" lesions compared to "low grade" lesions.

The ROC curves for the three spectroscopic modalities are presented in figure 3. The mean and standard deviation of the areas under the ROC curves, as well as the highest combined sensitivity and specificity for the three spectroscopic modalities are summarized in Table I. It is observed that DRS and DPS have larger areas under the ROC curves than AFS. Similarly, higher specificities and sensitivities were measured for DRS and DPS than for AFS.

The clinically relevant data set consists only of spectra measured on the 101 lesions found by autofluorescence imaging. For the analysis of this subset of spectra, the classification accuracy of AFS, DRS, and DPS was evaluated using the threshold value with the smallest classification error (corresponding to the highest combined sensitivity and specificity) derived from the ROC curves constructed using the complete data-set. For the classification results of the combination of the three spectroscopic techniques, the principle of majority voting was applied (the classification according to the majority of the 3 spectroscopic classifications determined the final classification). Table 2 summarizes the classification results of each of the three spectroscopic techniques and of their combination for bronchial lesions found by autofluorescence bronchoscopy. It must be noted that all these classification values are not absolute values but rather relative values since our data-set

consists of measurements on lesions already classified as abnormal by autofluorescence bronchoscopy. We find that all three spectroscopic techniques improve the positive predictive value (PPV) of bronchoscopic imaging. This improvement is combined with a high relative negative predictive value (rNPV), relative sensitivity (rSe) and relative specificity (rSp). White light reflectance spectroscopy (DRS and DPS) yielded better results than AFS. The best classification results were obtained when the three spectroscopic techniques were combined.

DISCUSSION

Autofluorescence bronchoscopy (AFB) is currently the diagnostic technique with the highest sensitivity for the detection of endobronchial (pre-)malignant lesions, but is hampered by a low specificity [1, 3]. We believe that combination of autofluorescence bronchoscopy with other real-time, non-invasive diagnostic techniques such as optical spectroscopy to minimize the amount of false positive findings would increase the acceptance of AFB in clinical practice. In this study, the classification accuracy of autofluorescence, diffuse reflectance and differential path length spectroscopy was investigated. We find that both autofluorescence and white light reflectance spectroscopy increase the positive predictive value of autofluorescence imaging alone. The highest relative positive predictive value was obtained when the three spectroscopic techniques were combined. Therefore, these results argue for a combined use of optical spectroscopy and autofluorescence bronchoscopy for the detection of bronchial tumors.

Optical spectroscopic techniques have been extensively studied for the *in vivo* detection of malignant and pre-neoplastic tissue [6, 9]. Combination of AFS and DRS has been shown to facilitate the detection of cancerous tissue with a high accuracy in the uterus [17-19], the breast [20], the ovary [21], the oesophagus [22] and the oral cavity [23]. In the lung, few data are available, mainly due to the inaccessibility of this organ. A decrease in autofluorescence intensity is a well know phenomena in malignant and dysplastic lesions of the bronchi [6, 24, 25]. However, the diagnostic accuracy of AFS for bronchial tumors has never been prospectively studied in a large cohort of patient. As for white light reflectance spectroscopy, our study is to the best of our knowledge the first report of its use during bronchoscopy. We find that the diagnostic accuracy of white light reflectance spectroscopy (both DRS and DPS) was superior to AFS. This result suggests that the optical properties of the bronchial mucosa contain the most discriminative information for tissue classification. In this view, the

classification accuracy of autofluorescence spectroscopy can be attributed to the fact that autofluorescence spectra depend on the optical properties as well, but that the accuracy of the classification is reduced by the large natural variations in fluorophore concentrations having less relevance for tissue diagnostics. Changes in tissue optical properties are related to changes in both the scattering and absorption properties of tissue. Scattering modifications are related to changes in tissue architecture such as thickening of the epithelial layer and to cellular changes such as an increase of the nucleus chromatin content, variations in the nucleus-cytoplasma ratio, and changes in the intra-cytosolic content [8]. Absorption modifications are mostly related to modifications of the concentration and distribution of light absorbers such as haemoglobin [9]. Tumors are known to be commonly more vascularized than normal tissue. Such increased blood content is related to the increased density of microvessels and the blood stasis occurring in tumoral tissue [16, 26]. Unfortunately, no information concerning the physiological changes in the bronchial cancerous tissue underlying the modifications of the tissue optical properties can be obtained from principal component analysis. However, we recently reported that several physiological parameters related to tissue microvasculature and blood oxygenation can be extracted from DPS spectra measured on bronchial mucosa [13]. We have reported that bronchial tumors are characterized by a higher blood content than normal and metaplastic/mild dysplastic bronchial mucosa. This suggests that the optical variations observed in bronchial tumors with DRS, DPS and AFS may be attributed largely to absorption of light by blood.

The equally good classification results observed with DRS and DPS suggests that the optical changes present in cancerous tissue are already detectable in the first 150-200μm of the tumor surface. We expect DPS to be superior in classifying superficial lesions such as severe dysplasia and carcinoma in situ, since DPS measures only the superficial layer of tissue, which is where the precancerous changes develop. Unfortunately, no conclusion

regarding this issue can be drawn from our data due to the nature of the population of lesions that was studied. During the examination of 191 bronchial lesions we found only 6 severe dysplasia/CIS lesions, and 4 of these lesions were detected without AFB, which leaves only 2 CIS lesions in the test set of 101 lesions found by AFB. Such a low fraction of superficial lesions hampers any comparison between the classification accuracy of DRS and DPS for these epithelial lesions. The exact prevalence of severe dysplasia and CIS in the bronchial tree is unknown. In a recent review on fluorescence bronchoscopy data in a selected population of smokers and former smokers with sputum atypia, prevalence of 6% and 1.6% were reported for severe dysplasia and CIS, respectively [27]. Further study of DPS in a selected population of patients suffering from severe dysplasia/CIS should be performed to show the benefit of DPS for the analysis of (pre-)malignant lesions confined to the epithelium.

In our study, the initial classification accuracy of the spectroscopic techniques was evaluated using areas under ROC-curves. In this procedure, the sensitivity and the specificity of the classifier were calculated with different threshold values to distinguish the "low grade" and "high grade" tissue. Based on these calculations for different thresholds, Receiver Operator Characteristics (ROC) curves are constructed by plotting (1-specificity) values against corresponding values of sensitivity. For the classification analysis of the subset of bronchial lesions detected using autofluorescence bronchoscopy, we chose to use threshold values giving the highest combined sensitivity and specificity. However, it must be noted that the choice of the classification threshold is flexible and can be adapted to the clinical aims. For example, if it is clinically more desirable to have a higher sensitivity at the cost of a lower specificity, the threshold value for the classifier can be adjusted to accommodate this desire.

CONCLUSION

Optical spectroscopy, especially white light reflectance spectroscopy, allows the real-time, non-invasive distinction of malignant from healthy bronchial mucosa with high accuracy. Combination of optical spectroscopy with autofluorescence bronchoscopy was shown to improve the specificity of autofluorescence bronchoscopy alone. Therefore, these non-invasive techniques may be well implemented in the panel of diagnostic techniques currently used for the detection of endobronchial cancer.

LEGENDS OF THE FIGURES

Figure 1. Schematic diagram of the experimental set-up.

Figure 2. Illustration of autofluorescence (Fig.2A), diffuse reflectance (Fig.2B), and differential path length (Fig 2C) spectra measured in "low grade" and "high grade" bronchial lesions.

Figure 3. Receiver-Operating Characteristic (ROC) curves for the three different spectroscopic modalities. Black triangle and solid line: differential path-length spectroscopy (DPS), white triangle and dotted line: diffuse reflectance spectroscopy (DRS), white circle and dotted line: autofluorescence spectroscopy (AFS).

REFERENCES

[1]   Hirsch FR, Prindiville SA, Miller YE, Franklin WA, Dempsey EC, Murphy JR, et al. Fluorescence versus white-light bronchoscopy for detection of preneoplastic lesions: a randomized study. J Natl Cancer Inst 2001;93:1385-91.

[2]   Kennedy TC, Hirsch FR, Miller YE, Prindiville S, Murphy JR, Dempsey EC, et al. A randomized study of fluorescence bronchoscopy versus white-light bronchoscopy for early detection of lung cancer in high risk patients. Lung Cancer 2000;29(S1):244-5.

[3]   Lam S, Kennedy T, Unger M, Miller YE, Gelmont D, Rusch V, et al. Localization of bronchial intraepithelial neoplastic lesions by fluorescence bronchoscopy. Chest 1998;113:696-702.

[4]   Sutedja TG, Venmans BJ, Smit EF,Postmus PE. Fluorescence bronchoscopy for early detection of lung cancer. A clinical perspective. Lung Cancer 2001;34:157-68.

[5]   Banerjee AK, Rabbitts PH,George J. Lung cancer. 3: Fluorescence bronchoscopy: clinical dilemmas and research opportunities. Thorax 2003;58:266-71.

[6]   Wagnières GA, Star WM,Wilson BC. In vivo fluorescence spectroscopy and imaging for oncological applications. Photochem Photobiol 1998;603-32.

[7]   Bartlett M, Huang G, Larcom L,Jiang H. Measurement of particle size distribution in mammalian cells in vitro by use of polarized light spectroscopy. Appl Optics 2004;43:1296-307.

[8]   Beauvoit B,Chance B. Time-resolved spectroscopy of mitochondria, cells and tissue under normal and pathological conditions. Mol Cell Bioch 1998;184:445-55.

[9]   Sokolov K, Follen M,Richards-Kortum R. Optical spectroscopy for detection of neoplasia. Cur Opin Chemical Biol 2002;6:651-8.

[10] Bard MPL, Amelink A, Skurichina M, den Bakker M, Burgers SA, van Meerbeeck JP, et al. Improving the specificity of fluorescence bronchoscopy for the analysis of neoplastic lesions of the bronchial tree by combination with optical spectroscopy: preliminary communication. Lung Cancer 2005;47:41-7.

[11] Amelink A,Sterenborg HJCM. Measurement of the local optical properties of turbid media by differential path-lenght spectroscopy. Appl Optics 2004;43:3048-54.

[12] Amelink A, Sterenborg HJCM, Bard MPL,Burgers SA. In vivo measurement of the local optical properties of tissue by use of differential path-length spectroscopy. Opt Lett 2004;29:1087-9.

[13] Bard MPL, Amelink A, Noordhoek-Hegt V, Graveland WJ, Sterenborg HJCM, Hoogsteden HC, et al. Measurement of hypoxia-related parameters in bronchial mucosa by use of optical spectroscopy. Am J Resp Crit Care Med 2005;February 11, as doi:10.1164/rccm.200501-046OC:

[14] Brambilla E, Travis WD, Colby TV, Corrinz B,Shimosato Y. The new World Health Association classification of lung cancer. Eur Respir J 2001;18:1059-68.

[15] Bigio IJ, Bown SG, Brigs G, Kelley C, Lakhani S, Pickard D, et al. Diagnosis of breast cancer using elastic-scattering spectroscopy: preliminary clinical results. J Biomed Opt 2000;5:221-8.

[16] Jain RK. Determinant of tumor blood flow: a review. Cancer Res 1988;48:2641-58.

[17] Mirabal YN, Chang SK, Atkinson EN, Malpica A, Follen M,Richards-Kortum R. Reflectance spectroscopy for in vivo detection of cervical precancer. J Biomed Opt 2002;7:587-94.

[18] Nordstrom RJ, Burke L, Nilodd JM,Myrtle JF. Identification of cervical intraepithelial neoplasia (CIN) using UV-excited fluorescence and diffuse-reflectance spectroscopy. Lasers Surg Med 2001;28:118-27.

[19] Georgakoudi I, Sheets EE, Müller MG, Backman V, Crum CP, Badizadegan K, et al. Trimodal spectroscopy for the detection and characterization of cervical precancers in vivo. Am J Obstet Gynecol 2002;186:374-82.

[20] Breslin TM, Xu F, Palmer GM, Zhu C, Gilchrist KW,Ramanujan N. Autofluorescence and diffuse reflectance properties of malignant and benign breast tissues. Ann Surg Oncol 2004;11:65-70.

[21] Utzinger U, Brewer M, Silva E, Gershenson D, Blast RC, Follen M, et al. Reflectance spectroscopy for in vivo characterization of ovarian tissue. Lasers Surg Med 2001;28:56-66.

[22] Wallace MB, Perelman LT, Backman V, Crawford JM, Fitzmaurice M, Seiler M, et al. Endoscopic detection of dysplasia in patients with Barrett's esophagus using light-scattering spectroscopy. Gastroenterology 2000;119:677-82.

[23] Müller MG, Valdez TA, Georgakoudi I, Backman V, Fuentes C, Kabani S, et al. Spectroscopic detection and evaluation of morphologic and biochemical changes in early human oral carcinoma. Cancer 2003;97:1681-92.

[24] Hung J, Lam S, LeRiche JC,Palcic B. Autofluorescence of normal and malignant bronchial tissue. Lasers Surg Med 1991;11:99-105.

[25] Kusunoki Y, Imamura F, Uda H, Mano M,Horai T. Early detection of lung cancer with laser-induced fluorescence endoscopy and spectrofluorometry. Chest 2000;118:1776-82.

[26] Shijubo N, Kojima H, Nagata M, Ohchi T, Suzuki A, Abe S, et al. Tumor angiogenesis of non–small cell lung cancer. Microsc Res Tech 2003;60:186-98.

[27] Lam S, MacAulay C, LeRiche JC,Palcic B. Detection and localization of early lung cancer by fluorescence bronchoscopy. Cancer 2000;89:2468-73.

Table I. Mean and standard deviation of the areas under the ROC curves, as well as the highest combined sensitivity and specificity for diffuse reflectance (DRS), differential path length (DPS), and autofluorescence (AFS) spectroscopy for the distinction between "high-grade" and "low-grade" bronchial lesions.

Spectroscopic technique	Area under ROC	Sensitivity	Specificity
DRS	0.90 ± 0.02	86%	81%
DPS	0.89 ± 0.03	81%	88%
AFS	0.82 ± 0.03	73%	82%

Table II. Classification results of autofluorescence (AFS), diffuse reflectance (DRS), differential path length (DPS) spectroscopy and of their combination for bronchial lesions found by autofluorescence (AF) bronchoscopic imaging (n=101).

Histology	AF-imaging normal	AF-imaging abnal.	AFS normal	AFS abnal.	DRS normal	DRS abnal.	DPS normal	DPS abnal.	AFS + DRS + DPS normal	AFS + DRS + DPS abnal.
low-grade	-	66	55	11	57	9	57	9	60	6
high-grade	-	35	10	25	2	33	5	30	5	30
rPPV	34.7%		69.4%		78.6%		76.9%		83.3%	
rNPV			84.6%		96.6%		91.9%		92.3%	
rSe			71.4%		94.3%		85.7%		85.7%	
rSp			86.4%		86.4%		86.4%		90.9%	

rPPV; relative positive predictive value, rNPV; relative negative predictive value, rSe; relative sensitivity, rSp; relative specificity
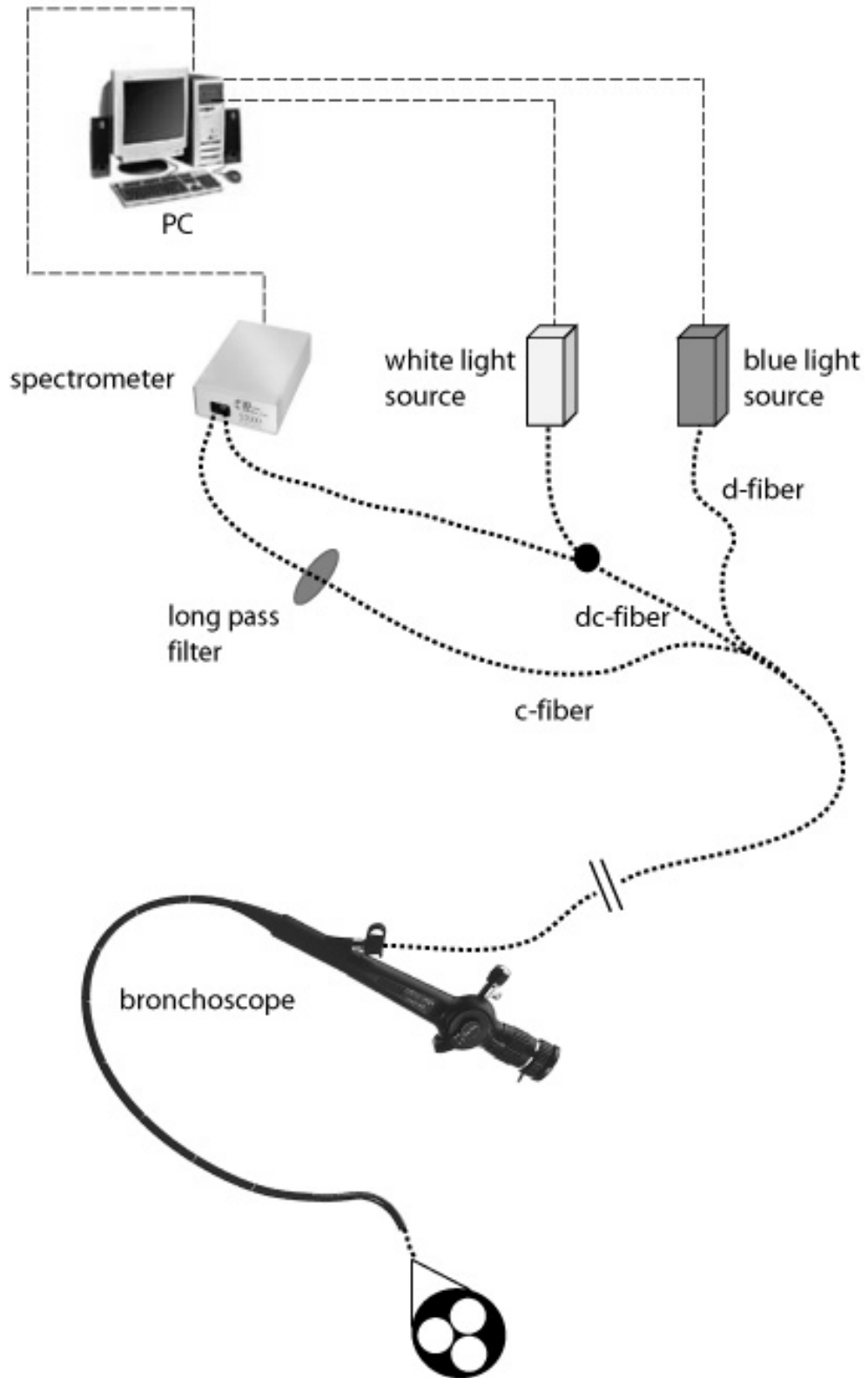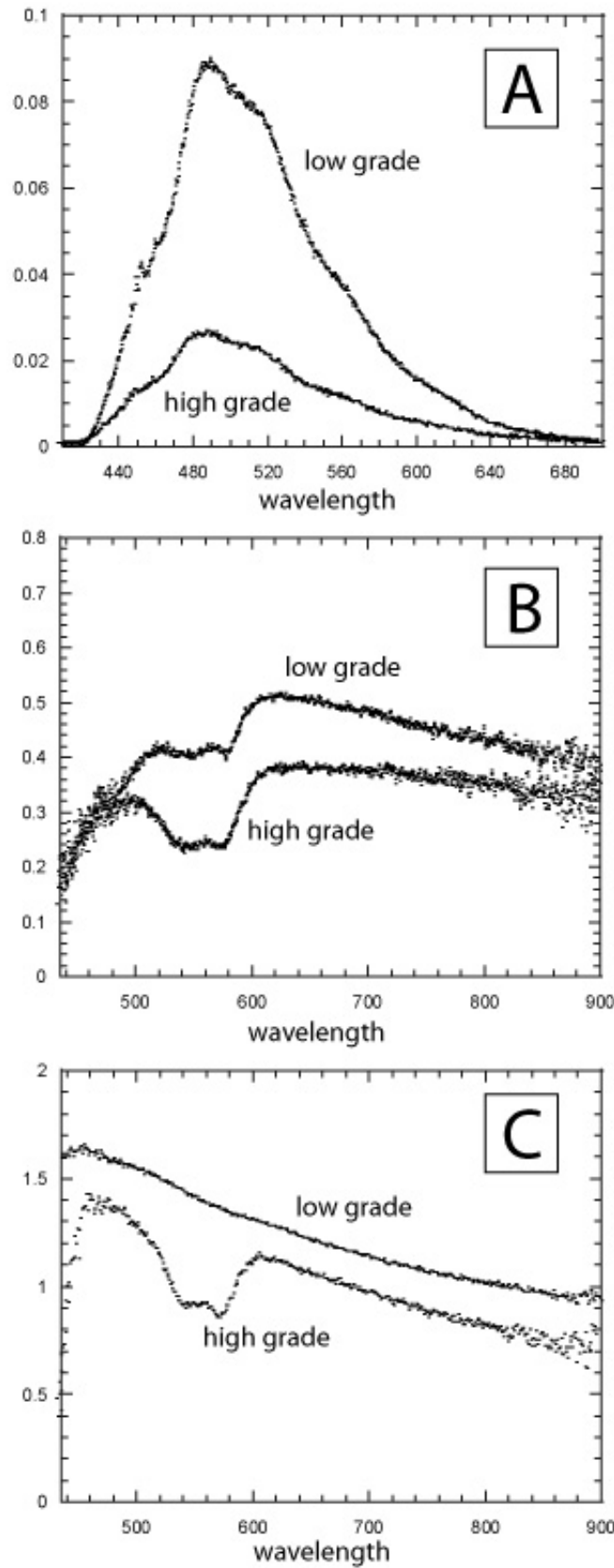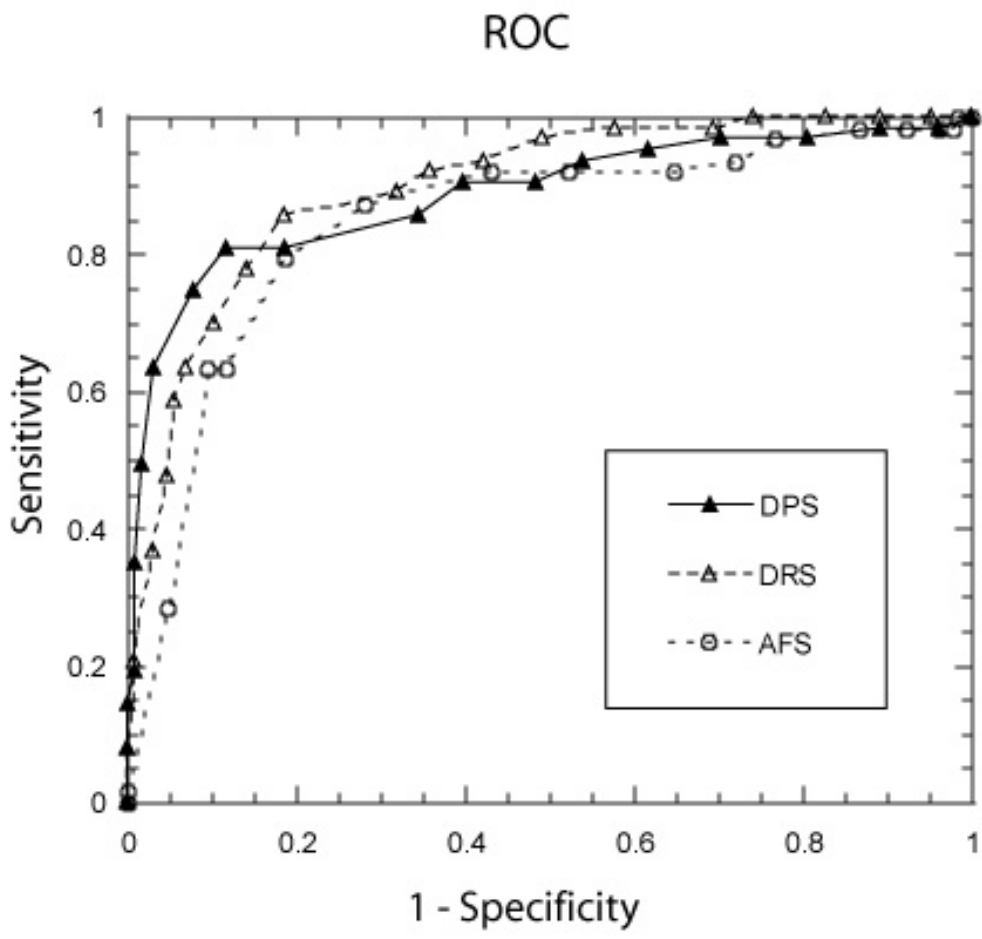
Figure 1

Figure 2

Figure 3

ROC

CHAPTER 8

General discussion and summary

Prognosis of lung cancer is severe because the majority of symptomatic patients are diagnosed in the late and not curable stage of the disease (1, 2). Early detection of localized cancer and pre-malignant diseases may improve the prognosis of this disease. Dysplastic and cancerous tissue are associated with chemical and morphological changes inducing modifications of the optical properties of the bronchial mucosa (3-5). Optical spectroscopic analysis of the bronchial mucosa may be a more specific technique than conventional bronchoscopic imaging in the detection of pre-malignant lesions and cancer of the proximal bronchial tree.

In this thesis we studied the diagnostic value of optical spectroscopy for cancerous lesions of the bronchial mucosa. We developed a fiber-optic instrument allowing the measurement of autofluorescence (AFS), diffuse reflectance (DRS), and differential path length (DPS) spectroscopy during bronchoscopy. DPS is an original spectroscopic technique which was developed in our institution for the purpose of studying the optical properties of the most superficial layer of the bronchial mucosa, i.e. the epithelium. DPS was initially studied in various tissue phantoms. Then, DPS was used *in vivo* for the analysis of hypoxia-related parameters measured in healthy and in malignant bronchial tissue. Finally, AFS, DRS and DPS were used during bronchoscopy in a large group of patients in order to examine their diagnostic accuracy. The capacity of optical spectroscopy to increase the specificity of autofluorescence bronchoscopy for the detection of bronchial cancerous lesions was studied.

Optical spectroscopy for the analysis of the bronchial mucosa.

Optical spectroscopy of the bronchial mucosa is challenging due to the difficulty of access to the bronchial tree. Recent progress in endoscopic imaging technology has allowed the development of high quality flexible bronchoscopes facilitating the exploration of the proximal bronchial tree. Combining optical spectroscopy to bronchoscopy would allow the *in*

situ real time spectral analysis of bronchial lesions detected by imaging. A first way to combine optical spectroscopy to imaging is to extract the spectroscopic spectra from the bronchoscopic images obtained during white light and/or blue light bronchoscopy (6, 7). However, the light spectra extracted from the bronchoscopic images are collected from a large tissue area and penetrate deep in the tissue impairing the specific analysis of localized lesions and of lesions limited to the most superficial (epithelial) layer of the bronchial mucosa. For our study, we chose to use a self made optical fiber probe to illuminate the bronchial mucosa and to collect the light signal reflected from the bronchial surface. This fiber probe was introduced via the work channel of the bronchoscope and positioned on the tissue surface. Advantages were: a better control of the illumination light signal (intensity, wavelength) and of the reflected light signal collection allowing the analysis of localized and superficial lesions of the bronchial mucosa. The use of this fiber-optic probe was easy and well tolerated. The probe could accurately be positioned on bronchial lesions without damaging the tissue.

An important feature of our spectroscopic instrument was the possibility to concomitantly measure both autofluorescence and white light reflectance spectroscopy. Auto fluorescence spectroscopy investigates the fluorescence of the endogeneous fluorophores present in the tissue, but the autofluorescence spectra are also affected by the optical properties (i.e. scattering and absorption) of the tissue (4). White light reflectance spectroscopy does not employ fluorophores but directly studies the optical properties of tissue. Reflectance spectra depend on the presence in the tissue of light absorbers such as haemoglobin, and of light scatterers such as collagen, elastin, and several membrane-bound cellular organelles (8-10). The concomitant measure of autofluorescence and white light reflectance spectroscopy allowed us to distinguish the role of the tissue fluorophores, scatterers and absorbers in the optical changes occurring during the cancerous transformation of the bronchial mucosa.

Optical spectroscopy for the analysis of the bronchial epithelium (role of differential path-length spectroscopy)

The study of the epithelium layer of the bronchial mucosa is particularly interesting because the majority of lung cancers arises in the epithelium and are preceded by precancerous changes that affect only the surface epithelium. DPS was developed for the purpose of studying the optical events occurring in the most superficial layer of the tissue. The superficial analysis was possible by using a single delivery and collection (dc-)fiber to deliver the light and detect the reflected light from tissue, optimizing the probability of detection of photons scattered from small sample depths.

In **chapter 2**, we used DPS to measure the scattering properties of various tissue phantoms consisting of one or two layers suspensions of polystyrene spheres. We observed that the signal collected by the dc-fiber was sensitive to scattering events occurring close to the fiber probe tip. Further analysis in tissue phantoms, demonstrated that, in the range of parameters relevant for biological tissue, the tissue depth explored by DPS is independent of the optical properties of the tissue but depends only of the diameter of the fiber (11). As a consequence, the diameter of the fibers can be adjusted according to the tissue depth studied. For the study of bronchial mucosa, we used fibers with a diameter of 400 μm for which the apparent differential path length of the DPS signal was 320 μm allowing the analysis of photons reflected roughly within 160 μm of the tissue surface.

Optical spectroscopy for the analysis of tissue hypoxia-related parameters in bronchial mucosa

In **chapter 3** we demonstrated that several hypoxia-related parameters such as the microvasculature blood oxygenation, the volume of blood and the diameter of microvessels

can be extracted from DPS spectra. In **chapter 4**, we reported that bronchial tumors were characterized by a lower blood oxygenation, a higher blood volume and larger microvessels in comparison with normal bronchial mucosa. No difference was found between normal mucosa and metaplastic/mild dysplastic mucosa. These results were in accordance with lung tumor oxygenation data obtained using functional imaging (12, 13) or hypoxic markers immunostaining (14-19) suggesting that tumor hypoxia is a common event in lung cancer.

In **chapter 5** we reported that poor prognosis lung cancer, such as small cell carcinomas and non-differentiated large cell carcinomas, were associated with the lowest blood oxygenation in comparison with other cancer cell types such as squamous cell and adenocarcinomas. Small cell carcinomas and non-differentiated large cell carcinomas were also characterized by a lower blood volume and smaller average blood diameter suggesting a poorer organization of the tumor microvasculature. Tumor hypoxia has been reported to be associated with a lower survival, a higher aggressiveness and a lower sensitivity to therapy (20). Association of poor prognosis lung cancer cell types with a lower blood oxygenation argues for a bad prognosis value of blood hypoxia measured in bronchial tumor using DPS.

Combination of optical spectroscopy with autofluorescence bronchoscopy for the detection of bronchial lesions of the bronchial tree

White light and fluorescence endoscopic imaging are commonly used for the detection of proximal endobronchial lesions. The sensitivity of autofluorescence bronchoscopy (AFB) has shown to be better than white light bronchoscopy for the detection of carcinoma in situ and dysplastic lesions (21-23). AFB is, however, characterized by a low specificity with a high rate of false positive findings. This induces unnecessary biopsies at greater costs and longer duration of the examination. Optical spectroscopic techniques have been extensively studied for the *in vivo* detection of malignant and pre-neoplastic tissue (4, 5). Combination of

AFS and DRS has been shown to facilitate the detection of cancerous tissue with a high accuracy in the uterus (24-26), the breast (27), the ovary (28), the oesophagus (29) and the oral cavity (30). In the lung, few data are available, mainly due to the inaccessibility of this organ.

We studied in **chapter 6** the feasibility of the combined use of optical spectroscopy and autofluorescence bronchoscopy for the detection of pre-malignant and invasive carcinomas of the bronchial tree. Preliminary data suggested that optical spectroscopy may improve the specificity of autofluorescence bronchoscopy imaging for the detection of bronchial cancerous lesions. In **chapter 7** the definitive results of the first autofluorescence and reflectance spectroscopic study of the bronchial mucosa were reported. We observed that the diagnostic accuracy of white light reflectance spectroscopy was better than of AFS. This result suggests that the optical properties of the bronchial mucosa are more important than their autofluorescence properties for tissue classification. We confirmed that white light reflectance and autofluorescence spectroscopy yielded higher "positive predictive values" in comparison with AFB imaging for the detection of bronchial tumor. Best results were obtained when reflectance and autofluorescence spectroscopy were combined.

General Conclusion

We demonstrated that optical spectroscopy can easily be used during bronchoscopy for the optical analysis of normal and of cancerous bronchial mucosa. We observed that the optical properties of the bronchial mucosa contain the most discriminative information for tissue classification and that the optical variations observed in bronchial tumors using DRS, DPS and AFS may be related to absorption of light by tissue blood. We observed that blood hypoxia is a common event in bronchial tumors especially in cases of poor prognosis tumors such as small cell lung carcinoma. Endobronchial tumors were also characterized by a higher

blood content and larger microvessels in comparison with non-cancerous mucosa. Finally, we demonstrated that combination of optical spectroscopy with autofluorescence bronchoscopy improves the specificity of autofluorescence bronchoscopy alone. Therefore, optical spectroscopy may be well implemented in the panel of diagnostic techniques currently used for the detection of endobronchial cancer.

REFERENCES

1. Mountain CF. The international system for staging lung cancer. Sem Surg Oncol 2000;18:106-115.
2. Naruke T, Tsuchiya R, Kondo H, Asamura H. Prognosis and survival after resection for bronchogenic carcinoma based on the 1997 TNM-staging classification: The Japanese experience. Ann Thorac Surg 2001;71:1759-1764.
3. Ramanujam N. Fluorescence spectroscopy of neoplastic and non-neoplastic tissues. Neoplasia 2000;2:89-117.
4. Wagnières GA, Star WM, Wilson BC. In vivo fluorescence spectroscopy and imaging for oncological applications. Photochem Photobiol 1998:603-632.
5. Sokolov K, Follen M, Richards-Kortum R. Optical spectroscopy for detection of neoplasia. Cur Opin Chemical Biol 2002;6:651-658.
6. Chiyoa M, Shibuyaa K, Hoshinoa H, Yasufukua K, Sekinea Y, Lizasaa T, et al. Effective detection of bronchial preinvasive lesions by a new auto.uorescence imaging bronchovideoscope system. Lung Cancer 2005:in press.
7. Zeng H, Petek M, Zorman MT, Mc Williams A, Palcic B, Lam S. Integrated endoscopy system for simultaneous imaging and spectroscopy for early lung cancer detection. Opt Letters 2004;29:587-589.
8. Bartlett M, Huang G, Larcom L, Jiang H. Measurement of particle size distribution in mammalian cells in vitro by use of polarized light spectroscopy. Appl Optics 2004;43:1296-1307.
9. Beauvoit B, Kitai T, Chance B. Contribution of the mitochondrial compartment to the optical properties of the rat liver: A theoretical and practical approach. Biophys J 1994;67:2501-2510.
10. Beauvoit B, Chance B. Time-resolved spectroscopy of mitochondria, cells and tissue under normal and pathological conditions. Mol Cell Bioch 1998;184:445-455.
11. Amelink A, Sterenborg HJCM. Measurement of the local optical properties of turbid media by differential path-lenght spectroscopy. Appl Optics 2004;43:3048-3054.
12. Urtasun RC, Parliament MB, McEwan AJ, Mercer JR, Manan RH, Wiebe LI, et al. Measurement of hypoxia in human tumours by non-invasive spect imaging of iodoazomycin arabinoside. Br J Cancer 1996;27:S209-S212.
13. Rasey JS, Koh W-J, Evans ML, Peterson LM, Lewellen TK, Graham MM, et al. Quantifying regional hypoxia in human tumors with positron emission tomography of [18F]fluoromisonidazole: a pretherapy study of 37 patients. Int J Radiat Oncol Biol Phys 1996;36:417-428.
14. Giatromanolaki A, Koukourakis MI, Sivridis E, Turley H, Talks K, Pezzela F, et al. Relation of hypoxia inducible factor 1a and 2a in operable non-small cell lung cancer to angiogenic/molecular profile of tumours and survival. Br J Cancer 2001;85:881-890.
15. Kayser G, Baumhakel JD, Szoke T, ITrojan I, Riede U, Werner M, et al. Vascular diffusion density and survival of patients with primary lung carcinomas. Virchows Arch 2003;442:462-467.
16. Fontanini G, Faviana P, Lucchi M, Boldrini L, M, A., Camacci T, et al. A high vascular count and overexpression of vascular endothelial growth factor are associated with unfavourable prognosis in operated small cell lung carcinoma. Br J Cancer 2002;86:558-563.
17. Swinson DEB, Jones JL, Richardson D, Wykoff C, Turley H, Pastorek J, et al. Carbonic anhydrase IX expression, a novel surrogate marker of tumor hypoxia, is asssociated with a poor prognosis in non-small-cell lung cancer. J Clin Oncol 2003;21:473-482.

18. Meert A-P, Paesmans M, Martin B, Delmotte P, Berghmans T, Verdebout J-M, et al. The role of microvessel density on the survival of patients with lung cancer: a systematic review of the literature with meta-analysis. Br J Cancer 2002;87:694-701.

19. Kim SJ, Rabbani ZN, Vollmer RT, Schreiber E-G, Oosterwijk E, Dewhirst MW, et al. Carbonic anhydrase IX in early-stage non-small cell lung cancer. Clin Cancer Res 2004;10:7925-7933.

20. Evans SM, Koch CJ. Prognostic significance of tumor oxygenations in humans. Cancer Lett 2003;195:1-16.

21. Hirsch FR, Prindiville SA, Miller YE, Franklin WA, Dempsey EC, Murphy JR, et al. Fluorescence versus white-light bronchoscopy for detection of preneoplastic lesions: a randomized study. J Natl Cancer Inst 2001;93:1385-1391.

22. Lam S, Kennedy T, Unger M, Miller YE, Gelmont D, Rusch V, et al. Localization of bronchial intraepithelial neoplastic lesions by fluorescence bronchoscopy. Chest 1998;113:696-702.

23. Kennedy TC, Hirsch FR, Miller YE, Prindiville S, Murphy JR, Dempsey EC, et al. A randomized study of fluorescence bronchoscopy versus white-light bronchoscopy for early detection of lung cancer in high risk patients. Lung Cancer 2000;29(S1):244-245.

24. Mirabal YN, Chang SK, Atkinson EN, Malpica A, Follen M, Richards-Kortum R. Reflectance spectroscopy for in vivo detection of cervical precancer. J Biomed Opt 2002;7:587-594.

25. Nordstrom RJ, Burke L, Nilodd JM, Myrtle JF. Identification of cervical intraepithelial neoplasia (CIN) using UV-excited fluorescence and diffuse-reflectance spectroscopy. Lasers Surg Med 2001;28:118-127.

26. Georgakoudi I, Sheets EE, Müller MG, Backman V, Crum CP, Badizadegan K, et al. Trimodal spectroscopy for the detection and characterization of cervical precancers in vivo. Am J Obstet Gynecol 2002;186:374-382.

27. Breslin TM, Xu F, Palmer GM, Zhu C, Gilchrist KW, Ramanujan N. Autofluorescence and diffuse reflectance properties of malignant and benign breast tissues. Ann Surg Oncol 2004;11:65-70.

28. Utzinger U, Brewer M, Silva E, Gershenson D, Blast RC, Follen M, et al. Reflectance spectroscopy for in vivo characterization of ovarian tissue. Lasers Surg Med 2001;28:56-66.

29. Wallace MB, Perelman LT, Backman V, Crawford JM, Fitzmaurice M, Seiler M, et al. Endoscopic detection of dysplasia in patients with Barrett's esophagus using light-scattering spectroscopy. Gastroenterology 2000;119:677-682.

30. Müller MG, Valdez TA, Georgakoudi I, Backman V, Fuentes C, Kabani S, et al. Spectroscopic detection and evaluation of morphologic and biochemical changes in early human oral carcinoma. Cancer 2003;97:1681-1692.

Samenvatting en conclusies

De prognose van longkanker is slecht omdat de diagnose bij het merendeel van de patiënten in het late en ongeneeslijke stadium van de ziekte wordt gesteld (1, 2). Vroegtijdig opsporen van gelokaliseerde kanker en premaligne afwijkingen kan de prognose van deze ziekte verbeteren. Dysplastische en kankerachtige weefsels worden in verband gebracht met chemische en morfologische veranderingen die leiden tot wijzigingen van de optische eigenschappen van de bronchiale slijmvliezen (3-5). Optische spectroscopische analyse van de bronchiale slijmvliezen kan een meer specifieke techniek zijn dan conventionele bronchoscopische beeldtechniek bij het opsporen van premaligne laesies en kanker van de proximale bronchiaalboom.

In dit proefschrift bestudeerden we de diagnostische waarde van optische spectroscopie voor kankerachtige laesies van de bronchiale slijmvliezen. We ontwikkelden een glasvezel-optisch instrument. waarmee "*autofluorescence*" (AFS), "*diffuse reflectance*" (DRS), en "*differential path length*" (DPS) spectroscopie gemeten kan worden tijdens bronchoscopie. DPS is van origine een spectroscopische techniek die in ons instituut werd ontwikkeld met het doel de optische eigenschappen te bestuderen van de meest oppervlakkige laag van de bronchiale slijmvliezen, n.l. het epitheel. DPS werd aanvankelijk bestudeerd in allerlei weefselfantomen. Daarna werd DPS *in vivo* gebruikt voor de analyse van hypoxie-gerelateerde parameters, gemeten in gezond en in maligne bronchiaal weefsel. Tenslotte werden AFS, DRS en DPS gebruikt tijdens bronchoscopie bij een grote groep patiënten om de diagnostische nauwkeurigheid te onderzoeken. De capaciteit van optische spectroscopie om de specificiteit van autofluorescentie-bronchoscopie voor het opsporen van bronchiale kankerachtige laesies te vergroten, werd bestudeerd.

Optische spectroscopie voor de analyse van de bronchiale slijmvliezen.

Optische spectroscopie van de bronchiale slijmvliezen is een uitdaging vanwege het probleem van toegankelijkheid van de bronchiaalboom. Recente vooruitgang in endoscopische beeldtechnologie heeft de ontwikkeling mogelijk gemaakt van hooggekwalificeerde flexibele bronchoscopen die het onderzoek van de proximale bronchiaalboom vergemakkelijken. Het combineren van optische spectroscopie met bronchoscopie zou de *in situ* "*real time*" spectraal-analyse mogelijk maken van bronchiale laesies die door beeldtechniek zijn opgespoord. Een eerste manier om optische spectroscopie te combineren met beeldtechniek is om de spectroscopische spectra te extraheren uit de bronchoscopische beelden die zijn verkregen tijdens wit licht en/of blauw licht - bronchoscopie (6, 7). De lichtspectra, echter, die zijn verkregen uit de bronchoscopische beelden worden verzameld uit een groot weefselgebied en dringen diep in het weefsel door, waardoor de specifieke analyse wordt geschaad van gelokaliseerde laesies en van laesies die zijn beperkt tot de meest oppervlakkige (epitheel) laag van de bronchiale slijmvliezen. Voor onze studie kozen we ervoor, om een zelfgemaakte optische glasvezelsonde te gebruiken om de bronchiale slijmvliezen te verlichten en om het lichtsignaal op te vangen dat wordt gereflecteerd door het bronchiale oppervlak. Deze glasvezelsonde werd ingebracht via het werkkanaal van de bronchoscoop en op het weefseloppervlak geplaatst. Voordelen waren een betere controle van het verlichtingssignaal (intensiteit, golflengte) en van het opgevangen gereflecteerde lichtsignaal wat de analyse mogelijk maakte van gelokaliseerde en oppervlakkige laesies van de bronchiale slijmvliezen. Het gebruik van deze glasvezel-optische sonde was gemakkelijk en werd goed verdragen. De sonde kon nauwkeurig worden geplaatst op bronchiaal-laesies zonder het weefsel te beschadigen.

Een belangrijke eigenschap van ons spectroscopisch instrument was de mogelijkheid om tegelijkertijd zowel autofluorescentie als witlicht-reflectie spectroscopie te meten.

Autofluorescentie spectroscopie onderzoekt de fluorescentie van de endogene fluorophoren die in het weefsel aanwezig zijn, maar de autofluorescentiespectra worden ook beïnvloed door de optische eigenschappen (n.l. verstrooiing en absorptie) van het weefsel (4). Wit licht reflectiespectroscopie gebruikt geen fluorophoren maar bestudeert rechtstreeks de optische eigenschappen van weefsel. Reflectiespectra zijn afhankelijk van de aanwezigheid in het weefsel van lichtabsorberend materiaal zoals hemoglobine, en van lichtverstrooiend materiaal zoals collageen, elastine, en verscheidene membraan-gebonden cellulaire organellen (8-10). Het gelijktijdig meten van autofluorescentie en witlicht reflectiespectroscopie maakte het ons mogelijk om de rol te onderscheiden van de weefselfluorophoren, verstrooiiende en absorberende materialen in de optische veranderingen die optraden tijdens de maligne transformatie van de bronchiale slijmvliezen.

Optische spectroscopie voor de analyse van het bronchiaal epithelium (rol van "*differential path length*" spectroscopie)

De studie van de epitheellaag van de bronchiale slijmvliezen is vooral interessant omdat het merendeel van de longkankers optreedt in het epitheel en wordt voorafgegaan door premaligne veranderingen die alleen het oppervlakte-epitheel aantasten. DPS werd ontwikkeld met het doel te bestuderen wat er optisch gebeurde in de meest oppervlakkige laag van het weefsel. De oppervlakkige analyse was mogelijk door een enkelvoudige "aanlevering" en "verzameling" dc-glasvezel te gebruiken om het licht te leveren en het door het weefsel gereflecteerde licht op te sporen, en op die manier tot een optimalisatie te komen van de waarschijnlijkheid van het opsporen van fotonen die worden verstrooid vanuit kleine proefdieptes.

In **hoofdstuk 2** gebruikten we DPS om de verstrooiingseigenschappen te meten van diverse weefselfantomen die bestonden uit één of twee lagen suspensie van polystyreen

bollen. We zagen dat het signaal dat werd opgevangen door de dc-glasvezel gevoelig was voor verstrooiingsmomenten die dichtbij de punt van de glasvezelsonde optraden. Verdere analyse in weefselfantomen toonde aan dat, in het scala van parameters dat relevant is voor biologisch weefsel, de weefseldiepte die door DPS wordt onderzocht, onafhankelijk is van de optische eigenschappen van het weefsel, maar slechts afhankelijk is van de diameter van de glasvezel (11). Dientengevolge kan de diameter van de glasvezels worden aangepast aan de weefseldiepte die wordt bestudeerd. Voor de studie van bronchiale slijmvliezen gebruikten we glasvezels met een diameter van 400 μm waarvoor de kennelijke differentiële weglengte van het DPS signaal 320 μm bedroeg, zodat analyse van gereflecteerde fotonen mogelijk werd van ruwweg binnen 160 μm van het weefseloppervlak.

Optische spectroscopie voor de analyse van weefselhypoxie-gerelateerde parameters in bronchiale slijmvliezen

In **hoofdstuk 3** toonden we aan dat verscheidene hypoxie-gerelateerde parameters zoals de oxygenatie in het bloed van de microvasculatuur, het bloedvolume en de diameter van microvaten kunnen worden afgeleid uit DPS spectra. In **hoofdstuk 4** meldden we dat bronchiale tumoren werden gekenmerkt door een lagere bloedoxygenatie, een hoger bloedvolume en grotere microvaten in vergelijking met normale bronchiale slijmvliezen. Er werd geen verschil gevonden tussen normale slijmvliezen en metaplastische/licht dysplastische slijmvliezen. Deze resultaten waren in overeenstemming met gegevens over longtumor-oxygenatie die waren verkregen met gebruikmaking van functionele beeldtechnieken (12, 13) van immunokleuringen met hypoxiemarkers (14-19) wat erop wees dat tumorhypoxie vaak optreedt bij longkanker.

In **hoofdstuk 5** meldden we dat longkanker met een slechte prognose, zoals kleincellig carcinomen en ongedifferentieerde grootcellig carcinomen in verband gebracht kon worden

met de laagste bloedoxygenatie in vergelijking met andere kankerceltypes zoals plaveiselcelcarcinomen en adenocarcinomen. Kleincellig carcinomen en ongedifferentieerde grootcellig carcinomen werden ook gekenmerkt door een lager bloedvolume en kleinere gemiddelde bloeddiameter, dat wees op een slechtere organisatie van de microvasculatuur van de tumor. Tumorhypoxie is eerder in verband gebracht met een lagere overleving, een hogere agressiviteit en een lagere gevoeligheid voor therapie (20). Het verband tussen longkankerceltypes met een slechte prognose met een lagere bloedoxygenatie pleit voor de slechte prognose waarde van bloedhypoxie gemeten in een bronchiale tumor met gebruikmaking van DPS.

Combinatie van optische spectroscopie met autofluorescentie bronchoscopie voor het opsporen van bronchiaallaesies van de bronchiaalboom

Wit licht en fluorescentie endoscopische beeldtechnieken worden veelal gebruikt voor het opsporen van proximale endobronchiaallaesies. De gevoeligheid van autofluorescentie bronchoscopie (AFB) heeft bewezen beter te zijn dan wit licht bronchoscopie voor het opsporen van carcinomen *in situ* en dysplastische laesies (21-23). AFB wordt echter gekenmerkt door een lage specificiteit met een hoge mate van "vals-positieve" resultaten. Dit brengt onnodige biopsieën met zich mee met hogere kosten en een langere duur van het onderzoek. Optische spectroscopische technieken zijn uitgebreid bestudeerd voor het *in vivo* opsporen van maligne en pre-neoplastisch weefsel (4, 5). Het blijkt, dat combinatie van AFS en DRS het met een hoge mate van nauwkeurigheid opsporen van maligne weefsel vergemakkelijkt in de uterus (24-26), de borst (27), de eierstok (28), de slokdarm (29) en de mondholte (30). Van de long zijn weinig gegevens beschikbaar, vooral vanwege de ontoegankelijkheid van dit orgaan.

We bestudeerden in **hoofdstuk 6** de haalbaarheid van het gecombineerd gebruik van optische spectroscopie en autofluorescentie-bronchoscopie voor het opsporen van pre-maligne en invasieve carcinomen van de bronchiaalboom. Voorlopige gegevens wekten de indruk dat optische spectroscopie de specificiteit kan verbeteren van autofluorescentie-bronchoscopie beeldtechniek voor het opsporen van bronchiale maligne laesies. In **hoofdstuk 7** werden de definitieve resultaten gemeld van de eerste autofluorescentie en reflectie-spectroscopische studie van de bronchiale slijmvliezen. We constateerden dat de diagnostische nauwkeurigheid van witlichtreflectie-spectroscopie beter was dan die van AFS. Dit resultaat doet vermoeden dat de optische eigenschappen van de bronchiale slijmvliezen belangrijker zijn dan hun autofluorescentie eigenschappen voor weefselclassificatie. We bevestigden dat witlicht-reflectie en autofluorescentie spectroscopie hogere "positieve voorspellende waarden" opleverden in vergelijking met AFB beeldtechnieken voor het opsporen van bronchiale tumoren. De beste resultaten werden verkregen wanneer reflectie- en autofluorescentie spectroscopie werden gecombineerd.

Algemene Conclusie

We lieten zien dat optische spectroscopie gemakkelijk kan worden gebruikt tijdens bronschoscopie voor de optische analyse van normaal en van cancereus bronchiaal slijmvlies. We zagen dat de optische eigenschappen van de bronchiale slijmvliezen de meest onderscheidende informatie bevatten voor weefselclassificatie en dat de optische variaties als waargenomen in bronchiaaltumoren met behulp van DRS, DPS en AFS in verband kunnen worden gebracht met de absorptie van licht door weefselbloed. We zagen dat bloedhypoxie vaak voorkomt in bronchiaaltumoren vooral in gevallen van tumoren met een slechte prognose zoals klein-cellige longcarcinomen.. Endobronchiale tumoren werden ook gekenmerkt door een hogere bloedinhoud en grotere microvaten in vergelijking met non-

cancereuze slijmvliezen. Tenslotte lieten we zien dat combinatie van optische spectroscopie met autofluorescentie-bronchoscopie de specificiteit verbetert van autofluorescentie-bronchoscopie alleen.. Daarom kan optische spectroscopie worden toegepast in de reeks diagnostische technieken die momenteel worden gebruikt voor het opsporen van endobronchiale kanker.

REFERENTIES

1. Mountain CF. The international system for staging lung cancer. Sem Surg Oncol 2000;18:106-115.
2. Naruke T, Tsuchiya R, Kondo H, Asamura H. Prognosis and survival after resection for bronchogenic carcinoma based on the 1997 TNM-staging classification: The Japanese experience. Ann Thorac Surg 2001;71:1759-1764.
3. Ramanujam N. Fluorescence spectroscopy of neoplastic and non-neoplastic tissues. Neoplasia 2000;2:89-117.
4. Wagnières GA, Star WM, Wilson BC. In vivo fluorescence spectroscopy and imaging for oncological applications. Photochem Photobiol 1998:603-632.
5. Sokolov K, Follen M, Richards-Kortum R. Optical spectroscopy for detection of neoplasia. Cur Opin Chemical Biol 2002;6:651-658.
6. Chiyoa M, Shibuyaa K, Hoshinoa H, Yasufukua K, Sekinea Y, Lizasaa T, et al. Effective detection of bronchial preinvasive lesions by a new auto.uorescence imaging bronchovideoscope system. Lung Cancer 2005:in press.
7. Zeng H, Petek M, Zorman MT, Mc Williams A, Palcic B, Lam S. Integrated endoscopy system for simultaneous imaging and spectroscopy for early lung cancer detection. Opt Letters 2004;29:587-589.
8. Bartlett M, Huang G, Larcom L, Jiang H. Measurement of particle size distribution in mammalian cells in vitro by use of polarized light spectroscopy. Appl Optics 2004;43:1296-1307.
9. Beauvoit B, Kitai T, Chance B. Contribution of the mitochondrial compartment to the optical properties of the rat liver: A theoretical and practical approach. Biophys J 1994;67:2501-2510.
10. Beauvoit B, Chance B. Time-resolved spectroscopy of mitochondria, cells and tissue under normal and pathological conditions. Mol Cell Bioch 1998;184:445-455.
11. Amelink A, Sterenborg HJCM. Measurement of the local optical properties of turbid media by differential path-lenght spectroscopy. Appl Optics 2004;43:3048-3054.
12. Urtasun RC, Parliament MB, McEwan AJ, Mercer JR, Manan RH, Wiebe LI, et al. Measurement of hypoxia in human tumours by non-invasive spect imaging of iodoazomycin arabinoside. Br J Cancer 1996;27:S209-S212.
13. Rasey JS, Koh W-J, Evans ML, Peterson LM, Lewellen TK, Graham MM, et al. Quantifying regional hypoxia in human tumors with positron emission tomography of [18F]fluoromisonidazole: a pretherapy study of 37 patients. Int J Radiat Oncol Biol Phys 1996;36:417-428.
14. Giatromanolaki A, Koukourakis MI, Sivridis E, Turley H, Talks K, Pezzela F, et al. Relation of hypoxia inducible factor 1a and 2a in operable non-small cell lung cancer to angiogenic/molecular profile of tumours and survival. Br J Cancer 2001;85:881-890.
15. Kayser G, Baumhakel JD, Szoke T, ITrojan I, Riede U, Werner M, et al. Vascular diffusion density and survival of patients with primary lung carcinomas. Virchows Arch 2003;442:462-467.
16. Fontanini G, Faviana P, Lucchi M, Boldrini L, M, A., Camacci T, et al. A high vascular count and overexpression of vascular endothelial growth factor are associated with unfavourable prognosis in operated small cell lung carcinoma. Br J Cancer 2002;86:558-563.
17. Swinson DEB, Jones JL, Richardson D, Wykoff C, Turley H, Pastorek J, et al. Carbonic anhydrase IX expression, a novel surrogate marker of tumor hypoxia, is asssociated with a poor prognosis in non-small-cell lung cancer. J Clin Oncol 2003;21:473-482.

18. Meert A-P, Paesmans M, Martin B, Delmotte P, Berghmans T, Verdebout J-M, et al. The role of microvessel density on the survival of patients with lung cancer: a systematic review of the literature with meta-analysis. Br J Cancer 2002;87:694-701.

19. Kim SJ, Rabbani ZN, Vollmer RT, Schreiber E-G, Oosterwijk E, Dewhirst MW, et al. Carbonic anhydrase IX in early-stage non-small cell lung cancer. Clin Cancer Res 2004;10:7925-7933.

20. Evans SM, Koch CJ. Prognostic significance of tumor oxygenations in humans. Cancer Lett 2003;195:1-16.

21. Hirsch FR, Prindiville SA, Miller YE, Franklin WA, Dempsey EC, Murphy JR, et al. Fluorescence versus white-light bronchoscopy for detection of preneoplastic lesions: a randomized study. J Natl Cancer Inst 2001;93:1385-1391.

22. Lam S, Kennedy T, Unger M, Miller YE, Gelmont D, Rusch V, et al. Localization of bronchial intraepithelial neoplastic lesions by fluorescence bronchoscopy. Chest 1998;113:696-702.

23. Kennedy TC, Hirsch FR, Miller YE, Prindiville S, Murphy JR, Dempsey EC, et al. A randomized study of fluorescence bronchoscopy versus white-light bronchoscopy for early detection of lung cancer in high risk patients. Lung Cancer 2000;29(S1):244-245.

24. Mirabal YN, Chang SK, Atkinson EN, Malpica A, Follen M, Richards-Kortum R. Reflectance spectroscopy for in vivo detection of cervical precancer. J Biomed Opt 2002;7:587-594.

25. Nordstrom RJ, Burke L, Nilodd JM, Myrtle JF. Identification of cervical intraepithelial neoplasia (CIN) using UV-excited fluorescence and diffuse-reflectance spectroscopy. Lasers Surg Med 2001;28:118-127.

26. Georgakoudi I, Sheets EE, Müller MG, Backman V, Crum CP, Badizadegan K, et al. Trimodal spectroscopy for the detection and characterization of cervical precancers in vivo. Am J Obstet Gynecol 2002;186:374-382.

27. Breslin TM, Xu F, Palmer GM, Zhu C, Gilchrist KW, Ramanujan N. Autofluorescence and diffuse reflectance properties of malignant and benign breast tissues. Ann Surg Oncol 2004;11:65-70.

28. Utzinger U, Brewer M, Silva E, Gershenson D, Blast RC, Follen M, et al. Reflectance spectroscopy for in vivo characterization of ovarian tissue. Lasers Surg Med 2001;28:56-66.

29. Wallace MB, Perelman LT, Backman V, Crawford JM, Fitzmaurice M, Seiler M, et al. Endoscopic detection of dysplasia in patients with Barrett's esophagus using light-scattering spectroscopy. Gastroenterology 2000;119:677-682.

30. Müller MG, Valdez TA, Georgakoudi I, Backman V, Fuentes C, Kabani S, et al. Spectroscopic detection and evaluation of morphologic and biochemical changes in early human oral carcinoma. Cancer 2003;97:1681-1692.

Dankwoord

Veel mensen hebben bijgedragen aan de voltooiing van dit proefschrift. Een aantal wil ik met name bedanken.

Allereerst, mijn promotor prof. dr. Henk Hoogsteden die mij de mogelijkheid heeft gegeven om deze promotie uit te voeren.

Mijn eerste copromotor, dr. Dick Sterenborg. Beste Dick, je bent de grote "Manitoe" van het optische spectroscopie project van het Erasmus MC waarvan mijn proefschrift slechts een heel klein onderdeel uitmaakt. Bedankt voor jouw ondersteuning en de prikkelende discussie over onze resultaten.

Mijn tweede copromotor, dr. Joachim Aerts. Beste Joachim, bedankt voor jouw hartstochtelijke samenwerking en jouw ondersteuning. Je hebt me laten zien hoe een vrolijk familieleven, zwaar klinisch werk en uitgebreide wetenschappelijke activiteiten gecombineerd kunnen worden. Bedankt voor de ontspannen en vriendelijke sfeer tijdens mijn werkzaamheden in het Sint Franciscus Gasthuis.

Mijn "copromentor", dr. Arjen Amelink. Beste Arjen, je bent de uitvinder van de "differential path length spectroscopy" techniek die, naar mijn overtuiging, in de toekomst een forse bijdrage zal leveren aan de behandeling van kanker patiënten. Je had de moeilijke taak om de wet van optische spectroscopie aan mij uit te leggen. Bedankt voor jouw geduld, jouw ondersteuning bij mijn gedachtenvorming en jouw hulp bij het schrijven.

Prof. dr. Jan van Meerbeeck en dr. Sjaak Burgers die de twee initiatiefnemers van het klinische project "optische spectroscopie in longkanker" waren. Beste Jan, sinds onze eerste ontmoeting in Barcelona, heb je altijd aandacht gehad voor deze Franse longarts die het gekke plan had om in Nederland te gaan werken. Bedankt voor het vertrouwen dat je in mij in de mogelijkheden die er voor mij in Nederland zijn, stelde. Beste Sjaak, onze samenwerking in het begin van het spectroscopische project blijft voor mij een uitstekende herinnering. Ik ben dankbaar voor jouw dynamisme en vriendelijke ondersteuning.

Arjan Rudolphus en Yoeke Tan, mijn aardige collega's van het Sint Franciscus Gasthuis. Bedankt voor jullie vriendelijke ontvangst en jullie hulp in mijn begin als zelfstandig specialist in jullie top periferiek ziekenhuis.

Het personeel van de afdeling en de polikliniek longziekten van het Sint Franciscus Gasthuis dat altijd nieuwsgierig en enthousiast met betrekking tot dit project was. Esther, Prina, Deerdre, Brigit, Bianca, Jolanda, Vivian, Liesbeth, Badria, Simone, Lies, Monique, Inge, Ans, Sabira en alle andere medewerkers van het Sint Franciscus Gasthuis die ik niet met naam heb genoemd; Bedankt voor jullie fijne samenwerking.

Prof. dr. Bart Lambrecht, hoofd van het Erasmus MC longziekten laboratorium. Beste Bart, ik blijf meer dan dankbaar voor jouw ondersteuning gedurende mijn hele werkzaamheid in het Erasmus MC. Je bent het levende bewijs ervoor dat humor en top wetenschap prima kunnen samengaan.

Joost Hegmans, mijn leuke collega gedurende mijn *fellowship* in het longziekten laboratorium. Beste Joost, je hebt me het voorrecht verleend om met jouw het proteomic project van het longziekten laboratorium te beginnen. Je bent in een paar jaar een wereldbekende referent in kanker proteomic en immunotherapie geworden. Na mijn *fellowship* bleef je altijd beschikbaar om me te helpen voor het *in vitro* deel van mijn spectroscopische werk. Bedankt voor de kameraadschap.

De huidige en ex-medewerkers van het Erasmus MC longziekten laboratorium, Alex, Harmjan, Leonie, Hamida, Hendrik Jan, Annabrita, Danielle, Femke, Karolina, Monique, Nanda, Thomas, Tanja, Hermelijn, Mirjam, Lous, Brigit, Jan Bas, Sophia, Pim, Victor; Hartelijk dank voor de plezierige samenwerking.

Annelies en Francine; Bedankt voor jullie hulp bij het oplossen van taalprobleempjes.

Curriculum Vitae

De auteur van dit proefschrift heeft de Franse nationaliteit en is geboren op 30 april 1965. In 1984 behaalde hij het "baccalaureaat" aan het "Rabelais" lyceum te Meudon. In hetzelfde jaar begon hij aan zijn studie Geneeskunde aan het academisch ziekenhuis "Kremlin Bicêtre" (Universiteit Paris XI). In 1990 slaagde hij voor het Franse landelijke selectieve toelatingsexamen voor de medische specialiteit (Concours d'Internat). Van 1992 tot 1993 vervulde hij zijn militaire dienstplicht in het militair ziekenhuis "Clermont-Tonnerre" te Brest. In de periode 1990-1996 doorliep hij de opleiding tot longspecialist in de regio Paris, Ile-de-France. Het medische doctoraat en het specialisatie diploma voor longgeneeskunde werden respectievelijk in 1995 en 1996 verkregen. Van 1996 tot 1999 was hij werkzaam als longarts in de longziekten unit van het academisch ziekenhuis "Kremlin Bicêtre" en van 1999 tot 2001 in het kanker instituut "Gustave-Roussy". In 2001 verkreeg hij het specialisatie diploma voor medische oncologie. In 2001 kwam hij naar Nederland in het kader van een *fellowship* van de *European Society for Medical Oncology*. Van 2001 tot 2002 deed hij mee aan een studie over tumor exosomen bij maligne pleural mesothelioom in het longziekten laboratorium van het Erasmus Medisch Centrum te Rotterdam (Prof. dr. Hoogsteden, Dr. Lambrecht). Vanaf 2001 was hij als longarts allereerst werkzaam in de longziekten afdeling van het Erasmus Medisch Centrum (Prof. dr. Hoogsteden) en vervolgens in de longziekten afdeling van het Sint Franciscus Gasthuis te Rotterdam. Tijdens deze periode werd een aanvang gemaakt met het onderzoek, onder leiding van Dr. Sterenborg en Dr. Aerts, waarvan de resultaten zijn beschreven in dit proefschrift. Sinds 2005 is hij werkzaam als longarts in het Kennemer Gasthuis te Haarlem.